Effects of HIV on the Longitudinal Development of Fronto-striatal Functional Connectivity in Children Aged 7 to 11

Author:
Cayleigh Brown

Student Number:
BRWCAY001

Division of Biomedical Engineering

Department of Human Biology

University of Cape Town, South Africa

Dissertation submitted in fulfilment of the requirements for the degree:

Master of Science in Biomedical Engineering

Supervisor:

Dr Frances Robertson

Co-supervisors:

Professor Ernesta Meintjes

Dr Jia Fan

February 2022

Declaration

I, Cayleigh Brown, hereby declare that the work on which this dissertation/thesis is based is my original work (except where acknowledgements indicate otherwise) and that neither the whole work nor any part of it has been, is being, or is to be submitted for another degree in this or any other university.

I empower the university to reproduce for the purpose of research either the whole or any portion of the contents in any manner whatsoever.

Signature Signed by candidate

Date: 13 February 2022

Acknowledgments

I would like to express my sincere gratitude to my supervisors for your continuous guidance and support throughout this dissertation. Thank you, Dr Frances Robertson, for being engaging and proactive. You provided me with direction and feedback when I needed clarity on my research. Thank you, Professor Ernesta Meintjes, for your insight of fMRI and knowledge of the CHER cohort, and to Dr Jia Fan, for familiarising me with AFNI and your assistance with preprocessing the data.

Thank you to the members of the MRI lab who provided me with daily encouragement and research advice.

Thank you to the National Research Foundation (NRF) for providing the funding that allowed me to pursue my studies.

And finally, thank you to my parents, brothers, and my pillar of strength, Joshua Arendse, for all your love and support.

Abstract

Despite the early initiation of antiretroviral therapy (ART), human immunodeficiency virus (HIV) in children is still associated with neurodevelopmental delay, with findings of neurocognitive deficits in executive, motor and language function.

The basal ganglia (BG) develop early in childhood and are known to be affected by HIV. Their main function is to control goal-directed behaviours. Although the BG are strongly interconnected with the cerebral cortex through fronto-striatal pathways, little is known about fronto-striatal network maturation during childhood or how perinatal HIV-infection (PHIV) affects its development. Using seed-based correlation analysis (SCA) of resting state functional magnetic resonance imaging (rs-fMRI), we conducted a longitudinal analysis to examine the effects of age and HIV on functional connectivity (FC) between the BG and the frontal cortex.

Rs-fMRI data were collected at ages 7, 9 and 11 from children with perinatal HIV (CPHIV) who were part of the Children with HIV Early AntiRetroviral (CHER) trial (n=79), along with age-matched uninfected children from similar neighbourhoods (n=80). For SCA, BG seeds and frontal cortex regions of interest (ROIs) were selected from known cortico-BG-thalamic functional networks. The BG seeds comprised the bilateral putamen, caudate, globus pallidus (GP) and thalamus. Functional regions located in the dorsolateral prefrontal cortex (DLPFC), paracentral lobule and pars opercularis were chosen as frontal ROIs because of their association with executive, motor and language function, respectively. FC was obtained via correlations between rs-fMRI time-series from the BG seeds and frontal ROIs. Linear mixed effect models were used to examine individual and synergistic effects of age and HIV status on FC.

We found age-related increases in FC between BG seeds and both DLPFC and pars opercularis regions, while age-related FC decreases were seen between the BG and paracentral lobule. HIV-related alterations in FC were seen between the paracentral lobule and left and right caudate ($P = 0.043$ and $P = 0.02$) and GP ($P = 0.023$ and $P = 0.041$), and between the right pars opercularis and left and right putamen ($P = 0.015$ and $P = 0.01$), left caudate ($P = 0.02$) and left and right GP ($P = 0.001$ and $P = 0.048$).

Attenuated FC between the BG and paracentral lobule and right pars opercularis suggests that HIV alters primarily motor function and inhibitory control, a component of executive function, in childhood. In contrast, there was no effect of HIV on FC of the BG to the DLPFC, a connection which is also considered to be important for executive functioning. Interaction of HIV and age on FC between the BG and paracentral lobule shows that although FC typically decreases with age, it remains unchanged in CPHIV. Similarly, increased FC between the BG and right pars opercularis with age in the control group but relatively constant FC in CPHIV provides evidence that HIV may hinder typical age-related development of BG FC.

Contents

List of Tables

List of Figures

Abbreviations

2D	2 dimensional
3D	3 dimensional
ADHD	Attention Deficit Hyper-activity Disorder
AIC	Akaike Information Criterion
AIDS	Acquired immune deficiency syndrome
AFNI	Analysis of functional neuroimages
ART	Anti-retroviral therapy
ATP	Adenosine triphosphate
BA	Brodmann area
BBB	Blood-brain barrier
BG	Basal ganglia
BOLD	Blood oxygenation level dependent
CBF	Cerebral blood flow
CHER	Children with HIV Early Antiretroviral
CNS	Central nervous system
CPHIV	Children with perinatal HIV
CSF	Cerebral spinal fluid
CUBIC	Cape Universities Brain Imaging Centre/Cape Universities Body Imaging Centre
DICOM	Digital Imaging and Communications in Medicine
DLPFC	Dorsal lateral prefrontal cortex
DMN	Default mode network
DOF	Degrees of freedom
DTI	Diffuser Tensor Imagining
EPI	Echo planar imaging
FC	Functional Connectivity
fMRI	Functional magnetic resonance imaging
FoV	Field of view
FWHM	Full width half maximum
GM	Grey matter
GP	Globus pallidus
GPi	Internal segment of the globus pallidus
GPe	External segment of the globus pallidus
GRE	Gradient echo
HAND	HIV-associated neurocognitive disorder

Abbreviations

HIV	Human immuno-deficiency virus
HRF	Hemodynamic response function
ICA	Independent component analysis
IFG	Inferior frontal gyrus
LME	Linear mixed effect
LOFC	Lateral orbital frontal cortex
MEMPRAGE	Multi-echo magnetization prepared rapid gradient echo
MR	Magnetic resonance
MRI	Magnetic resonance imaging
MTCT	Mother to child transmission
PCR	Polymerase-chain-reaction
PFC	Prefrontal cortex
PHIV	Perinatal human immuno-deficiency virus
PLV	Plasma viral load
PMTCT	Prevention mother to child transmission
PPN	Pedunculopontine nucleus
RF	Radiofrequency
ROI	Region of interest
RSFC	Resting-state functional connectivity
Rs-fMRI	Resting-state functional magnetic resonance imaging
SCA	Seed-based Correlation Analysis
SE	Spin echo
SNr	Substantia nigra pars reticulata
SNR	Signal-to-noise ratio
SSA	Sub Saharan Africa
TR	Repetition time
TE	Echo time
TI	Inversion time
WM	White matter
ZDV	Zidovudine

1. Introduction

In comparison to adults, there is a greater concern for the neurological effects that Human Immunodeficiency Virus (HIV) has on children due to their rapidly developing, yet still immature brains. Prior to the introduction of anti-retroviral therapy (ART), HIV infection in children manifested as a static or progressive HIV encephalopathy (Van Rie et al., 2010). This was reflected in the delay or loss of developmental milestones, impaired cognitive functioning, motor deficits, slower processing speeds and behavioural abnormalities (Lindsey et al., 2006; Van Rie et al., 2007, 2010). The Children with HIV Early Antiretroviral (CHER) trial in 2005 (Violari et al., 2008) investigated the possible long-term health benefits of infants receiving early ART (before 12 weeks). Children that were in the deferred ART treatment arm were more likely to develop illnesses or require hospitalisation, revealing that early ART decreases morbidity rates, as well as mortality. The results of the CHER trial showed the importance of early HIV diagnosis, and the early initiation of ART. Although the introduction of ART reduced the incidence of HIV encephalopathy, little is known about the long-term neurological effects of HIV in children who had access to early ART (Lindsey et al., 2006; Van Rie et al., 2010; Laughton et al., 2013).

Children with perinatal HIV (CPHIV) may still be vulnerable to structural and functional brain abnormalities owing to HIV infection during critical periods of brain development, and prolonged exposure to the virus and chronic inflammation (Lewis-de los Angeles et al., 2016). ART has led to a substantial increase in the survival rate of CPHIV, increasing the population of children living with HIV as a chronic condition (Davies et al., 2017). Consequently, there is a need to understand the effects of HIV-infection on brain development (Wade et al., 2019).

Although neuroimaging allows for further insight into brain development of children living with HIV, these studies are relatively rare, especially in developing countries (Musielak and Fine, 2016; Randall et al., 2017) . Additionally, some studies have reported conflicting results, possibly due to the large variation in ages among the sample groups. Notable limitations discussed in many of these clinical studies are the use of small sample sizes and cross-sectional designs. It is evident that longitudinal studies of CPHIV are required to confirm existing findings and add to the body of knowledge about how the trajectory of brain development may be altered by HIV.

Neuropathology caused by HIV is most evident in the basal ganglia (BG) and cerebral white matter (WM). The BG network demonstrates an essential role in learning complex and goal-directed behaviours (Smitha et al., 2017). Considering that the main function of the BG is to control movement, any interference in the BG network may mark the onset of a movement disorder (Lanciego, Luquin and Obeso, 2014). The BG, which includes the striatum, develop early in childhood and are known to be affected by HIV; therefore, it is of interest to examine the development of fronto-striatal networks in CPHIV. Although the BG are strongly interconnected with the cerebral cortex, relatively little is known about the maturation of this functional network during childhood or the way in which perinatal HIV (PHIV) may affect its development.

The FC of the caudate, one component of the BG, is of interest because of its documented atrophy in HIV patients; it is also the structure in which the highest concentration of HIV is observed (Thompson et al., 2005; Ances et al., 2013). In an adult HIV cohort, reduced intrinsic connectivity between the dorsolateral prefrontal cortex (DLPFC) and the dorsal caudate has been reported

(Ipser et al., 2015). Additionally, a task-based FC study revealed that the HIV group had lower connectivity between the left caudate and ventral prefrontal cortex than the control group (Melrose et al., 2008).

Despite these findings specifically implicating the caudate in HIV, whole-brain (WB) FC analysis in the CHER cohort at age 7 did not reveal any differences in FC of the BG as a whole between CPHIV and the control group (Toich et al., 2018). In combination with previous observations, this may indicate that HIV-related alterations in FC of the fronto-striatal network occur with age, and reduced connectivity in the HIV group may be more apparent when assessing the development of FC over time. Alternatively, early ART may prevent alterations to BG FC.

Based on previous findings in literature, it is hypothesised that:

i. HIV-infection is associated with compromised (i.e. reduced) BG FC in executive function, motor and language networks.

ii. HIV-infection is associated with slower rate of development of FC (smaller increases with age) within the fronto-striatal resting-state network. This will be shown as larger differences in FC measures between ages 7 and 11 in a control group compared to the FC measures between ages 7 and 11 in an HIV group.

The present study aims to compare the development of FC within the fronto-striatal network of PHIV children and compare these findings to that of uninfected controls by considering the individual and synergistic effects of age and HIV-status. This will be conducted as longitudinal study design, whereby a temporal profile of the change in FC between the BG and the frontal region will be constructed for the PHIV and control groups, by including FC measurements at ages 7, 9 and 11.

1.1 HIV within Sub-Saharan Africa

Although only accounting for 12% of the global population, in 2017 Sub-Saharan Africa (SSA) housed 71% of people living with HIV (Dwyer-lindgren et al., 2017). The primary mode of HIV-transmission in children is vertical transmission from mother to child (MTCT), which comprises about 90% of total pediatric HIV infections. In the absence of preventative measures, the rate of vertical transmission ranges from 15 - 45% (Al Sawai et al., 2020). The estimated pediatric fatality due to HIV has declined by nearly 50% compared to the number of deaths recorded in 2002 (S.A, 2020). The increased survival rate can be attributed to the access and advancements of ART. Although there is no cure for HIV, ART provides a means of vastly reducing the viral load and slowing the progression of the disease.

1.2 Neurophysiology of HIV

HIV has neurological effects due to the neurotropic properties of the virus (Hof et al., 2019). The virus enters the brain within days of primary infection by effectively penetrating the blood-brain barrier (BBB) via infected monocytes or blood lymphocytes, as proposed by the 'Trojan horse' theory. This is shown in Figure 1.1 where HIV binds to monocytes or CD4+ T-lymphocytes and uses these cells as a mask to cross the BBB. Subsequently, HIV uses the central nervous system

(CNS) to act as a reservoir for the viral infection (Hof et al., 2019; Ene, 2018; Le Doaré et al., 2012, Lindsey et al., 2006) and resides in macrophages and microglia within the perivascular space (Gartner, 2000). Regardless of the decline in HIV-complications owing to the use of ART, there has been a persistent prevalence in neurological diseases. This is explained by the fact that not all antiretroviral drugs cannot adequately penetrate the CNS to the same degree as HIV (Hof et al., 2019; Letendre et al., 2009). Therefore, the virus is not prevented from replicating in the CNS. Evidently, developmental dysfunction may be caused by damage to the CNS (Smith et al., 2005). Thus, there is concern regarding the neurodevelopmental delay and neurocognitive deficits associated with HIV-infection.

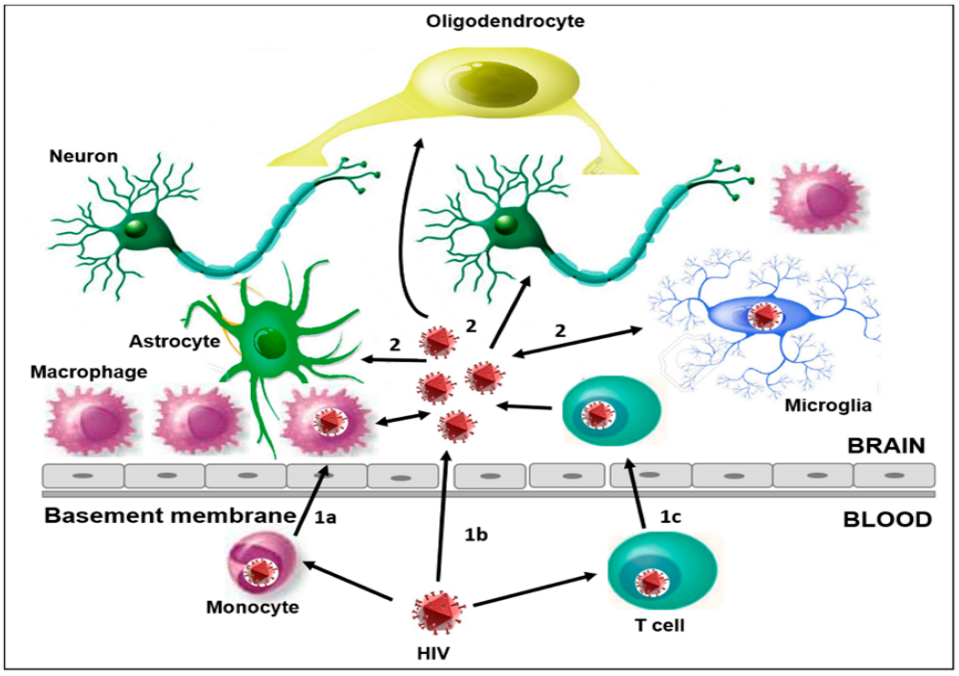

Figure 1.1: The proposed 'Trojan horse' theory suggests that the HIV virus uses monocytes and CD4+ T lymphocytes to penetrate the blood-brain barrier (Scutari et al., 2017).

1.3 Brain Abnormalities in Children Living with HIV

Neuroimaging studies conducted on vertically infected children and adolescents have found both morphometric and functional differences between these children and uninfected controls, providing evidence of abnormal or delayed neurodevelopment in HIV-infected youth. Previous neuroimaging studies conducted on CPHIV have found evidence of: WM abnormalities (van Arnhem et al., 2013; Sarma et al., 2014; Ackermann et al., 2016; Cohen et al., 2016; Uban et al., 2016; Jankiewicz et al., 2017); reduced gray matter (GM) volume (Lewis-de los Angeles et al., 2017; Li et al., 2018; Hoare et al., 2019); ventricular enlargement (van Arnhem et al., 2013); and cortical and sub-cortical morphometric deformations (Lewis-de los Angeles et al., 2016, 2020; Yadav et al., 2017; Hoare et al., 2019; Wade et al., 2019). A systematic review on the brain structure of CPHIV reported findings of differences in WM volume, WM hyperintensity, GM volume and cortical structures in CPHIV when compared with HIV-uninfected controls (Van den Hof et al., 2019), with further findings of increased CSF in WM and parts of the BG.

1.4 Effects of HIV on the Basal Ganglia

Abnormalities of the BG are frequently reported in both children and adults living with HIV. A study conducted on a cohort of Thai children found a strong negative correlation between the baseline CD4 count and morphometry of the left pallidum among adolescents with HIV (Wade et al., 2019). Additionally, Wade et al. (2019) observed that the medial inferior region of the right pallidum was thinner in HIV-infected group when compared with the healthy controls. Significantly reduced putamen volumes were observed in HIV-infected children at 7 years of age (Nwosu et al., 2018). Another Thai cohort revealed larger brain volumes of the caudate, nucleus accumbens, putamen and pallidum in vertically HIV-infected children than in HIV-infected children (Paul et al., 2018). Additionally, these volumes were more pronounced in children under the age of 12 years. Other reported abnormalities of the BG in children include altered neurometabolites (Mbugua et al., 2016; Holmes et al., 2017; Robertson et al., 2018) and increased cerebral blood flow (CBF) (Blokhuis et al., 2017) in CPHIV. Ances et al. (2013) observed that the caudate nuclei of the BG (together with the corpus collosum) had the highest HIV-concentration when compared to other brain regions. This may be caused by their proximity to the ventricles which allows for the ease of penetration of HIV-infected mononuclear cells (Ances et al., 2013; Randall et al., 2017). Furthermore, the study reported a reduced caudate volume for participants with HIV compared to controls.

2. Principles of Functional Magnetic Resonance Imaging

Different neuroimaging modalities can produce precise visualisations of the functions and structures of the brain at both a molecular and WB level. They have enabled the identification of neural networks that are involved in cognitive processes (Kasliwal, 2013). These functions are generally related to the performance of a particular behavioural or cognitive task. Analyses can produce inferences between brain processes and the location of brain activity (Hirsch et al., 2018).

2.1 Physics of Magnetic Resonance Imaging

Magnetic Resonance Imaging (MRI) is a non-invasive imaging technique that uses magnetic fields and low-energy radiofrequency signals to create topographic images of the body. Images are produced with contrast that relates to the magnetic properties and the molecular interactions of the investigated tissues, and are well-suited to the differentiation between soft tissue structures.

The main components of the magnetic resonance (MR) scanner are the superconducting magnet, gradient coils and radiofrequency (RF) coils. MRI machines are based on the principle that an electric current flowing through a wire will induce a magnetic field around that wire. To achieve negligible electric resistance, the conducting metal is extensively cooled to a superconducting state, thereby, enabling high-strength electric currents to produce high-strength magnetic fields. The primary magnet coils are comprised of a superconducting metal-alloy and are used to generate a strong, static magnetic field, B_0. For clinical applications, the strength of B_0 is usually 1.5T or 3T and is directed along the positive z-axis. The positive z-axis is denoted as the direction along the inferior-superior orientation of patient within the bore of the scanner. MR machines use three sets of orthogonal gradient coils: the x-, y-, and z-gradients. A secondary magnetic field is produced when an electric current is applied through these coils, causing the B_0 field to become spatially modulated in a predictable way. Thus, the main function of the gradient coil is to allow spatial encoding of the MR signal. The RF coils transmit and receive signals. The transmit coils generate an electromagnetic field perpendicular to the main magnetic field and the receiver coils are used to detect the produced MR signal.

MRI works by measuring the electromagnetic energy absorbed and released by protons in the body. Water (H_2O) and fat ($CH_2(OCOR)$–$CH(OCOR')$–$CH_2(OCOR'')$) contain an abundance of hydrogen atoms. Hydrogen nuclei are composed of a single, positively charged proton. These subatomic particles that contain an odd number of protons or neutrons exhibit *spin*, which refers to its angular momentum, and induce a randomly oriented magnetic (dipole) moment. When an external static magnetic field, B_0, is applied, protons align in the direction that is parallel or anti-parallel to the direction of the external field. Less energy is required for protons to align parallel than antiparallel to B_0. Consequently, more protons will align in the direction of external field than against it, as seen in Figure 2.1.

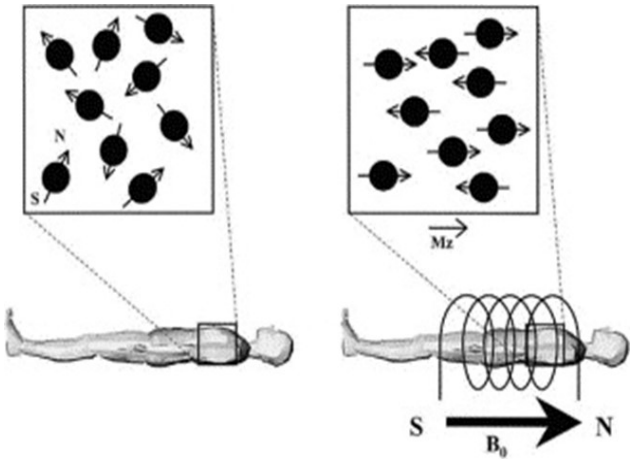

Figure 2.1: Protons will align parallel and anti-parallel to the direction of an external magnetic field (Geuns et al., 1999).

As individual nuclei are in constant motion, they do not precisely line up with the external field. Rather, they precess around the direction of the magnetic field. This precession can be described as a "wobbling" motion in which the nuclei rotate around the B_0 axis. The motion is often likened to that of a spinning gyroscope. The frequency at which nuclei precess is referred to as the Larmor frequency and is proportional to the field strength of the static magnetic field and the gyromagnetic ratio of the nucleus. The Larmor frequency (ω) is given by:

$$\omega = \gamma B_0 \tag{2.1.1}$$

where γ is the gyromagnetic ratio (42.6 MHz/T for hydrogen). The net magnetization vector, $\boldsymbol{M}_0$ is the resulting sum magnetic field of all individual nuclei and aligns parallel to the external magnetic field. This is also referred to as longitudinal magnetization.

M_0 cannot be measured in its static equilibrium state because it is in the same direction as B_0. To obtain a measurable signal, an RF pulse is applied to the tissue, thereby exciting the nuclei, and causing them to fall out of alignment with main magnetic field. This is achieved when the applied RF pulse has the same frequency as the precessing nuclei, the resonant frequency. Therefore, the RF pulse is applied at the Larmor frequency. Firstly, this allows some nuclei to absorb enough energy to transition to the higher energy state of being antiparallel to B_0. Secondly, nuclei begin moving in phase with one another. The result is non-zero transverse magnetization in which a new net magnetization vector is created, perpendicular to the main magnetic field. The transverse magnetization vector is an oscillating magnetic field.

When the RF pulse is terminated, nuclei will continue to precess but will gradually lose their phase coherence and return to their equilibrium state in which they again precess around B_0. The result is a decrease in transverse magnetization and an increase longitudinal magnetization, causing the induced signal within the RF coil to decrease over time. The reducing signal is referred to as free induction decay (FID). The process by which transverse magnetization decays is termed T2 relaxation. Small differences in the Larmor frequency of individual nuclei elicit energy exchange (spin-spin interactions) between the nuclei which brings about a decrease in phase coherence. The

net transverse magnetization is described according to:

$$\boldsymbol{M}_{xy} = \boldsymbol{M}_0 e^{\frac{-t}{\mathrm{T2}}} \tag{2.1.2}$$

where T2 relaxation time constant is the time taken for transverse magnetization to decay to 37% of its initial value. The length of T2 varies across tissues as its speed is determined by the nucleic spin-spin interactions. Additionally, inhomogeneity within B_0 causes nuclei to have different Larmor frequencies depending on their location within the magnetic field. This implies that they will no longer be spinning in sync. T2* relaxation is the term given to describe the combined effects of T2 relaxation and dephasing caused by inhomogeneities within the B_0 magnetic field.

The process of longitudinal magnetization recovery is referred to as T1 relaxation and requires a transfer of energy from nuclei. The nuclei emit their excess energy as they transition back to their previous orientation (low energy state). Notably, not all nuclei return to their original state at the same time as they need time to transfer their stored energy into the surrounding lattice tissue. Consequently, the longitudinal relaxation does not happen immediately but rather as a continuous process. Longitudinal relaxation recovers according to:

$$\boldsymbol{M}_z = \boldsymbol{M}_0(1 - e^{\frac{-t}{\mathrm{T1}}}) \tag{2.1.3}$$

where the T1 time constant is the time required for the longitudinal magnetization to recover from 0 to 63% of its equilibrium value. T1 does not only depend on the tissue properties, but also on the B_0 field strength of the scanner. T1 and T2 relaxation occur concurrently and independently. For biological tissues, T1 is generally 5 – 10 times slower than T2, and T1 increases with an increase in the applied B_0 field, whereas T2 remains nearly unchanged. The relaxation constants affect signal intensity, and consequently, the contrast of the MR image produced.

The FID undergoes dephasing that is caused by magnetic field gradients (discussed later). Therefore, it is not common practice to immediately measure the signal it generates. Instead, the signal is measured in the form of an 'echo'. The echo time (TE) is the time between the application of the RF pulse and the peak of the echo signal. The repetition time (TR) refers to the time between two consecutive RF pulses. The choice of TE and TR determines if the image contrast and brightness is predominantly weighted towards the T1 or T2 properties of the tissue.

To construct an MR image, the MR signal is localized using magnetic field gradients, namely: slice selection gradient, frequency encoding gradient ($\mathrm{G_F}$) and phase encoding gradient ($\mathrm{G_P}$). Slice selection aims to localize a tissue slice or slab to be excited by an RF pulse. This is accomplished through the generation of a linear magnetic gradient field perpendicular to the desired slice plane. This gradient field is superimposed on the main magnetic field, B_0. Thus, for a magnetic field gradient G·z that varies linearly in the z-direction, the total magnetic field at distance z has a value of B_0 + G·z. This implies that Larmor frequencies of the nuclei will vary along the z-axis. Therefore, to excite a particular slice, an RF pulse with a frequency bandwidth corresponding to the range of Larmor frequencies of the nuclei in that slice is applied. Different slices can be selected by altering the frequency of the RF pulse.

Frequency-encoding and phase-encoding gradients are applied to further localize regions within the selected slice. The G_F is used to differentiate the columns within the slice. By using a similar approach to slice-selection, the G_F is applied perpendicular to the slice-selection gradient, thereby introducing spatially dependent frequency along the excited slice. To subsequently localize slice regions in the third direction, the G_P is used to alter the phases of the nuclei. This is achieved by transiently turning on the G_P in the chosen direction for a short period of time between slice excitation and signal readout. When the gradient is switched off, the nuclei return to their precession frequency, determined by the G_F but will be out of phase. The phase-shift is determined by the position of the nuclei along the column.

K-space is the matrix in which the signal data is stored and represents the spatial frequency information of the scanned object. An MR image is formed by the application of a 2-dimensional (2D) Fourier Transform on the k-space data.

2.2 The BOLD Signal

FMRI signal is dependent on the measurement of T2* relaxation, which is sensitive to local changes in blood oxygenation (Ogawa et al., 1990). Blood oxygenation is affected by neural activity and neurovascular coupling. The fMRI Blood Oxygenation Level Dependent (BOLD) signal provides an indirect measure of neural activity by detecting the local changes in CBF, and concomitantly blood oxygenation, associated with brain activity. Neural activity requires energy in the form of adenosine triphosphate (ATP). Once a brain region becomes active, there is an increase in the local energy requirement. This elicits an increase in oxygen consumption to form more ATP (Glover, 2011; Harris, Reynell and Attwell, 2011). The consumption of oxygen leads to a localized increase in concentration of deoxyhemoglobin. This is shortly followed by an increase in local blood flow as blood vessels dilate to overcompensate for the requirement of additional oxygen and glucose (Hillman, 2014; Simon and Buxton, 2015; Gauthier and Fan, 2019). It is not fully understood why more oxygen is delivered than is required. The subsequent increase in blood flow leads to an increase in oxyhemoglobin concentration.

Oxygenated hemoglobin (HbO_2) deoxygenated hemoglobin (dHb) have different magnetic properties. The concentration of HbO_2 relative to dHb is the basis of the BOLD signal as BOLD contrast is formed by the change in the magnetic field that surrounds red blood cells. Because dHb is paramagnetic, an increase in its concentration causes local dephasing of hydrogen nuclei in water molecules, and thus a decrease in signal on T2*- weighted images, whereas a relative increase in HbO_2 as a result of neural activation causes increased signal, known as the BOLD response.

The mathematical transfer function that models the changes in BOLD signal intensity over time is referred to as the hemodynamic response function (HRF). A graph of the HRF is shown is Figure 2.2. It is seen that at the onset of neuronal activation, there is a greater metabolic demand for oxygen. This leads to a decrease in local oxygen in the blood, which causes the hemoglobin to become paramagnetic. Consequently, the distortions in the magnetic field result in a decrease T2*-weighted signal, as depicted by the initial dip. The increase in metabolic demand is followed by a surplus inflow of oxygenated blood to active brain regions, thereby decreasing the concentration of dHb and increasing signal intensity. This is illustrated by the peak in the BOLD response approximately 3–6 seconds after neuronal activation. After reaching its peak, the signal decreases

to an amplitude below baseline value before returning to baseline. This post stimulus undershoot is mainly due to the sustained increase in the cerebral metabolic rate of oxygen, along with reduced CBF and delayed vascular compliance (Zijl, Hua and Lu, 2012; Siero, Bhogal and Jansma, 2013).

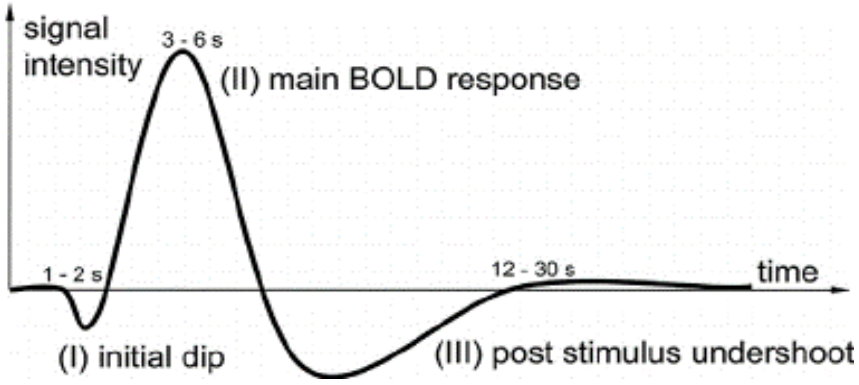

Figure 2.2: BOLD hemodynamic response function (Bhogal and Jansma, 2013).

FMRI data are collected over the whole brain by acquiring sequential volumes for each time point to create a time series. Spatial resolution, TE and the imaging acquisition methods are important scan parameters to consider to enhance BOLD specificity (Siero, Bhogal and Jansma, 2013). An echo planar imaging (EPI) sequence is commonly used for fMRI studies because of its speed of acquisition and sensitivity to T2- and T2*-imaging (Poustchi-Amin et al., 2001). EPI can be implemented using gradient echo (GRE), or spin echo (SE) sequences. However, for fMRI studies it is conventional to use GRE acquisition methods due to its higher BOLD contrast sensitivity (Siero, Bhogal and Jansma, 2013; Chiacchiaretta and Ferretti, 2015; Soares et al., 2016). GRE imaging uses a single RF pulse along with a bipolar readout gradient to produce a net gradient of zero at TE (Markl and Leupold, 2012) and a resulting gradient echo.

2.3 Temporal Resolution

The temporal resolution of fMRI is dependent on TR, which is usually 2-4 seconds (Constable and Spencer, 2001). This would be too slow to capture neuronal activity, but the BOLD response that is analysed when studying neural activity, peaks at 6-8 seconds after the stimulus (Lindquist and Wager, 2014). Therefore the temporal resolution is limited by the speed of the haemodynamic response. (Kim, Richter and Ugurbil, 1997; Glover, 2011; Lindquist and Wager, 2014) . While short TRs increase statistical power, longer TRs enhance the signal-to-noise ratio (SNR) of the images and allow more slices or higher resolution slices to be acquired but are inherently associated with increased motion sensitivity (Glover, 2011; Wald, 2012; Soares et al., 2016). Therefore there is a complicated trade-off between temporal and spatial resolution of fMRI. Parallel imaging and simultaneous multi-slice excitation are developments that allow increased temporal/spatial resolution to be attained.

2.4 Artifacts

BOLD signal fluctuations may be caused by non-neuronal activity. These artifactual signal variations predominantly arise from physiological noise, gradient system hardware and head motion, with the

effects of head motion representing one of the greatest confounds in fMRI data (Diedrichsen and Shadmehr, 2005; Lindquist and Wager, 2014; Soares et al., 2016; Maknojia et al., 2019; Fair et al., 2020). Head movements in the scanner cause alterations in the position of the brain in space, which interferes with the establishment of the required precise magnetic field gradients and the ensuing BOLD signal measurement (Power et al., 2012a). Studies have found that even sub-millimeter head movements introduce distortions in functional connectivity estimates (Power et al., 2012b; Satterthwaite et al., 2013).

2.5 Types of Functional Magnetic Resonance Imaging

FMRI can identify and delineate the change in activation of brain regions in response to experimental stimuli. Activation maps can be generated showing the BOLD signal response of different regions of the brain when completing a specific task or in reaction to a stimulus (Rogers et al., 2007). As fMRI formulation is based on the principle of the BOLD signal, it is associated with capturing the physiological changes in the brain (Hirsch et al., 2018). FMRI experiments may be one of two types: task-based or resting-state studies.

2.5.1 Task-based Functional Magnetic Resonance Imaging

Task-based fMRI studies are used to map regions of the brain that are functionally activated when subjects are instructed to perform a specific behavioural task (Chen and Glover, 2015; Zhang et al., 2018) that is intended to modulate the behaviour under investigation. Task-based fMRI is widely used in clinical and presurgical applications to assist with the planning of neurosurgical procedures (Asbury and Detre, 2019; Lemée et al).

2.5.2 Resting-state Functional Magnetic Resonance Imaging

Resting-state fMRI (rs-fMRI) data is acquired in the absence of a stimulus or task. Patients are simply instructed to rest. It can be argued that rs-fMRI is advantageous over other fMRI techniques as it is easily acquired. The lack of a task requires the least effort from patients, which makes it appropriate for patients who may have difficulty co-operating with task instructions, such as paediatric patients, individuals with neurological or psychiatric conditions, or paralyzed and comatose patients. Therefore, this technique reduces between-subject variability that may result from task-performance, in addition to improving patients' compliance (Smitha et al., 2017; Cieri, 2018; Lv et al., 2018; Connor and Zeffiro, 2019).

Resting-state Functional Connectivity Analysis Techniques

FC uses linear temporal correlation between the parameters of neuronal activity to find the connection between two different spatial regions (Smitha et al., 2017). The techniques that assess the connectivity and the relationships between different brain regions are referred to as functional integration methods. Computational methods that are used for evaluating resting-state FC (RSFC) include: seed-based correlation analysis (SCA), independent component analysis (ICA), and graph theory (Meszlényi et al., 2017; Smitha et al., 2017; Lv et al. 2018).

SCA uses a region of interest (ROI) or "seed" and discovers linear correlations between the ROI with other voxels in the brain. Synchronous activation between different brain regions suggests that

they may be involved in the same functional process and are therefore considered to be functionally connected. Iteratively calculating the linear correlation between the ROI time series and selected voxels will yield a seed-based FC map (Meszlényi et al., 2017; Smitha et al., 2017), which provides a clear visual display of voxels that are functionally correlated with the seed region. This allows for straightforward examination of FC within the brain. Seeds are required to be selected prior to the analysis, thus are based on hypotheses and previous findings. In addition, to determine the strength of the correlation between the ROI and the identified voxels, a threshold is employed for statistical significance (Rogers et al., 2007; Lee, Smyser and Shimony, 2014; Lv et al., 2018). The simplicity and interpretability of SCA makes it an advantageous technique for assessing RSFC (van den Heuvel and Hulshoff Pol, 2010; Smitha et al., 2017).

ICA (Comon, 1994; Mckeown et al., 1998) uses multivariate decomposition to separate a two-dimensional data matrix into several spatial and temporal components. Each functional component has an independent network of neurons with synchronised BOLD signal (Lv et al., 2018). ICA is a data-driven analysis technique which utilises a blind source separation algorithm (Mckeown et al., 1998). As opposed to SCA, ICA can be performed without prior knowledge or assumptions. While SCA only identifies single regions functionally connected to the seed, ICA extracts all detectable correlations between distinct brain networks (Smitha et al., 2017; Lv et al., 2018). A drawback of ICA is that the observed BOLD synchrony between functional networks may be non-neuronal, i.e., signal was derived from breathing or cardiac pulsation. Additionally, results may be divided into numerous subnetworks depending on the chosen number of components (Lv et al., 2018).

Graph theory analysis uses mathematical models or "graphs" to represent brain networks (Wang, Zuo and He, 2010; Medaglia, 2017). These networks are defined by a graph, G, as a function of nodes, N, and edges, E, and is shown by the model $G = f(N, E)$. Nodes represent the ROIs and edges describe the interaction between these ROIs. An edge is calculated by the correlation between the time-series data of 2 nodes (Lv et al., 2018). In comparison to SCA, graph theory is performed without prior assumptions and can determine the topological properties of an ROI within the whole brain (Smitha et al., 2017). However, results are often not intuitive, which make it difficult to interpret (Lv et al., 2018).

3. Neuroanatomy of the Basal Ganglia

The BG consist of sub-cortical nuclei situated deep within the cerebral hemispheres. They are involved in motor control, motor learning, executive functioning, behaviour control and emotional processing (Fazl and Fleisher, 2018; Florio et al., 2018; Yin, 2019). Based on their functional connections, these nuclei, Figure 3.1, can be classified as input, output, or intrinsic nuclei. The input nuclei primarily receive afferent information from cortical regions, thalamic nuclei and the brain stem (Lanciego, Luquin and Obeso, 2014). The caudate, putamen and nucleus accumbens are collectively referred to as the striatum and form the BG input nuclei. The output nuclei consist of the internal segment of the globus pallidus (GPi) and the substantia nigra pars reticulata (SNr). They send information from the BG to regions of the diencephalon and brain stem, which then project this information to regions of the frontal cortex (Martin, 2003). The external segment of the globus pallidus (GPe), subthalamic nucleus and substantia nigra pars compacta comprise the intrinsic nuclei and relay information between the input and output nuclei.

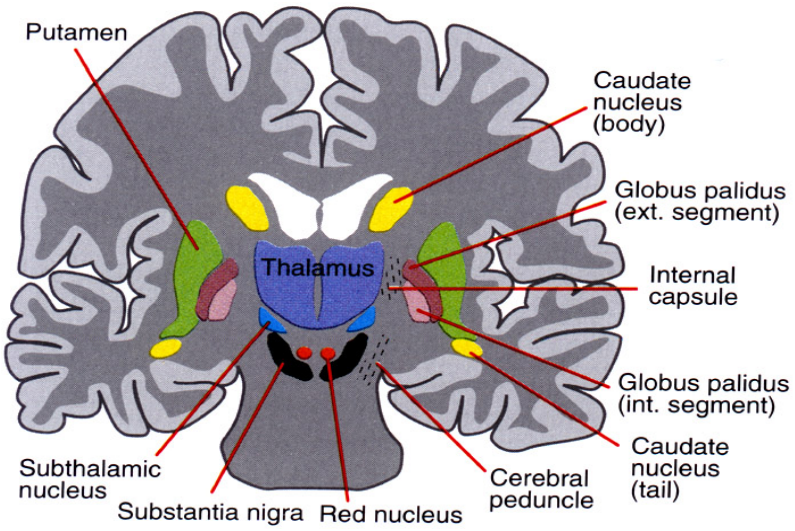

Figure 3.1: Nulcei of the Basal Ganglia (Leisman and Melillo, 2013).

The output nuclei innervate the thalamus, pedunculopontine nucleus (PPN) and superior colliculus. BG inneverations are shown in Figure 3.2. Through their thalamic innervation, the BG play a role in motor, sensory and cognitive information processing (Middleton and Strick, 2000). Through their PPN innervation, they affect limb and posture control during locomotion (Martin, 2003). Finally, via their superior colliculus innervation, the BG nuclei implicate saccadic eye movements (Hikosaka, Takikawa and Kawagoe, 2000). Evidently, operating with the frontal cortex, the BG function to achieve goal-directed behaviours.

Functional BG circuits have been proposed because of the main BG-thalamocortical projections. These have been classified as: the motor circuit, executive/association circuit, and the limbic circuit (Alexander, DeLong and Strick, 1986), as seen in Figure 3.3. The general organization of each circuit is as follows:

i. Each circuit receives inputs from multiple cortical regions.

ii. Inputs are projected from varying regions of the striatum to BG output nuclei, and then to thalamic nuclei.

iii. Projections terminate in the target frontal cortex region.

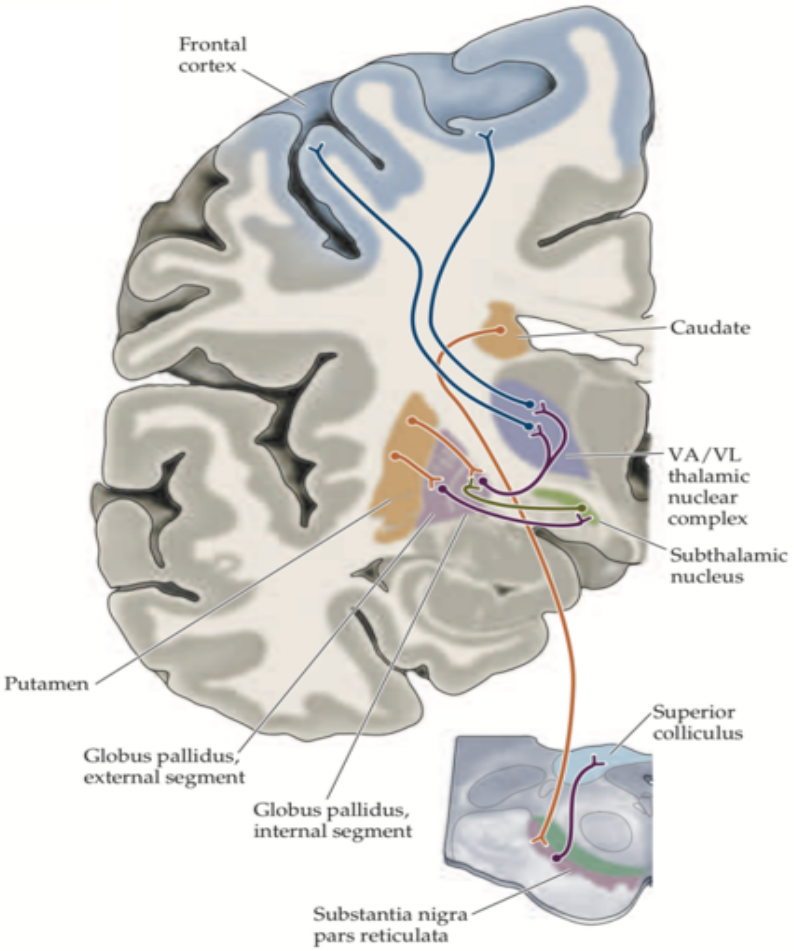

Figure 3.2: Innervations of the Basal Ganglia nuclei (van Kan, 2022).

3.1 Corticostriatal Projections

3.1.1 Motor Network

The BG motor circuit is primarily centred around the putamen and its connections. The postcommissural region of the putamen receives topographic projections from the primary motor, pre-motor, supplementary motor, and cingulate motor areas of the cortex (Künzle, 1975; Haber, Lynd-Balta and Spooren, 1994). Additionally, this region receives projections from parietal areas that are associated with somatosensory functions, resulting in a region that is somatotopically organized.

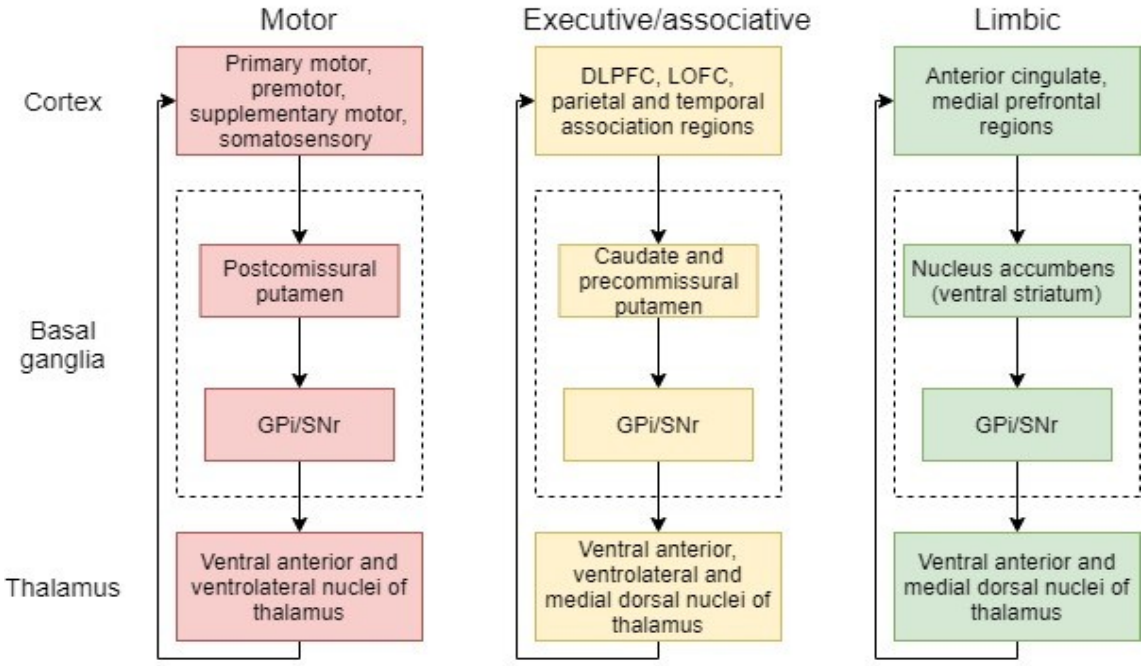

Figure 3.3: Basal ganglia-thalamo-cortical projection circuits.

A fundamental responsibility of the motor cortex is to control voluntary movement. BG connectivity to primary/supplementary motor cortex is of interest because of the BG's involvement in motor control (Middleton and Strick, 2000; Obeso et al., 2002; Lanciego, Luquin and Obeso, 2014).

3.1.2 Language Network

Several studies have found evidence that the BG support language processing (Booth et al., 2007; Ford et al., 2013; Copland, 2014). Results show that the putamen, specifically, has connections to the inferior frontal gyrus (IFG) (Booth et al., 2007; Ford et al., 2013). The pars opercularis and pars triangularis of the left posterior IFG, commonly referred to as Broca's area, are associated with language production and comprehension (Ferpozzi et al., 2018).

3.1.3 Executive Network

The DLPFC, lateral orbital frontal cortex (LOFC), and associative areas of the parietal and temporal cortices project to the caudate and precommissural region of the putamen (Alexander, DeLong and Strick, 1986; Haber, 2003). While, the DLPFC is associated with working memory and executive functions, the LOFC plays a role in decision making.

Executive functioning describes the higher-order cognitive control processes required to plan and achieve goals. It has been found to play an integral role in child development areas such as: social cognition and behaviour and emotional control (Anderson, 2002; Moriguchi, 2014; Lohndorf et al., 2019). It has further been reported that executive function develops rapidly during early childhood years and reaches adult-level performance by mid-adolescence (Anderson, 2002; Zelazo et al., 2003).

3.1.4 Limbic Network

The limbic system, comprising the amygdala, cingulate gyrus and hippocampal formation, project to the ventral striatum (Afsharpour, 1985).

3.2 Striato-pallidal Projections

Neurons travelling from the striatum to the globus pallidus (GP) are inhibitory GABAergic. They create "direct" and "indirect" pathways through their projections (not discussed here) and determine whether the output of the BG is excitation or inhibition (Haber, 2003; Obeso et al., 2008). Further, these projections are topographically organized (Haber et al., 1990). The sensorimotor areas of the striatum project to the ventrolateral GP and ventrolateral SNr, the dorsal striatum projects centrally to the GP and SNr; and the ventral striatum sends projections to the ventral GP and midbrain (Haber, 2003).

3.3 Thalamocortical Projections

The pallidal complex and SNr project to the ventral anterior, ventral lateral and medial dorsal nuclei of the thalamus. These projections are relayed back to the frontal cortex from the respective thalamus nuclei, thereby completing the BG-thalamocortical circuit. These projections remain functionally and topographically organized (Haber et al., 1990; Mcfarland and Haber, 2002; Haber, 2003) .

The motor, language and executive functions are relevant to child development. It is therefore of interest to investigate the BG networks which support these functions.

4. Methodology

4.1 Study Cohort

Participants of this study include CPHIV from the CHER trial, which was a randomised trial conducted from 2005 to 2011 by the Comprehensive International Program for Research in AIDS (Acquired Immuno-deficiency Syndrome) (Violari et al., 2008). The initial study trial took place at two centers in South Africa, namely: the Children's Infectious Diseases Clinical Research Unit at Tygerberg Children's Hospital, in Cape Town and the Perinatal HIV Research Unit at Chris Hani Baragwanath Hospital, in Soweto. The CHER trial enrolled infants aged 6–12 weeks who were diagnosed with HIV-infection and who had a CD4[i] percentage (CD4%) of at least 25%. HIV-infection was confirmed by a positive HIV DNA polymerase-chain-reaction (PCR) test and a plasma viral load (PVL) $>$ 1000 copies per millilitre. The infants were randomly assigned to one of the following treatment regimens: early limited ART, initiated before 12 weeks of age, and interrupted at 40 weeks (ART-40W); early limited ART, initiated before 12 weeks of age, and interrupted at 96 weeks (ART-96W); or had ART deferred (ART-def) until CD4% $<$ 25% in the first year, or below 20% thereafter. ART was restarted for children in the ART-40W or ART-96W treatment group if there was a decline in the CD4% or clinical symptoms of disease were observed (Violari et al., 2008; Mark F. Cotton et al., 2013). First-line of ART regimen comprised Zidovudine (ZDV), Lamivudine (3TC) and Lopinavir-Ritonavir (LPV/r, Kaletra) (Violari et al., 2008; Cotton et al., 2013).

Participants from the Cape Town community, as well as HIV-uninfected age-matched and socio-economic-matched controls, were enrolled into a follow-up neuroimaging and neurocognitive study to investigate the long-term effects of HIV on neurodevelopment. The current study includes children living in Cape Town who were enrolled into the follow-up study. Neuroimaging data, including rs-fMRI data were obtained from this subset at ages 7, 9 and 11 years old, which enabled a longitudinal study to be conducted.

4.2 MRI Acquisition

At age 7 and 9 years, neuroimaging was performed on a 3T Siemens Allegra MRI scanner (Siemens, Erlangen, Germany) located at the Cape Universities Brain Imaging Centre (CUBIC) in Tygerberg, South Africa using a single-channel head coil. At 9 and 11 years, children were scanned on a 3T Siemens Skyra MRI scanner using a 32-channel head coil. This scanner is located at the Cape Universities Body Imaging Centre (CUBIC) in Cape Town, South Africa. Neuroimaging was performed without sedation and in accordance with protocols approved by the Faculty of Health Sciences Research Ethics Committees of the University of Cape Town and the University of Stellenbosch. All parents or guardians provided written consent, in addition to the oral assent provided by the children.

[i]CD4 cells are a type of white blood cell that play a role in fighting infection by triggering the immune system (Tests, 2022). A CD4 cell count is the measure of the amount of CD4 cells in a cubic milliliter of blood. A higher CD4 cell count indicates a stronger immune system. Without treatment, HIV infects and destroys CD4 cells. A normal CD4 cell count ranges between 500 to 1500 cells per cubic millimeter of blood. A person with HIV with a CD4 cell count less than 200 (equivalent to a CD4% of 12-15%) is diagnosed with AIDS and is at risk of developing serious infections (HIV i-Base, 2022).

Scans Collected on the 3T Allegra MRI Scanner
T1-weighted structural images were acquired in the sagittal plane using a multi-echo magnetization prepared rapid gradient echo (MEMPRAGE) sequence (van der Kouwe et al., 2008) with a field of view (FoV) of 224mm × 224mm × 144mm, TR = 2530 ms, TE's = 1.53, 3.19, 4.86, 6.53 ms, TI = 1160 ms, flip angle = 7° and voxel size of 1.3 × 1.0 × 1.0mm^3, where TI is the inversion time. Rs-fMRI data were acquired using a 2D EPI sequence with FoV = 220mm × 220mm, TR = 2000ms, TE = 30ms, flip angle = 77° , voxel size = 3.44 × 3.44, slice thickness = 4mm, 1mm gap, 33 interleaved slices, and 180 volumes (6 minutes).

Scans Collected on the 3T Skyra MRI Scanner
T1-weighted structural images were acquired in the sagittal plane using a multi-echo magnetization prepared rapid gradient echo (MEMPRAGE) sequence (van der Kouwe et al., 2008) with a FoV of 224mm × 224mm × 176mm, TR = 2530ms, TE's = 1.69, 3.54, 5.39, 7.24ms, TI = 1100 ms, flip angle = 7° and voxel size of 1.0 × 1.0 × 1.0mm^3. RS-fMRI data was acquired using a 2D EPI sequence with FoV = 250mm × 250mm, TR = 2000ms, TE = 30ms, flip angle = 90° , voxel size = 2.98 × 2.98, slice thickness = 4mm, 1mm gap, 33 interleaved slices, and 180 volumes (6 minutes).

4.3 Rs-fMRI Preprocessing

First, structural and resting-state images were converted from the initial DICOM format to NIfTI format. All resting-state images were resampled to a voxel size of 3mm^3. Preprocessing was conducted using the afni_proc.py script in the AFNI (Analysis of Functional NeuroImages) software package, version 21.1.01 (Cox J.S., 1996). An overview of the preprocessing pipeline is presented in Section 4.3.1

4.3.1 Preprocessing Pipeline

A diagram of the afni_proc.py pipeline is depicted in Figure 4.1 and the pipeline code can be found in Appendix A.

First, motion was evaluated to identify a segment within each EPI series, that contained low motion. 3-dimensional (3D) motion is characterized by six degrees of freedom (DOF) and is described as a combination of translations and rotations. Motion correction calculates the spatial deviation in these 6 DOF between the reference EPI volume (in AFNI by default the 3rd volume) and all other EPI volumes. The motion parameters obtained from this first-pass motion correction were assessed for each subject in the dataset using an in-house python script. Subjects were required to have at least 134 consecutive volumes within their time series with motion not exceeding 3mm in translation or 3° in rotation from the reference volume. If these criteria were initially not met using the default reference volume, the reference volume was changed to a later volume in the time series to check whether this provided a better reference point to compare subsequent volumes against. This was usually the case when a motion event occurred early within the EPI series. The raw data of all the motion-evaluated EPI series that met the motion criteria were then trimmed to the selected 134 volumes.

The initial four volumes of the EPI data were removed for signal stabilization. This accounted for the time taken for the hydrogen nuclei to align with the magnetic field and reach steady-state (Park, Byeon and Park, 2019). Transient 'spikes' in the remaining time series were removed by

interpolation. Since it takes time to acquire each 2D slice in a series, individual slices within a 3D volume are recorded at different times. Consequently, there is an accumulation in time delays between the first slice and those acquired thereafter (Parker and Razlighi, 2019). Slice-timing alignment was performed to correct the time series of each slice by ensuring that individual slices were aligned to the same temporal reference (Sladky et al., 2011; Parker and Razlighi, 2019).

Motion correction was achieved by using rigid body volume registration. To spatially align the data to a standard space, linear affine transformation matrices were computed between EPI and anatomical volumes. Non-linear transforms were then calculated between the anatomical volumes and Haskins Pediatric template (Molfese et al., 2021). The choice of atlas was motivated by the age of the participants. All three transforms were simultaneously applied to warp the EPI data to Haskins Pediatric space. The data were spatially smoothed using a 6mm Full Width at Half Maximum (FWHM) Gaussian kernel to increase SNR. The anatomical data was segmented into three brain tissue masks: for WM, GM, and CSF. To correct for non-neuronal signal confounds, mean WM and CSF signals, along with motion parameter estimates and their derivatives, were regressed out of the time-series data.

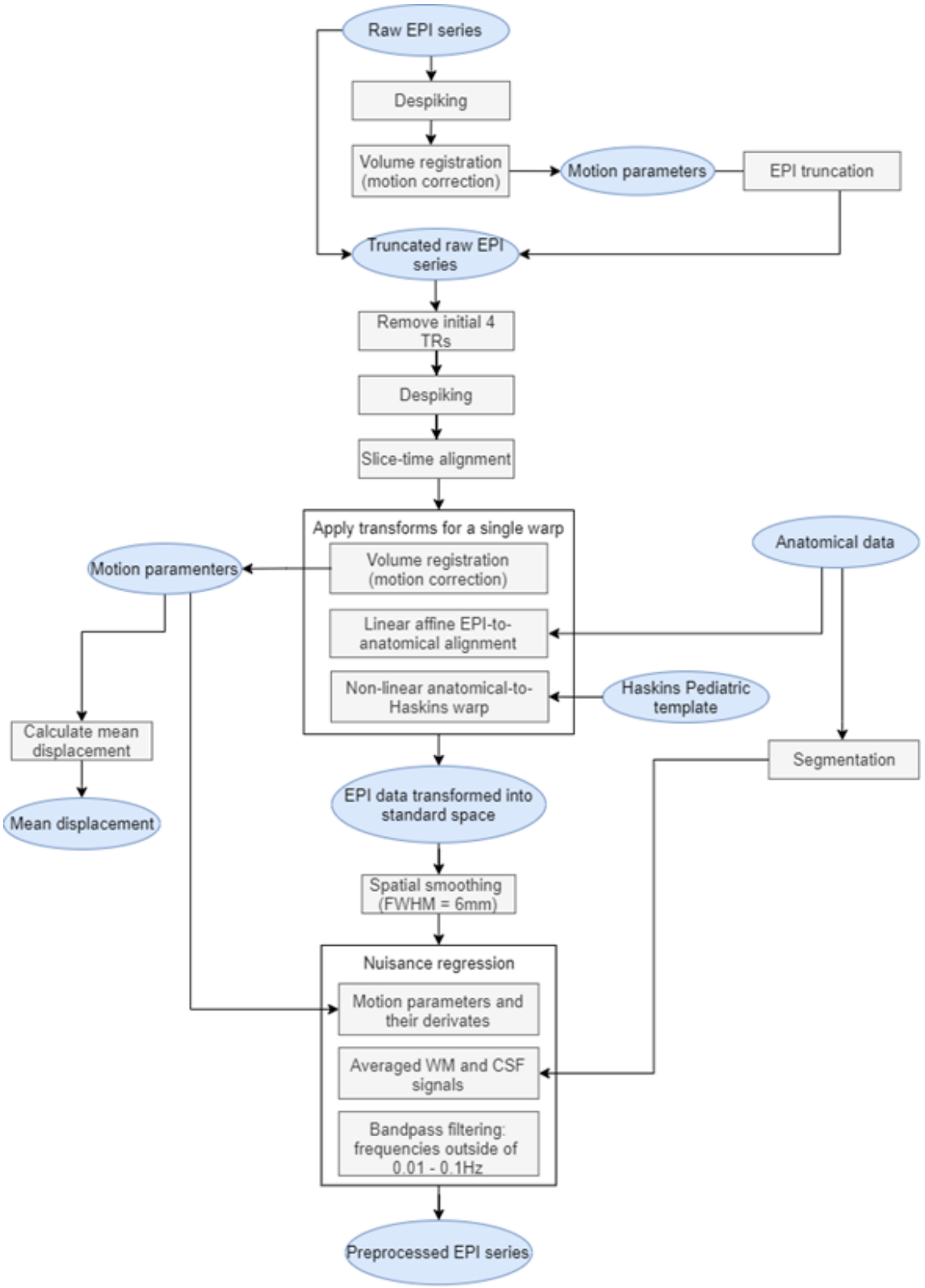

Figure 4.1: Pipeline for preprocessing rs-fMRI data.

4.4 Exclusion Criteria

Subjects were excluded from further analyses if they did not have at least 130 consecutive volumes within their time series that complied with the motion threshold criteria. Any subject with artifacts on their resting-state or anatomical datasets was excluded. Subjects were excluded if on visual inspection their data were poorly aligned to the Haskins Pediatric template. Additionally, any subject who had anatomical abnormalities was not included in the study.

4.5 Seed-based Correlation Analysis

To investigate the role of the BG in executive function, motor function and language networks, FC between the BG seeds and frontal cortex regions of interested were examined. Regions were selected from known cortico-BG networks.

4.5.1 Basal Ganglia Seeds

The primary aim of this dissertation involved assessing the development of FC between the BG and frontal cortex. Therefore, anatomical regions of the BG were chosen as seeds for SCA. Eight seeds were selected based on the functional anatomy of BG, Section 3.1, and previous findings of HIV-induced BG atrophy. BG seed masks, as seen in Figure 4.2, were extracted from the Haskins Pediatric atlas (Molfese and Glen, 2014) for the following regions: left and right putamen, left and right caudate, left and right globus pallidus, and left and right thalamus. Although the thalamus does not form part of the BG, it does play a significant role in the BG FC circuits as observed by the thalamo-cortical and thalamo-striatal projections found in animals (Cheatwood, Reep and Corwin, 2003; Cheatwood, Corwin and Reep, 2005; Kamishina et al., 2008). Individual masks were created by thresholding the Haskins Pediatric atlas to isolate the ROI, and then binarizing the outcome and resampling to match the orientation and voxel size of the preprocessed resting-state data. For each seed, WB SCA was performed by computing the average BOLD time series within the seed region and cross correlating the result with every voxel within the brain. This yielded subject-specific correlation maps for each seed. The Pearson correlation coefficients were Fisher Z-transformed to improve the normality of the sample distribution.

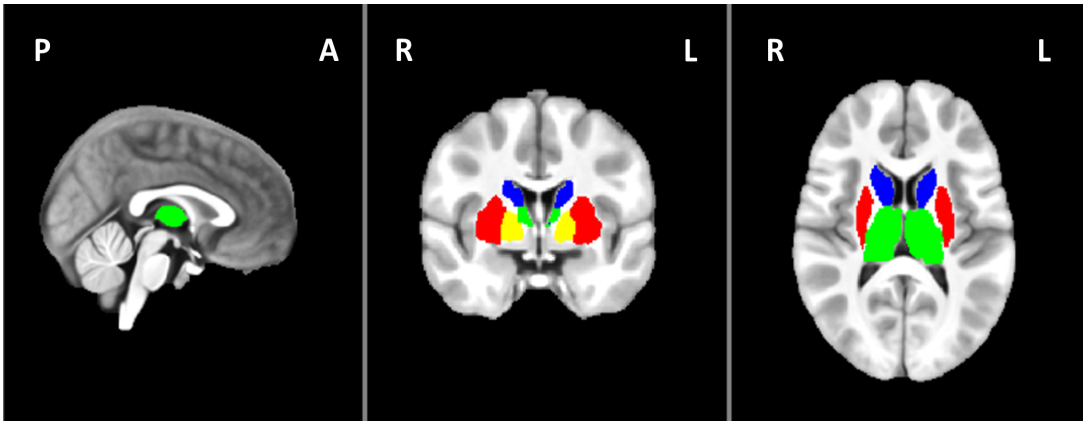

Figure 4.2: Basal ganglia regions of interest (ROIs) – left and right putamen (red), left and right caudate (blue), left and right globus pallidus (yellow), and left and right thalamus (green).

4.5.2 Frontal Cortex Regions of Interest

Frontal cortex regions of interest were defined using the Craddock atlas, which is which is a functional parcellation based on WB fMRI data (Craddock et al., 2012). These ROIs were warped from MNI space to Haskins Pediatric space via non-linear registration. The warped Craddock atlas overlaying the Haskins Pediatric template is shown in Figure 4.3.

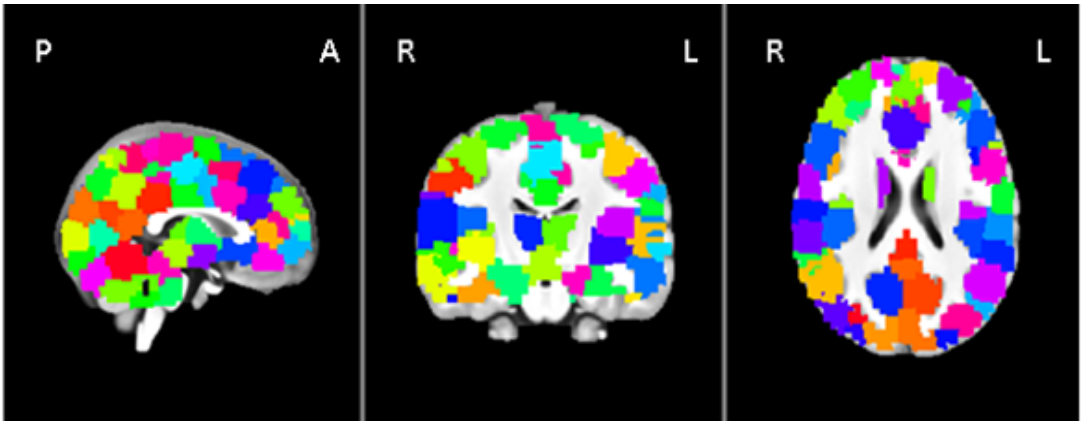

Figure 4.3: Warped Craddock atlas overlaid on the Haskins Paediatric template.

Functional ROIs were selected based on their spatial consistency with the DLPFC, motor cortices and left and right posterior IFG; known to be anatomically connected to the BG and involved in executive function, motor function and language and executive function, respectively.

To select frontal ROIs from the Craddock atlas, a python script, developed by Craddock (Craddock et al., 2012), was used to identify the spatial overlap of the Craddock functional regions with anatomically-defined atlas regions. The output of the script was a spreadsheet containing the numbered list of Craddock regions, the names of brain regions that they overlap in other atlases, and the percentage of overlap. Craddock regions were chosen as DLPFC ROIs if they overlapped Brodmann Area (BA) 9 or BA46, corresponding to the DLPFC. Two regions: Craddock regions 167 and 193 (Figure 4.4a) were found to overlap with BA9. Craddock region 111 (Figure 4.4b) was chosen as a motor ROI because it overlapped with both BA4 and BA6, representing primary motor cortex and premotor cortex respectively. BA44 and BA45 correspond to the posterior IFG. Craddock region 34 (Figure 4.4c) was chosen as left posterior IFG ROIs because it overlaps with BA44 , and Craddock region 164 was chosen as the right IFG ROI because it overlaps with BA44 and BA45. Table 4.1 provides a list of the five frontal cortex ROIs, the BAs and regions of the Haskins Pediatric atlas that they overlap. Hereafter, Craddock regions 167 and 193, Craddock region 111, and Craddock regions 34 and 164 are referred to as the left and right DLPFC regions, motor region, language region and right IFG region, respectively.

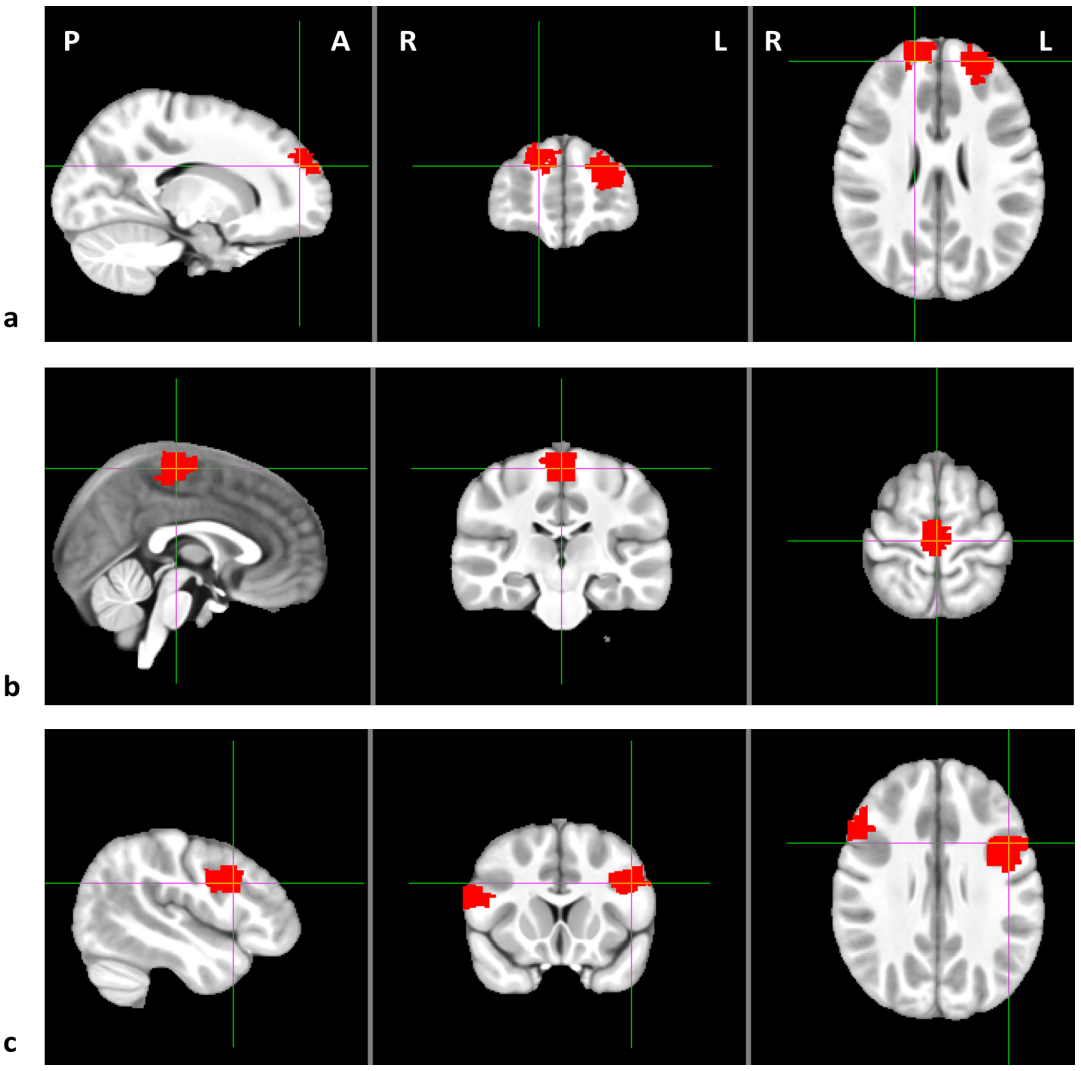

Figure 4.4: Craddock regions chosen as frontal cortex ROIs, overlaid on the Haskins Pediatric template. ROIs (red) are depicted here after they were warped to Haskins Pediatric space. a) Craddock regions 167 (anatomical left) and 193 (anatomical right). b) Craddock region 111. c) Craddock regions 34 (anatomical left) and 164 (anatomical right).

4.5.3 Functional Connectivity Extraction

For each of the 8 BG seed FC maps, the average Z-score was extracted in each frontal ROI. Therefore, for every subject, each of the 5 frontal ROIs had 8 different average Z-scores, corresponding to the 8 BG seeds.This meant that 40 variables were extracted for longitudinal analysis. The Z-score FC measures were modelled as dependent variables during the statistical analysis.

Table 4.1: Summary of the frontal cortex regions of interest and the corresponding frontal ROIs.

Functional Network	**Reference Name**	**Craddock Region**	**Volume Overlap of BA**	**Haskins Pediatric Region**
Executive	Left DLPFC region	167	21% BA9	Left rostral middle frontal gyrus (sub-region of DLPFC)
	Right DLPFC region	193	24% BA9	Right rostral middle frontal gyrus (sub-region of DLPFC)
Motor	Motor region	111	21% BA4 and 54% BA6	Paracentral lobule (region within motor corext)
Language	Language region	34	66% BA44	Left pars opercularis
Executive	Right IFG region	164	34% BA44 and 53% BA45	Right pars opercularis and pars triangularis

4.6 Statistical Analysis

4.6.1 Longitudinal Data Analysis

Longitudinal data refers to measurements of the same response variable collected at different occasions or points in time. In this study, the "response variable" is the FC measure and the "occasion" was the age at scan. Since the data contain repeated measurements from the same subjects, they are not independent observations as there is an inherent dependence between measurements recorded from the same subject.

Linear mixed-effect (LME) models can be used to describe and characterise the change of the response variable as a function of time. The underlying assumption is that individual subjects have their own subject-specific mean response profiles, which describe the unique change in their data over time. Consequently, LME is used to model the average response as a combination of covariates that are common to all subjects within the sample, together with subject-specific effects that are unique to individual subjects (Fitzmaurice and Ravichandran, 2008). The effects that are common to all subjects are referred to as "fixed effects", while those that are unique to particular subjects are called "random effects". Including subject-specific random effects accounts for within-subject variability within the dataset. Therefore, using LME models with fixed and random effects is a suitable approach for analysing longitudinal data that contain dependent repeated measures (Pinheiro and Bates, 2000).

Formulation of Linear Mixed Effect Model

A simple mixed effect model formulation is described as follows (Pinheiro and Bates, 2000):

$$y_{ij} = \beta + b_i + \epsilon_{ij} \tag{4.6.1}$$

where:

y_{ij} is the observed response for subject i at time j,

β is the overall mean over all the subjects and all occasions,

b_i is the subject-specific error, measuring between-subject variability and $b_i \sim \mathcal{N}(0, \sigma_b^2)$,

ϵ_{ij} is the random error, measuring within-subject variability and $\epsilon_{ij} \sim \mathcal{N}(0, \sigma_e^2)$,

and b_i and ϵ_{ij} are assumed to be independent.

The model presents a mean response with subject-specific deviations from the overall mean, along with occasion-specific deviations from subject-specific means. This is illustrated in Figure 4.5.

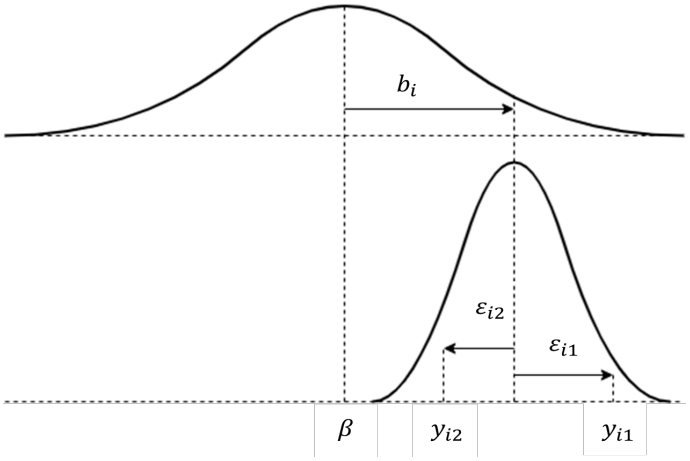

Figure 4.5: Concept of mixed effect modelling showing the distribution of error components for a single subject.

Generalised Mixed Effect Model

The generalised formula for an LME model is represented as:

$$y_i = X_i\beta + Z_i b_i + \epsilon_i \tag{4.6.2}$$

where:

$i = 1, ..., N$ subjects,

y_i is the response vector of length n_i for subject i,

X_i is a $n_i \times q$ design matrix for q fixed effect,

β is a $q \times 1$ vector of regression coefficients,

Z_i is an $n_i \times k$ design matrix for k random effects,

b_i is a $k \times 1$ vector subject-specific random effects and $b_i \sim \mathcal{N}(0, \sigma_b^2)$,

ϵ_i is an $n_i \times 1$ vector of sampling errors with $\epsilon_i \sim \mathcal{N}(0, \sigma_e^2)$.

4.6.2 Model Selection

Model selection criteria are used to identify the optimum model for the analysis of data by assessing the balance between model simplicity and goodness-of-fit (Cavanaugh and Neath, 2019). For model selection, a forward stepwise procedure was used with the Akaike Information Criterion.

Akaike Information Criterion

The Akaike Information Criterion (AIC) (Akaike, 1973) is a statistic used for model evaluation and comparison. It estimates the amount of information lost when a formulated model is used to approximate the fit of the data (Posada and Buckley, 2004). The model that produces the lowest AIC value is chosen to be the best fitting model. Individual AIC values cannot be interpreted because they may be biased by the sample size (Burnham and Anderson, 2004). Hence, it is more meaningful to evaluate the change in AIC value when comparing two models against one another. The difference in AIC is defined as:

$$\Delta_i = \text{AIC}_i - \text{AIC}_{min} \tag{4.6.3}$$

where AIC_{min} is the minimum of all AIC produced by model g_{min}, AIC_i is the AIC value calculated for model g_i, Δ_i is the information loss experienced when model g_{min} is used to fit the data instead of the best model g_i.

Forward Stepwise Procedure

Model formulation was done according to the forward stepwise selection procedure (Kutner et al., 2005):

1. First, a baseline model (equation 4.6.4) was established which included all the fixed effects of interest (age and HIV-status), and a subject-specific random effect.

2. Potential confounding variables were added to the baseline model, one at a time, and their effect was assessed by observing the change in AIC and the significance of the effect. The addition of a variable was deemed significant if the effect produced a P-value, or probability value, < 0.05. If the inclusion of the variable improved the model fit, it remained in the model.

3. Any relevant interaction[i] terms between variables were assessed in the same manner as described in 2.

The baseline model is described as:

$$Y_{ij} = \beta_0 + \beta_1 X_{1ij} + \beta_2 X_{2i} + b_i + \epsilon_{ij} \tag{4.6.4}$$

where:

Y_{ij} is the Fisher Z-transformed FC measure between a BG ROI and frontal cortex ROI,

β_0 is the constant,

X_{1ij} is the age of subject i at occasion j,

X_{2i} is the HIV-status of subject i,

β_1 and β_2 are the estimated coefficients for X_{1ij} and X_{2i}, respectively,

b_i is the subject-specific random effect $b_i \sim \mathcal{N}(0, \sigma_b^2)$,

ϵ_{ij} is the sampling error for subject i at occasion j and $\epsilon_{ij} \sim \mathcal{N}(0, \sigma_e^2)$

[i] An interaction effect occurs when an independent variable has a different effect on the response, depending on the value of another independent variable.

4.6.3 Variable selection

The aim of the study was to determine the potential effects of HIV on development of FC between the BG and frontal regions. Therefore, model formulation was aimed at identifying any relationship between HIV-infection and the change in FC.

The explanatory variables required in the model formulation were HIV-status, age, and their interaction. In addition, it was necessary to control for confounding variables and other sources of variance that could have distorted the association between HIV and BG FC.

Average displacement and sex were considered as possible confounding variables, consistent with previous RSFC studies e.g. (Toich et al., 2018). Because of the unknown effect of scanner on FC measures, a categorical variable was created to account for the scanner effect. (At age 9, ten subjects were scanned on both the Siemens Allegra and Siemens Skyra scanner).

Despite preprocessing procedures that aid in subject-level motion correction, they do not circumvent the requirement for group-level correction (Yan et al., 2013). Therefore, to control for motion-related confounds within data, the mean displacement for each subject was considered as a possible covariate in the group-level analyses.

AFNI calculates spatial deviation as the Euclidean norm of the change between the 6 motion parameters of consecutive EPI volumes. Therefore, the rigid body displacement, d_n can be described as follows:

$$d_n = \sqrt{(x_i - x_{i-1})^2 + (y_i - y_{i-1})^2 + (z_i - z_{i-1})^2 + (\psi_i - \psi_{i-1})^2 + (\varphi_i - \varphi_{i-1})^2 + (\theta_i - \theta_{i-1})^2} \tag{4.6.5}$$

where:

x, y, and z are translations in the respective axes,

ψ, φ and θ are the rotations: roll, pitch and yaw, respectively.

The mean displacement, D, is then calculated as the sum of d_n over time series divided by the number of volumes within the time series. AFNI provides this value, as well as maximum displacement during the time series, in the subject review scripts generated from the afni_proc.py (Appendix A).

Table 4.2 summarises the list of explanatory variables and potential covariates, that were considered for inclusion in the final LME model.

Table 4.2: Variables that were considered for inclusion in the LME model. This does not include the list of interactions that were assessed during the model comparison stage.

Variable	**Variable Type**	**Explanatory/Covariate**
HIV-status	Categorical	Explanatory
Age (years)	Continuous	Explanatory
Sex	Categorical	Covariate
Average displacement	Continuous	Covariate
Maximum motion	Continuous	Covariate
Scanner	Categorical	Covariate
BG seed volume	continuous	Covariate

4.6.4 Outlier Removal

Outliers were identified as values that were beyond 3 standard deviations from the mean Z-score. Individual outliers were removed from the statistical model, Equation 5.2.1, to determine if they were influential i.e. if their removal changed the significance of any of the effects of interest.

5. Results

This section first presents the number of participants who were included in the study at each age, along with a description of their demographic and clinical data. LME model results are presented describing the effects of age, HIV-status, and their interaction on FC between each of the BG seeds and each of the five frontal cortex ROIs.

5.1 Sample Demographics

The final analysis included data from 159 children (79 PHIV and 80 control). Notably, not all children were scanned at each time point and some subjects were excluded at particular time points because of motion or artifacts within the dataset. From the T1 structural imaging data, BG abnormalities were observed in 3 participants (2 PHIV and 1 control) and enlarged ventricles in 1 (PHIV) participant. These subjects were removed from the study and are not included in the description below.

At age 7 years, rs-fMRI data were successfully obtained from 86 children (49 PHIV and 37 control) . Of these, 26 were excluded from further analyses: rs-fMRI data from 25 participants (13 PHIV and 12 control) did not meet the motion criteria, as described in Section 4.4, and 1 PHIV participant's anatomical data failed to align to the Haskins Pediatric template.

At age 9 years, 35 children (13 PHIV and 22 control) were scanned on the Allegra scanner, but 18 (7 PHIV and 11 control) were excluded from the analyses for not meeting the motion criteria.

On the Skyra scanner, 110 children (62 PHIV and 48 control) were scanned at age 9. Following preprocessing, 15 children (9 PHIV and 6 control) did not meet the motion criteria and 3 participants (2 PHIV and 1 control) had artifacts present on their T1 or EPI data.

At age 11, rs-fMRI was successfully obtained from 143 children (76 PHIV and 67 control), but 8 participants were excluded from the analyses for the following reasons: 6 participants (5 PHIV and 1 control) failed to meet the motion criteria and anatomical data from 1 PHIV child and 1 control child could not be accurately aligned to the Haskins Pediatric template.

The demographic characteristics of the sample group, and clinical and treatment measures of the PHIV participants are presented in Tables 5.1 and 5.2. All the CPHIV within the sample group had detectable viral loads at the time of enrolment, whereas, within 6 months of the 11-year scan, 96% of PHIV children had viral loads of < 400 copies/ml.

Table 5.1: Demographic data of the PHIV and control participants at each time point.

	PHIV	**Control**
Demographic characteristics		
7-year-olds (Allegra scanner)		
N, subjects	35	25
Age (years)	7.19 ± 0.08	7.23 ± 0.15
Sex: Female	21 (60%)	11 (44%)
9-year-olds (Allegra scanner)		
N, subjects	6	11
Age (years)	9.24 ± 0.13	9.25 ± 0.17
Sex: Female	2 (33%)	4 (36%)
9-year-olds (Skyra scanner)		
N, subjects	51	41
Age (years)	9.28 ± 0.25	9.56 ± 0.49
Sex: Female	26 (51%)	16 (39%)
11-year-olds (Skyra scanner)		
N, subjects	70	65
Age (years)	11.63 ± 0.27	11.55 ± 0.26
Sex: Female	37 (53%)	27 (42%)
N, single time point	23	38
N, two time points	32	25
N, three time points	23	12
N, four time points	1	5

Table 5.2: Summary of clinical and treatment measures of the PHIV children scanned.

	PHIV
Treatment measures	
Age at ART initiation (weeks)	9 (7 - 12)[ii]
Clinical measures at enrolment	
CD4 cell count (cell/μl)	1726 (1178 - 2240)[ii]
CD4%	35 (28 - 40)[ii]
Viral load (RNA copies/ml)[iii]	
>750000	44 (56%)
400 - 750000	33 (42%)
<400	0 (0%)
Clinical measures around time of 7-year scan	
CD4 cell count (cell/μl)	1068 (848 - 1233)[ii]
CD4%	37 (34 - 39)[ii]
Viral load (RNA copies/ml)	
>750000	0 (0%)
400 - 750000	2 (6%)
<400	33 (94%)
Clinical measures around time of 9-year scan	
CD4 cell count (cell/μl)[iv]	958 (820 - 1219)[ii]
CD4% [iv]	37 (35 - 44)[ii]
Viral load (RNA copies/ml)[v]	
>750000	0 (0%)
400 - 750000	1 (2%)
<400	47 (92%)
Clinical measures around time of 11-year scan	
CD4 cell count (cell/μl)	787 (610 - 977)[ii]
CD4%	37 (33 - 43)[ii]
Viral load (RNA copies/ml)[vi]	
>750000	0 (0%)
400 - 750000	2 (3%)
<400	67 (96%)

[ii] Value is represented by median (interquartile range)
[iii] Viral load at enrolment was not recorded for 2 participants.
[iv] CD4 count and CD4% for 1 participant was acquired more than 6 months after time of 9-year (Skyra) scan.
[v] Viral loads for 3 participants were acquired more than 6 months after time of 9-year (Skyra) scan.
[vi] Viral load around time of 11-year scan was not recorded for 1 participant.

5.2 Final LME Model

All the covariates, except sex and volume, improved the model fit in the forward stepwise model-building process. This can be seen in Appendix C, where a forward stepwise approach was used. Additionally, the fixed effect estimate produced by the volume covariate was notably small. Although both effects of average motion and maximum motion were significant, including both terms seemed unnecessary. Thus, based on previous literature (Toich et al., 2018), the former was chosen over the latter. The final model chosen to analyse the data is defined as:

$$Y_{ij} = \beta_0 + \beta_1 X_{1ij} + \beta_2 X_{2i} + \beta_3 X_{3ij} + \beta_4 X_{4ij} + \beta_5 X_{1ij} \times X_{2i} + b_i + \epsilon_{ij} \tag{5.2.1}$$

where:

Y_{ij} is the Fisher Z-transformed FC measure between a BG seed and a frontal cortex ROI,

β_0 is the constant,

X_{1ij} is the age of subject i at occasion j,

X_{2i} is the HIV-status of subject i,

X_{3ij} is the scanner used for image acquisition of subject i at occasion j,

X_{4ij} is the average motion for subject i at occasion j,

$X_{1ij} \times X_{2i}$ is the interaction term between age and HIV-status,

b_i is the subject-specific random effect and $b_i \sim \mathcal{N}(0, \sigma_b^2)$,

ϵ_{ij} is the sampling error for subject i at occasion j and $\epsilon_{ij} \sim \mathcal{N}(0, \sigma_e^2)$.

Statistical analysis code can be found in Appendix B.

5.3 Effects of Age and HIV on FC Between the BG and DLPFC ROIs

5.3.1 Left DLPFC ROI Functional Connectivity

Significant age effects were found on FC to the left and right putamen, left and right caudate, and left GP, Table 5.3. All these estimates were positive, which suggests that FC between the left DLPFC region and the abovementioned BG regions increases with age. No significant effects of HIV-status or HIV-status/age interaction were revealed. Trajectories of FC to left DLPFC vs age for PHIV children and controls are shown in Figure 5.1.

5.3.2 Right DLPFC ROI Functional Connectivity

Like the left DLPFC region, significant age effects were identified on connectivity to the left and right putamen, and left and right caudate, as seen in Table 5.4. Trajectories of FC to right DLPFC vs age for PHIV children and controls are shown in Figure 5.2.

Table 5.3: LME model estimates for FC between BG seeds and the left DLPFC region.

BG Seed	Fixed Effect	Estimate	Standard Error	P-value
Left Putamen	Intercept	-0.30	0.11	0.008
	Age	0.05	0.01	**<0.001**
	Status (HIV)	0.18	0.12	0.153
	Scanner (Skyra)	-0.13	0.04	<0.001
	Average motion	-0.01	0.08	0.884
	Age*status (HIV)	-0.02	0.01	0.202
Right Putamen	Intercept	-0.25	0.11	0.024
	Age	0.04	0.01	**0.001**
	Status (HIV)	0.09	0.12	0.438
	Scanner (Skyra)	-0.14	0.04	<0.001
	Average motion	-0.08	0.08	0.324
	Age*status (HIV)	<-0.01	0.01	0.465
Left Caudate	Intercept	-0.21	0.10	0.046
	Age	0.04	0.01	**0.001**
	Status (HIV)	0.15	0.11	0.189
	Scanner (Skyra)	-0.06	0.04	0.075
	Average motion	0.30	0.08	<0.001
	Age*status (HIV)	-0.02	0.01	0.133
Right Caudate	Intercept	-0.14	0.11	0.183
	Age	0.03	0.01	**0.025**
	Status (HIV)	0.12	0.12	0.302
	Scanner (Skyra)	-0.085	0.04	0.020
	Average motion	0.20	0.08	0.011
	Age*status (HIV)	-0.01	0.01	0.291
Left GP	Intercept	-0.13	0.10	0.222
	Age	0.03	0.01	**0.023**
	Status (HIV)	0.08	0.11	0.507
	Scanner (Skyra)	-0.05	0.03	0.119
	Average motion	-0.33	0.08	<0.001
	Age*status (HIV)	<-0.01	0.01	0.656
Right GP	Intercept	-0.03	0.10	0.722
	Age	<0.01	0.01	0.365
	Status (HIV)	-0.02	0.11	0.826
	Scanner (Skyra)	-0.02	0.03	0.507
	Average motion	-0.28	0.07	<0.001
	Age*status (HIV)	<0.01	0.01	0.778
Left Thalamus	Intercept	-0.06	0.11	0.594
	Age	<0.01	0.01	0.227
	Status (HIV)	0.04	0.12	0.755
	Scanner (Skyra)	-0.09	0.037	0.022
	Average motion	-0.38	0.08	<0.001
	Age*status (HIV)	<-0.01	0.01	0.897
Right Thalamus	Intercept	0.04	0.12	0.715
	Age	0.01	0.01	0.833
	Status (HIV)	-0.06	0.13	0.649
	Scanner (Skyra)	-0.08	0.04	0.049
	Average motion	-0.43	0.09	<0.001
	Age*status (HIV)	0.01	0.01	0.635

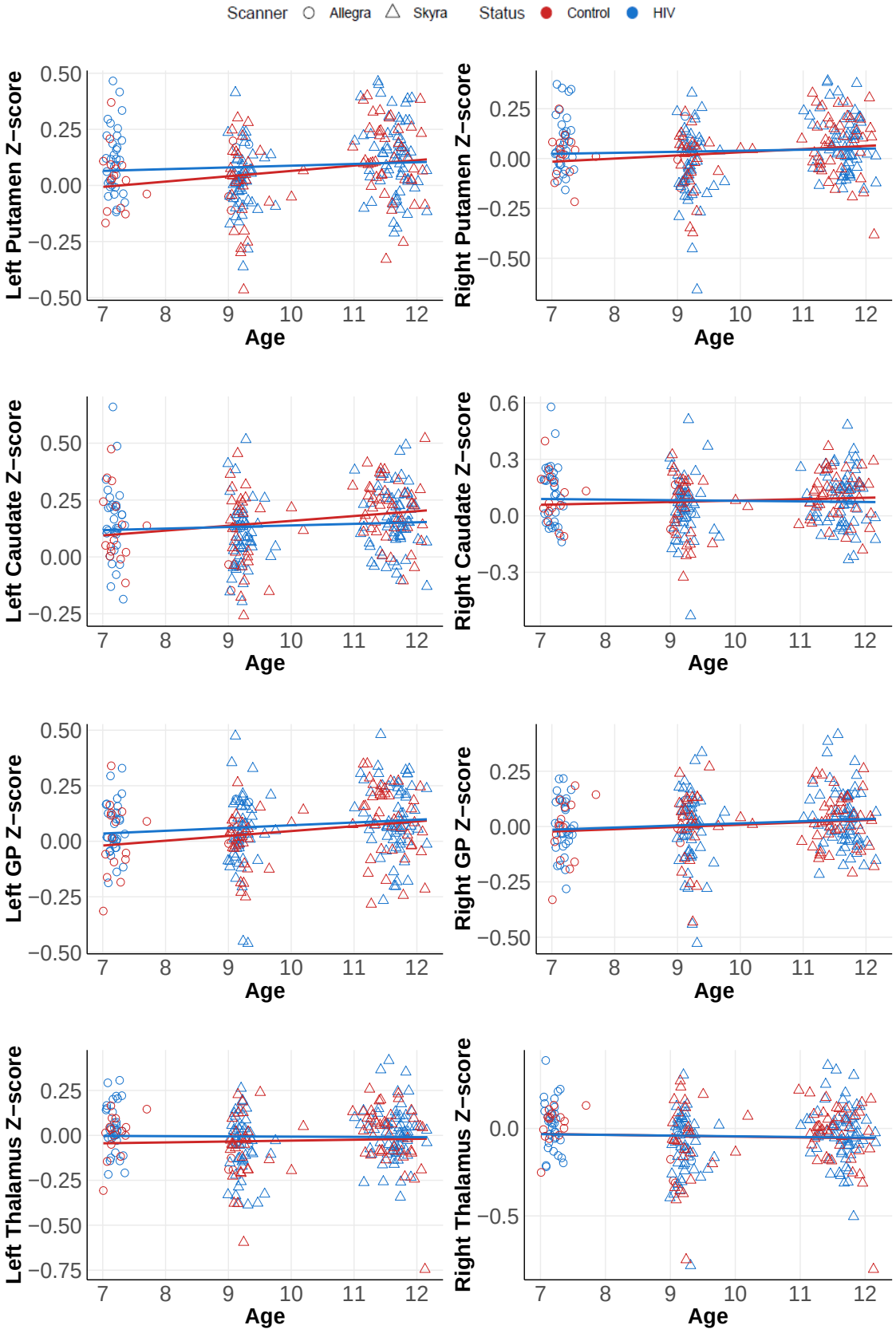

Figure 5.1: Graphical representation of the change in FC, from ages 7 to 11, between the BG seeds and left DLPFC region.

Table 5.4: LME model estimates for FC between the BG seeds and right DLPFC region.

BG Seed	Fixed Effect	Estimate	Standard Error	P-value
Left Putamen	Intercept	-0.24	0.11	0.024
	Age	0.03	0.01	**0.018**
	Status (HIV)	0.23	0.12	0.069
	Scanner (Skyra)	-0.12	0.04	0.002
	Average motion	0.01	0.08	0.89
	Age*status (HIV)	-0.02	0.01	0.145
Right Putamen	Intercept	-0.39	0.11	<0.001
	Age	0.05	0.01	**<0.001**
	Status (HIV)	0.18	0.12	0.149
	Scanner (Skyra)	-0.14	0.04	<0.001
	Average motion	0.18	0.08	0.031
	Age*status (HIV)	-0.01	0.01	0.233
Left Caudate	Intercept	-0.24	0.11	0.027
	Age	0.03	0.01	**0.007**
	Status (HIV)	0.20	0.12	0.090
	Scanner (Skyra)	-0.07	0.04	0.073
	Average motion	0.35	0.08	<0.001
	Age*status (HIV)	-0.02	0.01	0.148
Right Caudate	Intercept	-0.30	0.11	0.008
	Age	0.04	0.01	**0.002**
	Status (HIV)	0.24	0.12	0.057
	Scanner (Skyra)	-0.06	0.04	0.098
	Average motion	0.30	0.08	<0.001
	Age*status (HIV)	-0.02	0.01	0.128
Left GP	Intercept	-0.13	0.10	0.205
	Age	0.02	0.01	0.055
	Status (HIV)	0.08	0.11	0.465
	Scanner (Skyra)	-0.08	0.03	0.032
	Average motion	-0.31	0.08	<0.001
	Age*status (HIV)	-0.01	0.01	0.601
Right GP	Intercept	-0.12	0.10	0.244
	Age	0.02	0.01	0.069
	Status (HIV)	-0.01	0.12	0.922
	Scanner (Skyra)	-0.08	0.04	0.020
	Average motion	-0.19	0.08	0.018
	Age*status (HIV)	0.04	0.01	0.747
Left Thalamus	Intercept	-0.03	0.12	0.774
	Age	0.01	0.01	0.592
	Status (HIV)	0.07	0.13	0.622
	Scanner (Skyra)	-0.07	0.04	0.083
	Average motion	-0.43	0.09	<0.001
	Age*status (HIV)	-0.01	0.01	0.744
Right Thalamus	Intercept	-0.12	0.12	0.307
	Age	0.02	0.01	0.117
	Status (HIV)	0.07	0.13	0.612
	Scanner (Skyra)	-0.11	0.04	0.008
	Average motion	-0.45	0.09	<0.001
	Age*status (HIV)	-0.01	0.01	0.740

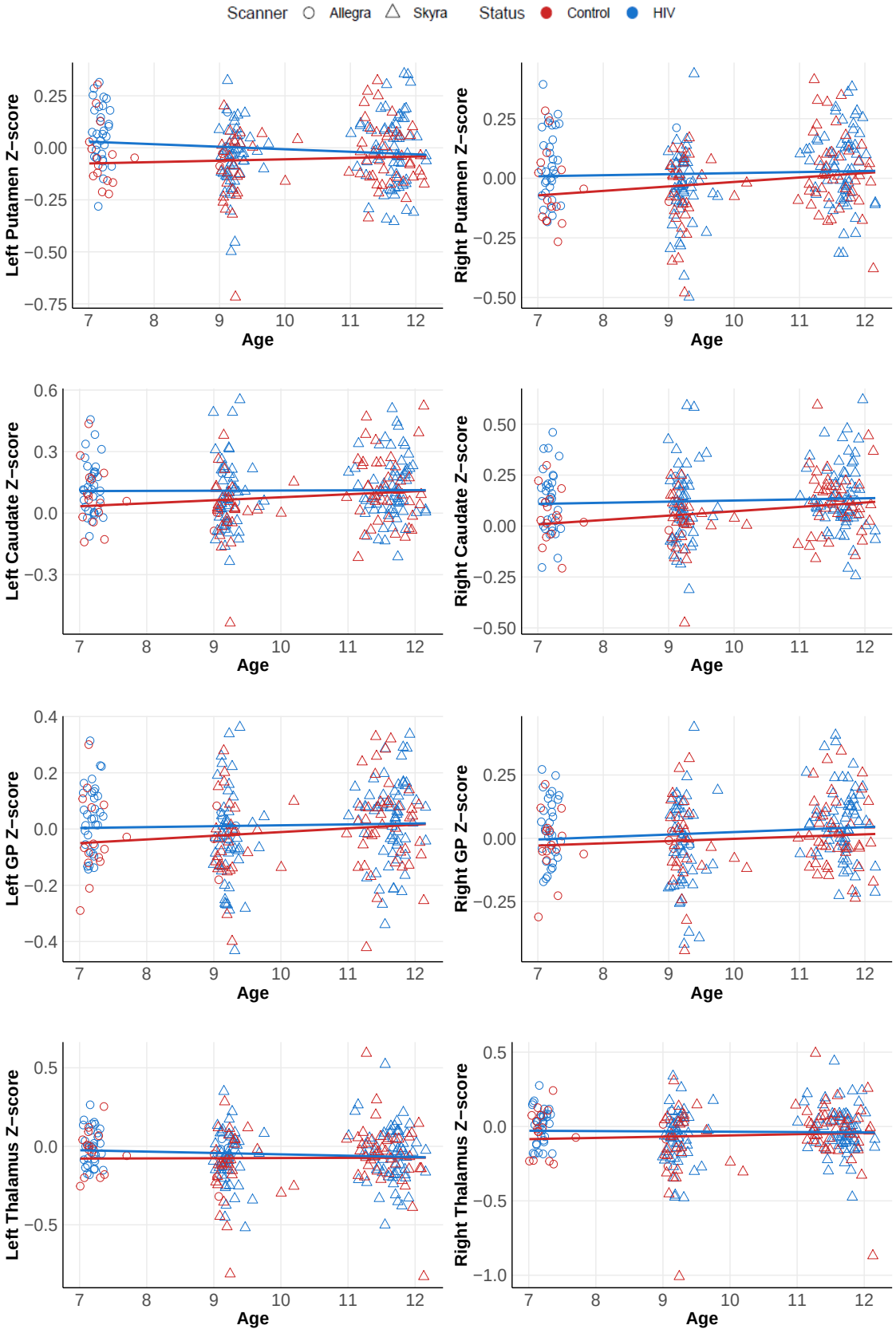

Figure 5.2: Graphical representation of the change in FC, from ages 7 to 11, between the BG seeds and the right DLPFC region.

5.4 Effects of age and HIV on FC Between the BG and Motor ROI

Significant age effects were identified on FC measures between the motor region and the left and right GP, seen in Table 5.5. The negative estimate for the age effect suggests that FC between motor region and the GP decreases with age. This is also shown by the negative slopes in the left and right GP Z-score plots in 5.3.

HIV-status was a significant effect on FC measures with the left and right caudate and GP, with large negative effects for CPHIV relative to controls observed in both caudate regions. However, 1 PHIV subject at age 11 was an influential outlier and when the subject was removed from the left caudate LME model, status was no longer significant.

Significant age/status interaction effects were observed on FC measures with the left and right caudate, GP and thalamus. Notably significant effects of age, status, and their interaction were all seen on FC with the GP. The effects of age and status were not statistically significant when modelling FC between the motor ROI and the left thalamus. However, when a PHIV influential outlier at age 7 was removed from the model, age and status effects became significant.

Table 5.5: LME model estimates for FC between BG seeds and the motor region.

BG Seed	Fixed Effect	Estimate	Standard Error	P-value
Left Putamen	Intercept	0.26	0.13	0.038
	Age	-0.02	0.01	0.187
	Status (HIV)	-0.07	0.14	0.598
	Scanner (Skyra)	-0.09	0.04	0.889
	Average motion	-0.02	0.09	0.809
	Age*status (HIV)	0.01	0.01	0.436
Right Putamen	Intercept	0.29	0.13	0.029
	Age	-0.02	0.01	0.228
	Status (HIV)	-0.18	0.15	0.228
	Scanner (Skyra)	-0.03	0.04	0.475
	Average motion	-0.08	0.10	0.420
	Age*status (HIV)	0.02	0.01	0.203
Left Caudate	Intercept	0.06	0.12	0.651
	Age	-0.01	0.01	0.388
	Status (HIV)	-0.28	0.14	**0.043**
	Scanner (Skyra)	-0.04	0.04	0.371
	Average motion	0.07	0.09	0.456
	Age*status (HIV)	0.04	0.01	**0.015**
Right Caudate	Intercept	0.05	0.13	0.680
	Age	-0.01	0.01	0.382
	Status (HIV)	-0.34	0.14	**0.020**
	Scanner (Skyra)	-0.03	0.04	0.440
	Average motion	0.05	0.09	0.616
	Age*status (HIV)	0.04	0.01	**0.010**
Left GP	Intercept	0.33	0.11	0.005
	Age	-0.03	0.01	**0.010**
	Status (HIV)	0.29	0.13	**0.023**
	Scanner (Skyra)	<-0.01	0.04	0.998
	Average motion	0.01	0.08	0.927
	Age*status (HIV)	0.03	0.01	**0.013**
Right GP	Intercept	0.30	0.12	0.016
	Age	-0.03	0.01	**0.037**
	Status (HIV)	-0.28	0.14	**0.041**
	Scanner (Skyra)	-0.02	0.04	0.665
	Average motion	-0.05	0.09	0.615
	Age*status (HIV)	0.03	0.01	**0.045**
Left Thalamus	Intercept	0.21	0.12	0.094
	Age	-0.02	0.01	0.105
	Status (HIV)	-0.27	0.14	0.056
	Scanner (Skyra)	0.01	0.04	0.880
	Average motion	0.25	0.09	0.007
	Age*status (HIV)	0.03	0.01	**0.040**
Right Thalamus	Intercept	0.21	0.12	0.092
	Age	-0.02	0.01	0.168
	Status (HIV)	-0.27	0.14	0.056
	Scanner (Skyra)	-0.03	0.04	0.464
	Average motion	0.18	0.09	0.054
	Age*status (HIV)	0.03	0.01	**0.046**

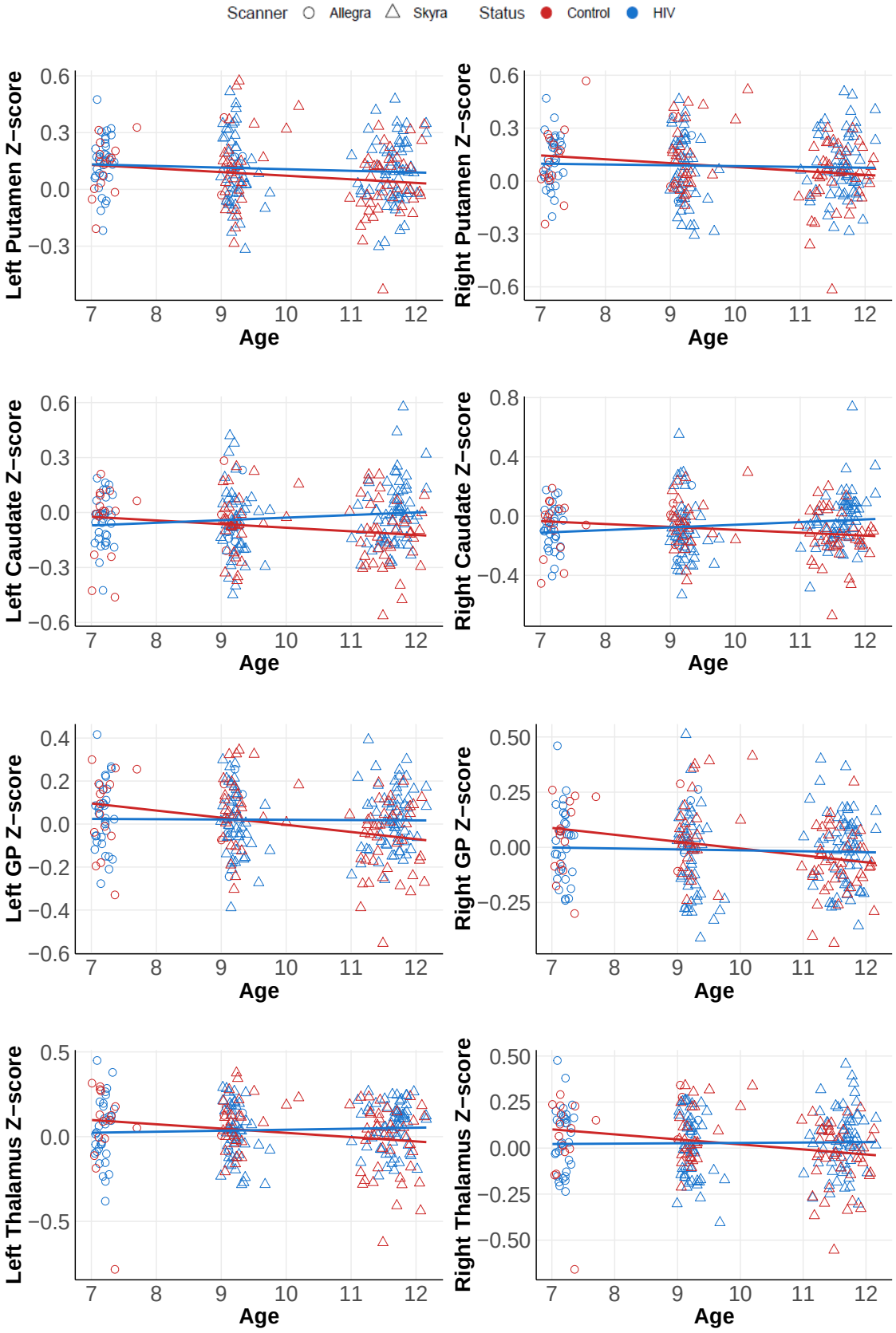

Figure 5.3: Graphical representation of the change in FC, from ages 7 to 11, between the BG seeds and the motor region.

5.5 Effects of age and HIV on FC Between the BG and Language ROI

Table 5.6 shows that all BG seeds revealed significant age effects. These were all positive estimates, with the largest estimates seen in the left and right putamen. The increase in FC with age between the BG ROIs and the left language ROI was apparent from the positive slopes on all the plots in Figure 5.4. There were no significant effects of HIV status.

5.6 Effects of age and HIV on FC Between the BG and Right Inferior Frontal Gyrus

FC between right IFG and BG seeds showed significant age effects within the left and right putamen, caudate, GP and right thalamus, as seen in Table 5.7. Significant HIV-status effects were seen in the left and right putamen, GP and left caudate. Additionally, the left and right putamen, left caudate and left GP revealed significant interaction effects. The negative estimates for the interaction effects suggests that the rate of FC development between the right IFG region and the BG seeds is slower for CPHIV. This is corroborated by positive slopes for controls in the putamen, left caudate and left GP Z-score plots shown in Figure 5.5, while the same Z-score plots for CPHIV have a gradient of approximately zero.

Table 5.6: LME model estimates for FC between BG seeds and the language region.

BG Seed	Fixed Effect	Estimate	Standard Error	P-value
Left Putamen	Intercept	-0.36	0.10	<0.001
	Age	0.06	0.01	**<0.001**
	Status (HIV)	0.13	0.11	0.240
	Scanner (Skyra)	-0.14	0.04	<0.001
	Average motion	0.26	0.08	0.001
	Age*status (HIV)	-0.01	0.01	0.288
Right Putamen	Intercept	-0.30	0.10	0.005
	Age	0.05	0.01	**<0.001**
	Status (HIV)	0.20	0.12	0.074
	Scanner (Skyra)	-0.15	0.04	<0.001
	Average motion	0.08	0.08	0.287
	Age*status (HIV)	-0.02	0.01	0.085
Left Caudate	Intercept	-0.31	0.10	0.003
	Age	0.05	0.01	**<0.001**
	Status (HIV)	0.09	0.11	0.421
	Scanner (Skyra)	-0.12	0.03	0.001
	Average motion	0.14	0.08	0.072
	Age*status (HIV)	-0.01	0.01	0.618
Right Caudate	Intercept	-0.18	0.10	0.071
	Age	0.03	0.01	**0.005**
	Status (HIV)	0.01	0.11	0.934
	Scanner (Skyra)	-0.11	0.03	0.001
	Average motion	0.06	0.07	0.399
	Age*status (HIV)	<0.01	0.01	0.885
Left GP	Intercept	-0.23	0.10	0.021
	Age	0.04	0.01	**<0.001**
	Status (HIV)	0.11	0.11	0.312
	Scanner (Skyra)	-0.05	0.03	0.173
	Average motion	-0.06	0.08	0.412
	Age*status (HIV)	-0.01	0.01	0.447
Right GP	Intercept	-0.15	0.10	0.161
	Age	0.02	0.01	**0.031**
	Status (HIV)	0.03	0.12	0.820
	Scanner (Skyra)	-0.06	0.04	0.078
	Average motion	-0.10	0.08	0.204
	Age*status (HIV)	<0.01	0.01	0.982
Left Thalamus	Intercept	-0.31	0.11	0.004
	Age	0.05	0.01	**<0.001**
	Status (HIV)	0.03	0.12	0.791
	Scanner (Skyra)	0.79	0.04	0.019
	Average motion	-0.05	0.08	0.571
	Age*status (HIV)	<-0.01	0.01	0.915
Right Thalamus	Intercept	-0.23	0.11	0.036
	Age	0.04	0.01	**<0.001**
	Status (HIV)	<-0.01	0.12	0.977
	Scanner (Skyra)	-0.13	0.04	<0.001
	Average motion	-0.10	0.08	0.206
	Age*status (HIV)	<0.01	0.01	0.882

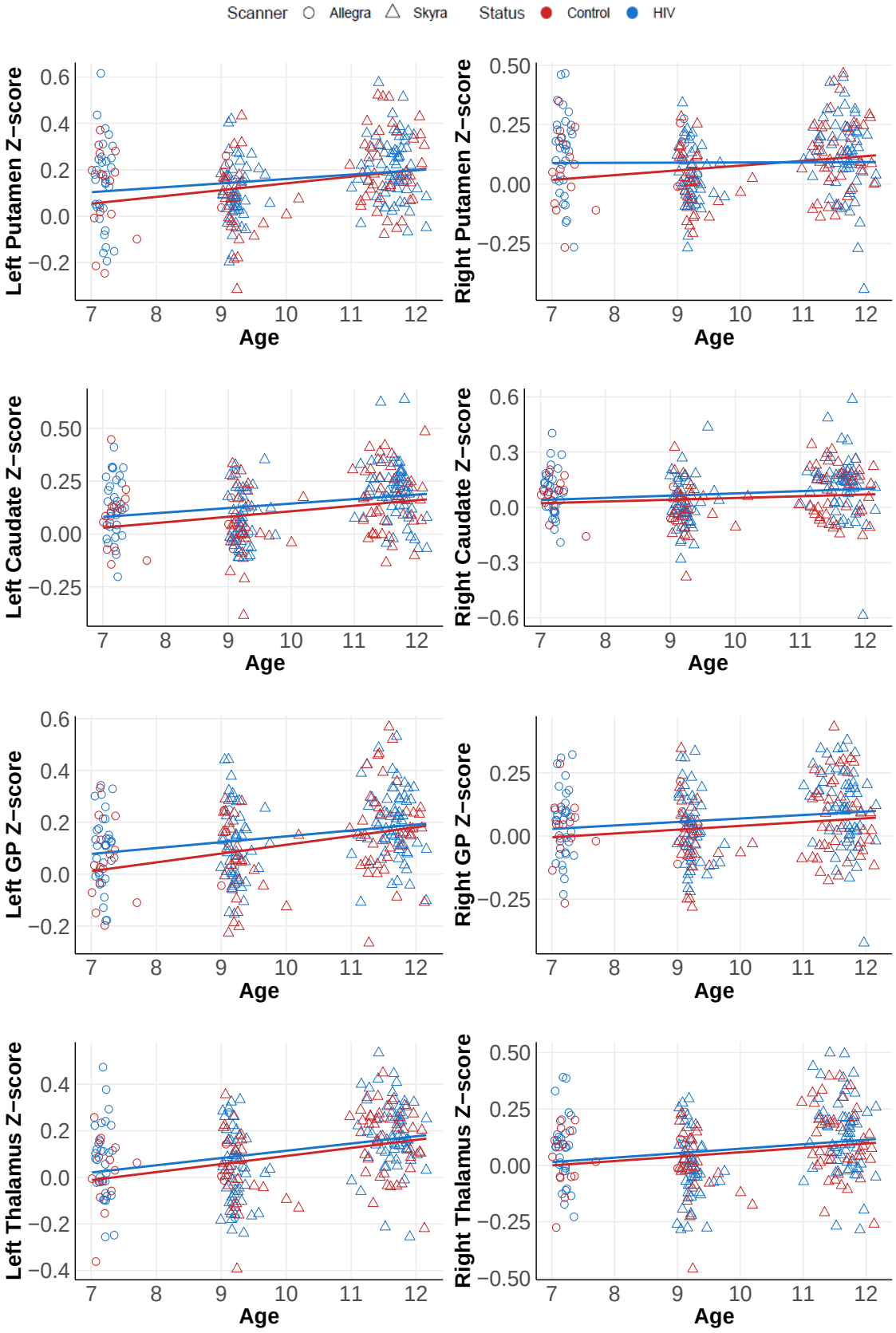

Figure 5.4: Graphical representation f change in FC, from ages 7 to 11, between BG seeds and the language region.

Table 5.7: LME model estimates for FC between BG seeds and the right IFG region.

BG Seed	Fixed Effect	Estimate	Standard Error	P-value
Left Putamen	Intercept	-0.26	0.10	0.008
	Age	0.04	0.01	**<0.001**
	Status (HIV)	0.27	0.11	**0.015**
	Scanner (Skyra)	-0.09	0.03	0.005
	Average motion	0.15	0.07	0.039
	Age*status (HIV)	-0.03	0.01	**0.012**
Right Putamen	Intercept	-0.36	0.10	0.001
	Age	0.05	0.01	**<0.001**
	Status (HIV)	0.30	0.11	**0.010**
	Scanner (Skyra)	-0.06	0.04	0.069
	Average motion	0.30	0.08	<0.001
	Age*status (HIV)	-0.03	0.01	**0.012**
Left Caudate	Intercept	-0.27	0.09	0.003
	Age	0.04	0.01	**<0.001**
	Status (HIV)	0.23	0.10	**0.020**
	Scanner (Skyra)	-0.06	0.03	0.066
	Average motion	0.21	0.07	0.002
	Age*status (HIV)	-0.02	0.01	**0.016**
Right Caudate	Intercept	-0.20	0.10	0.039
	Age	0.03	0.01	**0.012**
	Status (HIV)	0.17	0.11	0.107
	Scanner (Skyra)	<0.01	0.03	0.942
	Average motion	0.34	0.07	<0.001
	Age*status (HIV)	-0.02	0.01	0.141
Left GP	Intercept	-0.40	0.09	<0.001
	Age	0.05	0.01	**<0.001**
	Status (HIV)	0.35	0.11	**0.001**
	Scanner (Skyra)	-0.06	0.03	0.061
	Average motion	0.07	0.07	0.317
	Age*status (HIV)	-0.03	0.01	**0.002**
Right GP	Intercept	-0.28	0.10	0.006
	Age	0.04	0.01	**<0.001**
	Status (HIV)	0.22	0.11	**0.048**
	Scanner (Skyra)	-0.04	0.03	0.261
	Average motion	0.08	0.07	0.262
	Age*status (HIV)	-0.02	0.01	0.073
Left Thalamus	Intercept	-0.10	0.10	0.284
	Age	0.02	0.01	0.074
	Status (HIV)	0.01	0.11	0.944
	Scanner (Skyra)	-0.03	0.03	0.426
	Average motion	-0.14	0.074	0.052
	Age*status (HIV)	<-0.01	0.01	0.876
Right Thalamus	Intercept	-0.19	0.10	0.063
	Age	0.03	0.01	**0.003**
	Status (HIV)	0.07	0.11	0.555
	Scanner (Skyra)	-0.03	0.03	0.325
	Average motion	-0.16	0.08	0.038
	Age*status (HIV)	<-0.01	0.01	0.463

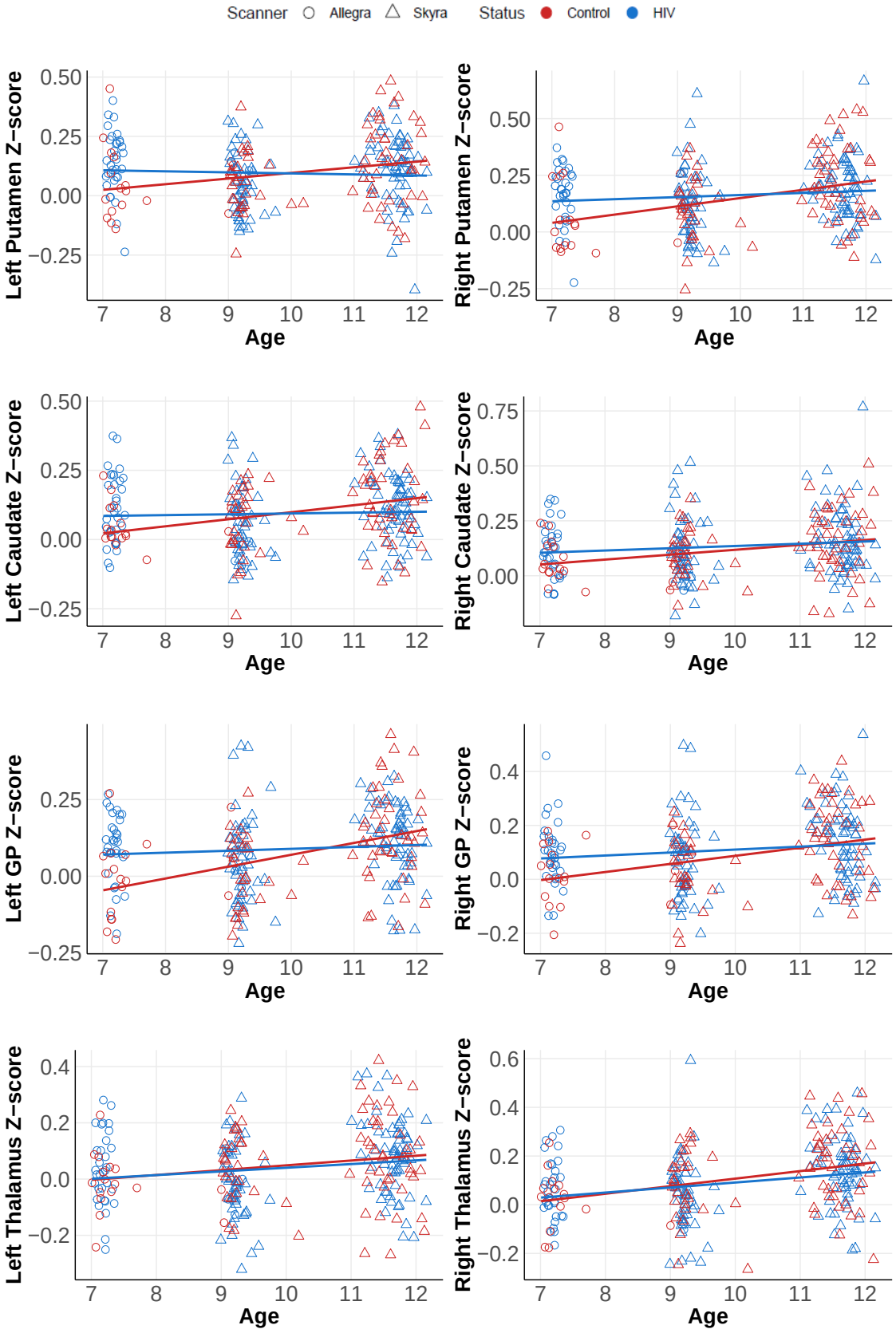

Figure 5.5: Graphical representation of the change in FC, from ages 7 to 11, between BG seeds and the right IFG region.

5.7 Model Validation

The LME models were formulated to have normally distributed between- and within-subject residuals. Figure 5.6 shows the histograms of the between- and within-subject residuals, confirming that they follow a normal distribution. The random scatter of the between-subject residuals plotted against the fitted values provides no evidence of heteroscedasticity, confirming that the model fit appropriately captures the associations. Residual plots for the remaining 39 models are provided in Appendix D. All models satisfied the assumptions underlying the model. Furthermore, the K-S test statistic for each model was calculated and is presented in Appendix E.

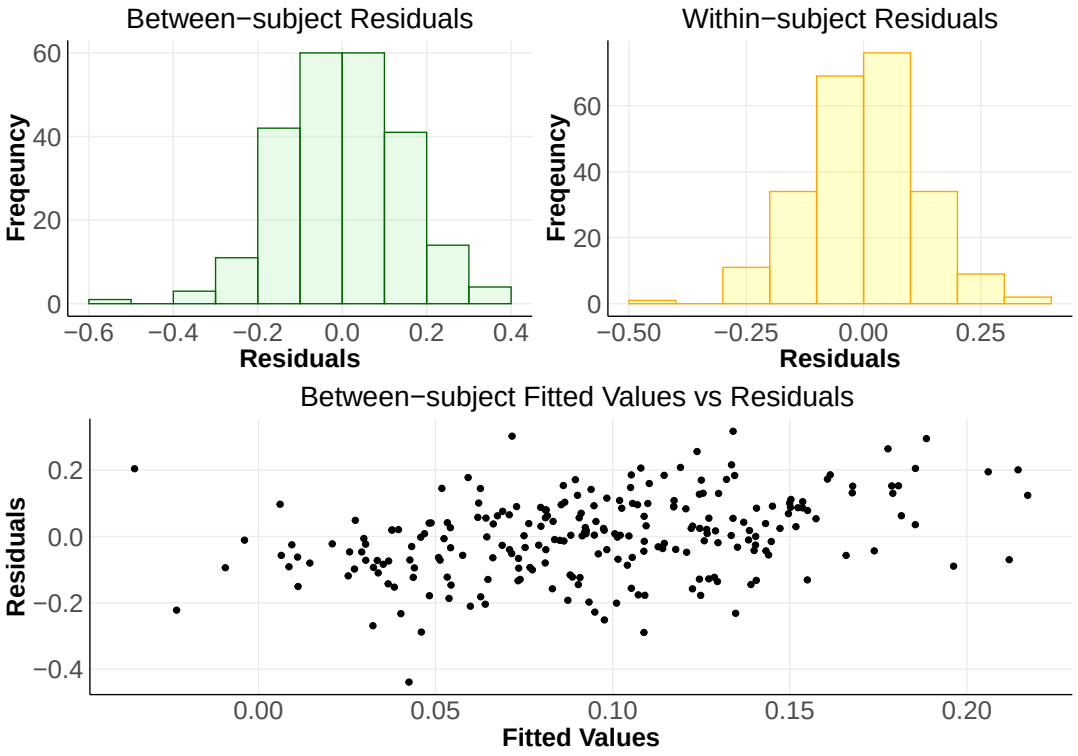

Figure 5.6: Between-subject and within-subject residuals are represented by histograms and a scatter plot for Z-score FC measures between the left putamen and right IFG region.

6. Discussion

This study assessed the effects of HIV on the development of FC between the BG and frontal cortex in children aged 7 to 11. To the authors' knowledge, this is the first study to examine longitudinal development of fronto-striatal RSFC in CPHIV. FC was calculated between 8 BG regions and 5 frontal regions (left and right DLPFC regions, a motor region, language region and the right IFG region). Longitudinal data analysis was used to statistically analyse the results over the study age range to determine if HIV-infection altered FC. In addition to identifying potential effects of HIV, the study examined the development of these functional connections with age and determined whether HIV-infection altered the rate of this development.

During the age range studied, the BG undergo volumetric changes. Linear decreases in GM volumes of the putamen and caudate have been observed, while the GM volumes of the GP and thalamus have shown to present an inverted U-shape developmental trajectory (Wierenga et al., 2014). Similarly, age has been found to generally influence FC (López-Vicente et al., 2021)

6.1 BG Executive Function Network

Age was a significant effect on FC measures between the putamen and caudate and both DLPFC ROIs. Notably, these findings are bilateral for both BG seeds. These positive estimates, although small, indicate that connectivity increases with age, affirming the projections of the DLPFC to the caudate and putamen. Martino et al. (2008) indicated that the dorsal caudate and rostral ventral putamen primarily showed FC with the DLPFC and other executive regions. As the DLPFC is involved in executive functioning (Nee, Wager and Jonides, 2007; Barbey, Koenigs and Grafman, 2012; Szczepanski and Knight, 2014), it makes sense that these functional connections strengthen during childhood. Executive functioning develops rapidly during early childhood years and reaches adult-level performance by mid-adolescence (Anderson, 2002; Zelazo et al., 2003).

Children living with HIV perform below average in the areas of processing speed, working memory and cognitive function (Koekkoek et al., 2008; Ruel et al., 2012), suggesting that HIV may adversely affect the development of executive function. However, this may depend on disease history, as executive function in children and adolescents with PHIV without previous severe disease[vii] has been found to be similar to that of uninfected (HIV-exposed) controls (Nichols et al 2016).

At age 5 the CHER PHIV group scored significantly lower than the control group in visual perception (Laughton et al., 2018), which involves components of cognitive processing. Additionally, at age 7 and 9, the PHIV grouped performed worse in executive functioning and working memory (VanWyhe et al., 2021). Toich et al. (2018) observed that the CHER cohort had reduced FC between the middle frontal gyrus of the executive control network and a cluster in the R supramarginal gyrus/inferior parietal lobule. The same study found that better immune health (higher CD4 count) in infancy was associated with lower connectivity within the BG network.

[vii] Centre for disease Control Class C diagnosis (AIDS-defining)

Contrary to one of the initial hypotheses, the current study found no significant group differences in FC between the executive frontal regions and the BG. A possible explanation for this is that the hypothesis was based on studies conducted on adults living with HIV, with longer duration of infection and not all of whom were on ART (Melrose et al., 2008; Ipser et al., 2015). Zhuang et al. (2017) showed that combinational ART improves the cognitive performance and default mode network FC in treatment-naïve individuals living with HIV. Similarly, Ortega et al. (2015) observed that, although HIV+ patients showed impaired FC, patients on ART had higher FC between the striatum and pre-SMA (default mode network) and superior frontal cortex (ventral attention network) than patients not on treatment. The current findings may provide evidence of benefits of early ART in preventing HIV-induced reductions in FC between DLPFC and the BG in children or the possibility that deficits only become apparent in adulthood.

6.2 BG Motor Function Network

The age effect was only significant in motor cortex correlations with the GP. These results are consistent with a BG development study that identified functional correlations between the posterior putamen/GP and the somatomotor face system, which decreased with development, with reduced FC already apparent between ages 7 and 12, and stabilised during early adulthood (Greene et al., 2014). Similarly, a graph theory analysis on cortical thickness revealed a connectivity decrease with age in primary sensorimotor regions (Khundrakpam et al., 2013). A study in adults found that cortico-BG motor circuit FC changes with age (Marchand et al., 2011) and connectivity between the supplementary motor area and subcortical structures was greater in the younger age groups. Furthermore, a longitudinal analysis conducted on young to middle-aged adults showed that GP and posterior putamen FC to the left somatomotor cortices decreases with age (Manza et al., 2015).

Because of the known anatomical connections of the putamen, which receives projections from the motor, pre-motor and somatosensory cortices (Künzle, 1975; Alexander, DeLong and Strick, 1986; Haber, Lynd-Balta and Spooren, 1994), we expected to observe a change in motor connectivity to this region during development. Movement execution, such as sequential finger tapping, has been associated with the activation in the putamen (Moritz et al., 2000; Romero et al., 2008; Andersen, Madsen and Siebner, 2020) and the degree of activation in the putamen has been found to be dependent on the complexity or frequency of the task being performed (Lehéricy et al., 2006). However, no significant age effects were observed in RSFC between the motor region and the putamen . This may be because motor connectivity to the putamen develops earlier, so that no change is observable by the time of the start of our longitudinal study, at age 7 years.

In the current study, reduced FC was observed for the PHIV group between the paracentral lobule (motor region) and the bilateral caudate and right GP, and increased FC between the motor region and left GP. Notably, the magnitude of the observed effects of HIV on FC measures are greater than that of age (Table 5.5), suggesting that HIV-infection may play a more dominant role the development of FC. In addition, significant age-status interactions are seen in the bilateral caudate, GP and thalamus. FC measures decrease (or increase in strength in the negative direction) with increasing age in control subjects, while remaining nearly unchanged for the PHIV subjects. This suggests that HIV may compromises normal FC development.

At age 7 years BG-motor connectivity is generally lower in PHIV children, while the negative slope in FC seen in the PHIV children by age 11 FC is higher than that of controls. Neurodevelopmentally, the Griffiths Mental Developmental Scales (GMDS) at infancy revealed that the CHER cohort performed lower on the locomotor scale when compared with the uninfected group (Laughton et al., 2012). However, this locomotor delay was resolved by age 5 (Laughton et al., 2018). Additionally, the Beery-Buktenica development tests of visual and motor integration administered at age 5 revealed no differences in motor coordination scores between the two groups (Laughton et al., 2018). The PHIV group initially performed worse in fine motor dexterity, however, this improved to the level of children without HIV by age 9 (VanWyhe et al., 2021). It appears that there are periods in which PHIV group lag in motor development, which is then resolved in later years.

Rs-fMRI findings of the same cohort at age 7, indicated attenuated FC between a seed in the paracentral lobule and the anterior cingulate in the PHIV group (Toich et al., 2018). Increased FC in the BG and somatosensory networks was also associated with poorer immune healthy at infancy, as expressed by a low CD4 count or CD % at enrolment. Structural analysis also shows that PHIV youth have reduced cortical thickness in the left and right primary motor areas (Angeles et al., 2020) and lower gyrification in the paracentral region (Nwosu et al., 2018). Yadav et al. (2017) found that children living with HIV had lower amplitude of low frequency fluctuations (ALFF) in the precentral and postcentral gyrus, reduced FC between a seed within the left precentral gyrus and a cluster in the right vermis region and FC between a seed within the left postcentral gyrus and middle temporal region. These observations may reveal that HIV-infection alters the flow of information within motor cortex regions, thus impacting motor function.

6.3 BG Language Function Network

Age was a significant effect on the FC Z-score between the language region (left IFG) and all eight BG regions. Interestingly, this was the only frontal cortex ROI which presented significant age effects for FC measures with all the BG ROIs. FC between the BG and regions within the pars opercularis increases with age, with the largest age effect seen in FC measures with the bilateral putamen.

The BG are more commonly known for their role in motor control, whereas their involvement in language is not well-established. However, research has provided evidence of their involvement in phonological, lexical and semantic processing (Crosson et al., 2003; Teichmann, Darcy and Dupoux, 2009; Cherodath et al., 2017). A study conducted on bilingual children found strong associations between putamen GM volume and phonological awareness (Cherodath et al., 2017). Vinas-Guasch and Wu (2017) conducted a meta-analytic connectivity analysis to assess the coactivation networks for the anterior and posterior putamen in language domain experiments. Coactivations for the left anterior putamen were predominantly in the left hemisphere, in regions directly associated to language comprehension and production (including the left IFG), lexical processing and language control (Vinas-Guasch and Wu, 2017). A DTI analysis revealed direct connectivity between two functionally distinct regions within Broca's area - one involved in semantic processing and the other in phonology and syntax - and the anterior one-third of the putamen (Ford et al., 2013). The output of the circuitry was then tracked to the ventral anterior thalamus.

A longitudinal study conducted on children from 5 to 11 years old found an age-related increase in the participation of IFG in language processing (Szaflarski et al., 2006). Hence, the increase in FC between the BG and left IFG within this current study's findings may reflect the BG's support of these processes.

No group differences were observed in FC measures between the BG and the language region. Correspondingly, the CHER cohort, at age 5, showed limited differences in language performance compared to controls (Laughton et al., 2018). This was also the case at age 7 and 9, where the only significant effect was the improvement in test scores between the two ages (VanWyhe et al., 2021). These findings corroborate the current study's results.

In HIV+ adults, increased activation in the bilateral putamen and caudate was observed during verbal fluency tasks (Thames et al., 2016). A meta-analysis of fMRI studies found converging evidence that HIV causes hyperactivation in the left caudate and left IFG (Du Plessis et al., 2014). Melrose et al. (2008) suggested that the increased BG-parietal FC during a semantic-sequencing task was a compensatory mechanism in individuals living with HIV. Similar to the negative findings in the executive function network, the lack of significant HIV effects in the current study may suggest that there are neurodevelopmental benefits to early ART or that differences in language ability are more pronounced in adult years.

6.4 BG and the Right IFG Network

The right IFG, which was selected in this study as the right hemisphere analogue for Broca's area, has been commonly implicated in inhibitory control (Aron, Robbins and Poldrack, 2004; Cai et al., 2014), an element of executive function, which refers to the suppression of a planned action which is not required anymore or deemed inappropriate (Verbruggen and Logan, 2008). Studies have found that BG-thalamo-cortical networks play a role in inhibitory control (Aron, Robbins and Poldrack, 2004, 2014). In a stop-signal task analysis, projections from the GPe to the striatum were essential for response inhibition (Wei and Wang, 2016). These previous findings confirm the presence of functional connections between the BG and right IFG.

The current study's results reveal that age was a significant effect on FC between the right IFG and seven of the eight BG regions (all except the left thalamus), suggesting that FC between these regions develops with age. Methods pertaining to response inhibition and interference suppression have been used to assess the development of inhibition in children. An analysis of two groups of children, aged 7 and 9, with a two-year follow-up, found that interference suppression improved for both groups between the two-year period (Richardson et al., 2018). In contrast, a stop-signal and go/no-go task assessment revealed little developmental change for children between 7 and 12 years of age (Johnstone et al., 2007).

We found significant differences in FC between the right IFG to the bilateral putamen and GP and left caudate in the PHIV group when compared to the control group. Additionally, significant age-status interaction effects were seen in FC measures between the right IFG and the bilateral putamen, left caudate and left GP. Following the FC developmental trajectories, the CPHIV had greater mean FC Z-scores at age 7 than controls but these values remained approximately constant throughout the age range studied, whereas the mean FC Z-scores for the control grouped increased

with age and were evidently greater than that of the HIV group after 11 years of age. These results may provide evidence of hindered maturation of processes related to inhibitory control in CPHIV.

Children with attention deficit hyperactivity disorder (ADHD) have poor inhibitory control (Schachar et al., 2000). ADHD is characterized by age-inappropriate levels of inattentiveness, hyperactivity and impulsivity (Arruda, Arruda and Anunciação, 2020). If CPHIV have a deficit in inhibitory control, they may be susceptible to ADHD. This is supported a Ugandan study on children and adolescents living with HIV which found that 6% of the sample population met the criteria for ADHD (Mpango et al., 2017). Additionally, the prevalence of ADHD was 29.4% in a sample group of adults living with HIV which was higher than percentage ADHD in the general population (7.3%) (Uysal et al., 2020). It remains to be investigated whether the children in this cohort display deficits in attention or inhibitory control during adolescence.

6.5 Limitations and Future Work

There are several limitations to this study. Although this longitudinal analysis allows for the assessment of the development of FC, the study did not have data for all participants at all time points. Some participants dropped out of the study, while others were only recruited at later time points. Additionally, data were lost when participants were excluded from the analysis because of excess motion. Motion was more prevalent in the younger age groups, consequently, there were fewer participants for which RSFC data could be statistically analysed, without motion confounds, at age 7 than at ages 9 and 11.

Scanning was transferred to a new scanner at age 9, thus at that at age 7 children were scanned on a different scanner from age 9 and 11. This introduced a variable of uncertainty in the analyses because it was unknown if and how the change of scanner influenced the FC measures and therefore the FC developmental trajectories. We included a scanner variable in the analysis to account for possible scanner-related differences . These effects were often significant, however, but were not able to investigate the full extent of the confounding. This is a common problem with longitudinal studies and methods are being explored how best to address this. One such technique is referred to as ComBat (Beer et al., 2020).

Several significant age, HIV-status and age-status interaction effects were found during the analysis. However, the study did not adjust for multiple comparisons as a post-hoc analysis. The results should therefore be considered exploratory. Future work would correct for multiple comparisons prior to any expansion on the results that were found.

The use of LME to model the development of FC assumes that all FC varies linearly over time. More complex non-linear mixed effect models may be better suited to predict some of the developmental trajectories.

This study used anatomical regions of the BG as seeds, which can be regarded as quite limited. Frontal regions do not project to entire BG regions but segments thereof. It is noted that more accurate results could be obtained by using smaller BG ROIs (Porter et al., 2015). Another approach is to place spherical seeds at coordinates of anatomical regions. More specific BG regions can be selected investigated as seeds for future work.

Finally, this study cannot differentiate between the effects of HIV or possible side-effects of ART. Numerous studies have described the potential neurotoxicity and CSF viral escape associated with the use of ART (Shah et al., 2016; Patel et al., 2018; Joseph et al., 2019; Manesh et al., 2019). All children living with HIV were grouped together in this analysis, regardless of the treatment regimen they were assigned to (ART-40W, ART-96W or ART-def), and their FC was compared to that of uninfected controls. A recommendation for future work would be to assess any associations between treatment group and development of fronto-striatal RSFC.

7. Conclusion

In conclusion, the findings of age-related changes in fronto-striatal FC confirm that childhood maturation influences the development of FC to the BG. Increased FC with age was predominantly seen between the BG and the DLPFC and language regions. These are indicative of the increased development of executive functioning and language processing during the age range studied, and the increased involvement of the BG to assist in these functions. Age-related decreases in FC were observed between the GP and motor region. This is supported by similar findings from another BG FC study on a cohort of a similar age (Manza et al., 2015).

HIV-induced atrophy within the BG has been well-reported. Therefore, the primary objective of this study was to analyse the potential effects of HIV on the BG FC in CPHIV. Contrary to the hypothesis, no significant HIV effects were seen in FC measures between the BG and DLPFC. This may be attributed to the initiation of early ART and viral load suppression. However, the same is not true for FC between the BG and the motor region and right IFG, in which HIV-altered FC was observed. FC with the motor region changed with age for controls, and remained fairly constant in CPHIV, providing evidence of altered development. This agrees with the second hypothesis. As the BG's main role is to control voluntary movement, altered FC in the motor region could indicate adverse effects on motor function. Additionally, the HIV-altered FC in the right IFG region may indicate that CPHIV are more likely to have inhibitory control deficits, and may therefore be more susceptible to developing ADHD. These FC alterations suggest possible HIV-related neurodevelopmental deficits and require further investigation.

8. References

Akaike, H. (1973) 'Information Theory and an Extension of the Maximum Likelihood Principle', pp. 199–213. doi: 10.1007/978-1-4612-1694-0_15.

Al Sawai, A. et al. (2020) 'The changing profile of paediatric HIV infection: An experience from the Middle East', International Journal of Infectious Diseases. International Society for Infectious Diseases, 97, pp. 347–351. doi: 10.1016/j.ijid.2020.06.013.

Alexander, G. E., DeLong, M. R. and Strick, P. L. (1986) 'Parallel organization of functionally segregated circuits linking basal ganglia and cortex', Annual Review of Neuroscience, VOL. 9, pp. 357–381. doi: 10.1146/annurev.ne.09.030186.002041.

Ances, B. M., Ortega, M., Vaida, F., and Heaps, J. (2013). Independent Effects of HIV, Aging, and HAART on Brain Volumetric Measures. 59(5), 469–477.

Andersen, K. W., Madsen, K. H. and Siebner, H. R. (2020) 'Discrete finger sequences are widely represented in human striatum', Scientific Reports. Nature Publishing Group UK, 10(1), pp. 1–12. doi: 10.1038/s41598-020-69923-x.

Anderson, P. (2002) 'Assessment and development of executive function (EF) during childhood', Child Neuropsychology, 8(2), pp. 71–82. doi: 10.1076/chin.8.2.71.8724.

Angeles, C. P. L. L. et al. (2020) 'NeuroImage: Clinical Brain morphometric differences in youth with and without perinatally-acquired HIV: A cross-sectional study', NeuroImage: Clinical. Elsevier, 26(October 2019). doi: 10.1016/j.nicl.2020.102246.

Aron, A.R., Robbins, T.W. and Poldrack, R.A. (2004) "Inhibition and the right inferior frontal cortex," Trends in Cognitive Sciences, pp. 170–177. doi:10.1016/j.tics.2004.02.010.

Aron, A.R., Robbins, T.W. and Poldrack, R.A. (2014) "Inhibition and the right inferior frontal cortex: One decade on," Trends in Cognitive Sciences. Elsevier Ltd, pp. 177–185. doi:10.1016/j.tics.2013.12.003.

Arruda, M.A., Arruda, R. and Anunciação, L. (2020) "Psychometric properties and clinical utility of the executive function inventory for children and adolescents: a large multistage populational study including children with ADHD," Applied Neuropsychology: Child [Preprint]. doi:10.1080/21622965.2020.1726353.

Asbury, C. H. and Detre, J. A. (2019) 'Brain Imaging Technologies: Clinical and Neuroscience Applications'.

Barbey, A. K., Koenigs, M. and Grafman, J. (2012) 'Dorsolateral prefrontal contributions to human working memory', CORTEX. Elsevier Ltd, 49(5), pp. 1195–1205. doi: 10.1016/j.cortex.2012.05.022.

Beer, J. C., Tustison, N. J., Cook, P. A., Davatzikos, C., Sheline, Y. I., Shinohara, R. T., and Linn, K. A. (2020). Longitudinal ComBat: A method for harmonizing longitudinal multi-scanner imaging data. NeuroImage, 220. https://doi.org/10.1016/j.neuroimage.2020.117129

Biswal, B. B. (2012) 'NeuroImage Resting state fMRI: A personal history', NeuroImage. Elsevier Inc., 62(2), pp. 938–944. doi: 10.1016/j.neuroimage.2012.01.090.

Biswal, B. B. et al. (2010) 'Toward discovery science of human brain function', Proceedings of the National Academy of Sciences of the United States of America, 107(10), pp. 4734–4739. doi: 10.1073/pnas.0911855107.

Booth, J. R. et al. (2007) 'The role of the basal ganglia and cerebellum in language processing', Brain Research, 1133(1), pp. 136–144.

Burnham, K. P. and Anderson, D. R. (2004) 'Multimodel inference: Understanding AIC and BIC in model selection', Sociological Methods and Research, 33(2), pp. 261–304. doi: 10.1177/0049124104268644.

Caballero-Gaudes, C. and Reynolds, R. C. (2017) 'Methods for cleaning the BOLD fMRI signal', NeuroImage. Elsevier, 154(December 2016), pp. 128–149. doi: 10.1016/j.neuroimage.2016.12.018.

Cai, W. et al. (2014) "Dissociable roles of right inferior frontal cortex and anterior insula in inhibitory control: Evidence from intrinsic and task-related functional parcellation, Connectivity, And response profile analyses across multiple datasets," Journal of Neuroscience, 34(44), pp. 14652–14667. doi:10.1523/JNEUROSCI.3048-14.2014.

Cavanaugh, J. E. and Neath, A. A. (2019) 'The Akaike information criterion: Background, derivation, properties, application, interpretation, and refinements', Wiley Interdisciplinary Reviews: Computational Statistics, 11(3), pp. 1–11. doi: 10.1002/wics.1460.

Chaganti, J. R. et al. (2017) 'Functional connectivity in virally suppressed patients with HIV-associated neurocognitive disorder: A resting-state analysis', American Journal of Neuroradiology, 38(8), pp. 1623–1629. doi: 10.3174/ajnr.A5246.

Cheatwood, J. L., Corwin, J. V and Reep, R. L. (2005) 'Overlap and interdigitation of cortical and thalamic afferents to dorsocentral striatum in the rat', Brain Research, 1036, pp. 90–100. doi: 10.1016/j.brainres.2004.12.049.

Cheatwood, J. L., Reep, R. L. and Corwin, J. V (2003) 'The associative striatum: cortical and thalamic projections to the dorsocentral striatum in rats', Brain Research, 968, pp. 1–14.

Chen, J. E. and Glover, G. H. (2015) 'Functional Magnetic Resonance Imaging Methods Jingyuan', Nature Reviews Neuroscience, 16(12), pp. 756–767. doi: 10.1007/s11065-015-9294-9.Functional.

Cherodath, S. et al. (2017) 'A role for putamen in phonological processing in children', Bilingualism: Language and Cognition, 20(2), pp. 318–326. doi: 10.1017/S1366728916000614.

Cieri, F. (2018) 'Neuroaging through the Lens of the Resting State Networks'. Hindawi, 2018. doi: 10.1155/2018/5080981.

Connor, E. E. O. and Zeffiro, T. A. (2019) 'Why is Clinical fMRI in a Resting State?', 10(April), pp. 1–8. doi: 10.3389/fneur.2019.00420.

Copland, D. (2014) 'The basal ganglia and semantic engagement: Potential insights from semantic priming in individuals with subcortical vascular lesions , Parkinson ' s disease , The basal ganglia and semantic engagement: Potential insights from semantic priming in individ', (December 2003). doi: 10.1017/S1355617703970081.

Cotton, M. F. et al. (2013) 'Early limited antiretroviral therapy is superior to deferred therapy in HIV-infected South African infants: results from the CHER (Children with HIV Early antiRetroviral) Randomized Trial', 23(1), pp. 1–7. doi: 10.1016/S0140-6736(13)61409-9.Early.

Cox J.S., R. W. H. (1996) ' AFNI: Software for analysis and visualization of functional magnetic resonance neuroimages.', Computers and Biomedical Research, 29(29), pp. 162–173.

Craddock, R. C. et al. (2012) 'A whole rain fMRI tlas generated via spatially constrained spectral clustering', Human Brain Mapping, 33(8), pp. 1914–1928. doi: 10.1002/hbm.21333.

Crosson, B. et al. (2003) 'Left and right basal ganglia and frontal activity during language generation: Contributions to lexical, semantic, and phonological processes', Journal of the International Neuropsychological Society, (2003), pp. 1061–1077.

da Silva, R. C. et al. (2013) 'HIV mother-to-child transmission: A complex genetic puzzle tackled by Brazil and Argentina research teams', Infection, Genetics and Evolution. Elsevier B.V., 19, pp. 312–322. doi: 10.1016/j.meegid.2013.03.005.

Davies, M. et al. (2017) 'Survival of HIV-1 vertically infected children', 11(5), pp. 455–464. doi: 10.1097/COH.0000000000000303. . DeLong, M. R. and Wichmann, T. (2007) 'Circuits and circuit disorders of the basal ganglia', Archives of Neurology, 64(1), pp. 20–24. doi: 10.1001/archneur.64.1.20.

Du Plessis, S. et al. (2014) 'HIV infection and the fronto-striatal system: A systematic review and meta-analysis of fMRI studies', Aids, 28(6), pp. 803–811. doi: 10.1097/QAD.0000000000000151.

Durston, S. et al. (2006) 'A shift from diffuse to focal cortical activity with development: Commentary', Developmental Science, 9(1), pp. 1–8. doi: 10.1111/j.1467-7687.2005.00454.x.

Dwyer-lindgren, L. et al. (2017) 'Mapping HIV prevalence in sub-Saharan Africa between 2000 and 2017', Nature. Springer US. doi: 10.1038/s41586-019-1200-9. Eggleton JS, N. S. (2020) Highly Active Antiretroviral Therapy (HAART), StatPearls. Available at: https://www.ncbi.nlm.nih.gov/books/NBK554533/

Ene, L. (2018) 'Human Immunodeficiency Virus in the Brain — Culprit or Facilitator?' doi: 10.1177/1178633717752687.

Fazl, A. and Fleisher, J. (2018) 'Anatomy , Physiology , and Clinical Syndromes of the Basal Ganglia: A Brief Review', Seminars in Pediatric Neurology. Elsevier, 25, pp. 2–9. doi: 10.1016/j.spen.2017.12.005.

Ferpozzi, V. et al. (2018) 'Broca's Area as a Pre-articulatory Phonetic Encoder: Gating the Motor Program', Frontiers in Human Neuroscience, 12(February), pp. 1–17. doi: 10.3389/fnhum.2018.00064.

Fitzmaurice, G. M. and Ravichandran, C. (2008) 'A Primer in Longitudinal Data Analysis', Circulation. doi: 10.1161/CIRCULATIONAHA.107.714618. Florio, T. M. et al. (2018) 'The Basal Ganglia: More than just a switching device', (May), pp. 677–684. doi: 10.1111/cns.12987.

Ford, A. A. et al. (2013) 'Broca's area and its striatal and thalamic connections: a diffusion-MRI tractography study', 7(May), pp. 1–12. doi: 10.3389/fnana.2013.00008.

Fox, M. D. et al. (2005) 'The human brain is intrinsically organized into dynamic, anticorrelated functional networks'.

Geuns, R. M. van, Wielopolski, P. A., Bruin, H. G. de, Rensing, B. J., Ooijen, P. M. A. van, Hulshoff, M., Oudkerk, M., and Feyter, P. J. de. (1999). Basic Principles of Magnetic Resonance Imaging. Progress in Cardiovascular Diseases, 42(2), 149–156.

Global HIV & AIDS statistics—2020 fact sheet (2020) UNAIDS. Available at: https://www.unaids.org/en/resources/fact-sheet (Accessed: 15 July 2020). Glover, G. H. (2011) 'Overview of functional magnetic resonance imaging', Neurosurgery Clinics of North America, 22(2), pp. 133–139. doi: 10.1016/j.nec.2010.11.001.

Goyal, A. and Dhamija, R. K. (2016) 'Neuroimaging in Parkinson's disease', Journal International Medical Sciences Academy, 29(1), pp. 55–58. doi: 10.1007/bf03206608.

Greene, D. J. et al. (2014) 'Developmental changes in the organization of functional connections between the basal ganglia and cerebral cortex', Journal of Neuroscience, 34(17), pp. 5842–5854. doi: 10.1523/JNEUROSCI.3069-13.2014.

Guha, A. et al. (2016) 'Intrinsic network connectivity abnormalities in HIV-infected individuals over age 60', Journal of NeuroVirology, 22(1), pp. 80–87. doi: 10.1007/s13365-015-0370-y.

Haber, S. , Lynd-Balta, E. and Spooren, W. P. J. M. (1994) 'Integrative Aspects of Basal Ganglia Circuitry', in The Basal Ganglia IV. Advances in Behavioral Biology. Springer, Boston, MA, pp. 71–80. doi: https://doi.org/10.1007/978-1-4613-0485-2_7.

Heine, L. et al. (2012) 'Resting state networks and consciousness Alterations of multiple resting state network connectivity in physiological , pharmacological , and pathological consciousness states', 3(August), pp. 1–12. doi: 10.3389/fpsyg.2012.00295.

Hirsch, G. V et al. (2018) 'Using structural and functional brain imaging to uncover how the brain adapts to blindness'.

Hof, M. Van Den et al. (2019) 'Brain structure of perinatally HIV-infected patients on long-term treatment'. doi: 10.1212/CPJ.0000000000000637. Ipser, J. C. et al. (2015) 'HIV infection is associated with attenuated frontostriatal intrinsic connectivity', 21(3), pp. 203–213. doi: 10.1017/S1355617715000156.HIV.

Jankiewicz, M. et al. (2017) 'White Matter Abnormalities in Children with HIV Infection and Exposure', 11(September), pp. 1–9. doi: 10.3389/fnana.2017.00088. Jo, H. J. et al. (2013) 'Effective preprocessing procedures virtually eliminate distance-dependent motion artifacts in resting state FMRI', Journal of Applied Mathematics, 2013(May). doi: 10.1155/2013/935154.

Johnstone, S.J. et al. (2007) “The development of stop-signal and Go/Nogo response inhibition in children aged 7-12 years: Performance and event-related potential indices,” International Journal of Psychophysiology, 63(1), pp. 25–38. doi:10.1016/j.ijpsycho.2006.07.001.

Joseph, S. B. et al. (2019) ‘What can characterization of cerebrospinal fluid escape populations teach us about viral reservoirs in the central nervous system?’, AIDS, (August 2018), pp. 171–179. doi: 10.1097/QAD.0000000000002253. Kamishina, H. et al. (2008) ‘Striatal projections from the rat lateral posterior thalamic nucleus’, Brain Research, 04. doi: 10.1016/j.brainres.2008.01.094.

Kasliwal, M. K. (2013) ‘Functional Neuroimaging: Current Status’, OMICS Journal of Radiology, 01(04), pp. 4–5. doi: 10.4172/2167-7964.1000e111. Kharsany, A. B. M. and Karim, Q. A. (2016) ‘HIV Infection and AIDS in Sub-Saharan Africa: Current Status ’, pp. 34–48. doi: 10.2174/1874613601610010034.

Khundrakpam, B. S. et al. (2013) ‘Developmental Changes in Organization of Structural Brain Networks’, Cerebral Cortex, (September), pp. 2072–2085. doi: 10.1093/cercor/bhs187.

Koekkoek, S. et al. (2008) ‘Neurocognitive function profile in HIV-infected school-age children’, European Journal of Paediatric Neurology. doi: 10.1016/j.ejpn.2007.09.002.

Künzle, H. (1975) ‘Bilateral projections from precentral motor cortex to the putamen and other parts of the basal ganglia. An autoradiographic study in Macaca fascicularis’, Brain research, 88(2), pp. 195–209. Kutner, M. H. et al. (2005) Applied Linear Statistical Models. doi: 10.1080/00224065.1997.11979760.

Lanciego, J. L., Luquin, N. and Obeso, J. A. (2014) ‘Functional Neuroanatomy of the Basal Ganglia Functional Neuroanatomy of the Basal Ganglia’, (October 2012). doi: 10.1101/cshperspect.a009621.

Lanciego, J. L., Luquin, N. and Obeso, J. A. (2014) ‘Functional Neuroanatomy of the Basal Ganglia Functional Neuroanatomy of the Basal Ganglia’, (October 2012). doi: 10.1101/cshperspect.a009621.

Laughton, B. et al. (2012) ‘Early antiretroviral therapy improves neurodevelopmental outcomes in infants’, AIDS, 26(13), pp. 1685–1690. doi: 10.1097/QAD.0b013e328355d0ce.Early.

Laughton, B. et al. (2013) ‘Review article Neurodevelopment in perinatally HIV-infected children: a concern for adolescence’.

Laughton, B. et al. (2018) ‘Five year neurodevelopment outcomes of perinatally HIV-infected children on early limited or deferred continuous antiretroviral therapy’, Journal of the International AIDS Society, 21(5), p. e25106. doi: 10.1002/jia2.25106.

Le Doaré, K., Bland, R. and Newell, L. (2012) ‘Neurodevelopment in Children Born to HIV-Infected Mothers by Infection and Treatment Status abstract’, (082384). doi: 10.1542/peds.2012-0405.

Lee, M. H., Smyser, C. D. and Shimony, J. S. (2014) 'Resting state fMRI: A review of methods and clinical applications', AJNR Am J Neuroradiol, 34(10), pp. 1866–1872. doi: 10.3174/ajnr.A3263.Resting.

Lee, W. H. and Frangou, S. (2017) 'Linking functional connectivity and dynamic properties of resting-state networks', Scientific Reports. Springer US, (November), pp. 1–10. doi: 10.1038/s41598-017-16789-1.

Lehéricy, S. et al. (2006) 'Motor control in basal ganglia circuits using fMRI and brain atlas approaches', Cerebral Cortex, 16(2), pp. 149–161. doi: 10.1093/cercor/bhi089.

Lemée, J. M. et al. (2019) 'Resting-state functional magnetic resonance imaging versus task-based activity for language mapping and correlation with perioperative cortical mapping', Brain and Behavior, 9(10), pp. 1–17. doi: 10.1002/brb3.1362.

Letendre, S. et al. (2009) 'Validation of the CNS Penetration-Effectiveness Rank for Quantifying Antiretroviral Penetration Into the Central Nervous System', 65(1), pp. 65–70. doi: 10.1001/archneurol.2007.31.Validation.

Lewis-de los Angeles, C. P. et al. (2016) 'Deformed Subcortical Structures Are Related to Past HIV Disease Severity in Youth With Perinatally Acquired HIV Infection', Journal of the Pediatric Infectious Diseases Society, 5, pp. S6–S14. doi: 10.1093/jpids/piw051.

Li, W. et al. (2020) 'Longitudinal functional connectivity changes related to dopaminergic decline in Parkinson's disease', NeuroImage: Clinical. Elsevier, 28(April), p. 102409. doi: 10.1016/j.nicl.2020.102409.

Lindsey, J. C. et al. (2006) 'Neurodevelopmental Functioning in HIV-Infected Infants and Young Children Before and After the Introduction of Protease Inhibitor – Based Highly Active Antiretroviral Therapy', 119(3). doi: 10.1542/peds.2006-1145.

Lohndorf, R. T. et al. (2019) 'Preschoolers' problem behavior, prosocial behavior, and language ability in a Latin-American context: The roles of child executive functions and socialization environments', Early Childhood Research Quarterly. Elsevier Inc., 48, pp. 36–49. doi: 10.1016/j.ecresq.2019.02.005.

López-Vicente, M., Agcaoglu, O., Pérez-Crespo, L., Estévez-López, F., Heredia-Genestar, J. M., Mulder, R. H., Flournoy, J. C., van Duijvenvoorde, A. C. K., Güroğlu, B., White, T., Calhoun, V., Tiemeier, H., Muetzel, R. L. (2021). Developmental Changes in Dynamic Functional Connectivity From Childhood Into Adolescence. Frontiers in Systems Neuroscience, 15. https://doi.org/10.3389/fnsys.2021.724805

Lu, H., Jaime, S. and Yang, Y. (2019) 'Origins of the Resting-State Functional MRI Signal: Potential Limitations of the "Neurocentric" Model', Frontiers in Neuroscience, 13(October), pp. 1–8. doi: 10.3389/fnins.2019.01136.

Lv, H. et al. (2018) 'Resting-state functional MRI: Everything that nonexperts have always wanted to know', American Journal of Neuroradiology, 39(8), pp. 1390–1399. doi: 10.3174/ajnr.A5527.

Manesh, A. et al. (2019) 'International Journal of Infectious Diseases Symptomatic HIV CNS viral escape among patients on effective cART', International Journal of Infectious Diseases. International Society for Infectious Diseases, 84, pp. 39–43. doi: 10.1016/j.ijid.2019.03.033.

Manza, P. et al. (2015) 'The effects of age on resting state functional connectivity of the basal ganglia from young to middle adulthood', NeuroImage. Elsevier Inc., 107, pp. 311–322. doi: 10.1016/j.neuroimage.2014.12.016.

Marchand, W. R. et al. (2011) 'Age-related changes of the functional architecture of the cortico-basal ganglia circuitry during motor task execution', NeuroImage. Elsevier B.V., 55(1), pp. 194–203. doi: 10.1016/j.neuroimage.2010.12.030.

Martino, A. Di et al. (2008) 'Functional Connectivity of Human Striatum: A Resting State fMRI Study', Cerebral Cortex, (December). doi: 10.1093/cercor/bhn041.

Masami, G. et al. (2016) 'Head Motion and Correction Methods in Resting-state Functional MRI', 15(2), pp. 178–186. doi: 10.2463/mrms.rev.2015-0060.

Medaglia, J. D. (2017) 'Graph Theoretic Analysis of Resting State Functional MR Imaging', Neuroimaging Clinics of North America. Elsevier Inc, 27(4), pp. 593–607. doi: 10.1016/j.nic.2017.06.008.

Melrose, R. J. et al. (2008) 'Compromised fronto-striatal functioning in HIV: An fMRI investigation of semantic event sequencing', Behavioural Brain Research. doi: 10.1016/j.bbr.2007.11.021.

Meszlényi, R. J. et al. (2017) 'Resting State fMRI Functional Connectivity Analysis Using Dynamic Time Warping', 11(February), pp. 1–17. doi: 10.3389/fnins.2017.00075.

Middleton, F. A. and Strick, P. L. (2000) 'Basal ganglia and cerebellar loops: Motor and cognitive circuits', Brain Research Reviews, 31(2–3), pp. 236–250. doi: 10.1016/S0165-0173(99)00040-5.

Mier, W. and Mier, D. (2015) 'Advantages in functional imaging of the brain', Frontiers in Human Neuroscience, 9(MAY), pp. 1–6. doi: 10.3389/fnhum.2015.00249.

Molfese, P. and Glen, D. (2014) Haskins Pediatric Atlas Anouncement. Available at: https://afni.nimh.nih.gov/afni/community/board/read.php?1,146551,146551

Molfese, P. J. et al. (2021) 'The Haskins pediatric atlas: a magnetic-resonance-imaging-based pediatric template and atlas', Pediatric Radiology. Pediatric Radiology, (51), pp. 628–639.

Moriguchi, Y. (2014) 'The early development of executive function and its relation to social interaction: A brief review', Frontiers in Psychology, 5, pp. 1–6. doi: 10.3389/fpsyg.2014.00388.

Moriguchi, Y. and Hiraki, K. (2011) 'Longitudinal development of prefrontal function during early childhood', Developmental Cognitive Neuroscience. Elsevier Ltd, 1(2), pp. 153–162. doi: 10.1016/j.dcn.2010.12.004.

Moritz, C. H. et al. (2000) 'Whole-brain functional MR imaging activation from a finger-tapping task examined with independent component analysis', American Journal of Neuroradiology, 21(9), pp. 1629–1635.

Mpango, R.S. et al. (2017) "Prevalence and correlates for ADHD and relation with social and academic functioning among children and adolescents with HIV/AIDS in Uganda," BMC Psychiatry, 17(1). doi:10.1186/s12888-017-1488-7.

Nalcia, A., Raob, B. D. and Liua, T. T. (2019) 'Nuisance Effects and the Limitations of Nuisance Regression in Dynamic Functional Connectivity fMRI', NeuroImage, 176(3), pp. 139–148. doi: 10.1016/j.neuroimage.2018.09.024.Nuisance.

Nee, D. E., Wager, T. D. and Jonides, J. (2007) 'Interference resolution: Insights from a meta-analysis of neuroimaging tasks', Cognitive, Affective, and Behavioral Neuroscience, 7(1), pp. 1–17.

Nichols, S. L., Chernoff, M. C., Malee, K. M., Sirois, P. A., Woods, S. P., Williams, P. L., Yildirim, C., Delis, D., and Kammerer, B. (2016). Executive functioning in children and adolescents with perinatal HIV infection and perinatal HIV exposure. Journal of the Pediatric Infectious Diseases Society, 5, S15–S23. https://doi.org/10.1093/jpids/piw049

Nwosu, E. C. et al. (2018) 'Altered brain morphometry in 7-year old HIV-infected children on early ART'. Metabolic Brain Disease, pp. 523–535.

Obeso, J. A. et al. (2002) 'The Basal Ganglia and Disorders of Movement: Pathophysiological Mechanisms', News in Physiological Sciences, 17, pp. 51–55.'

Ortega, M., Brier, M. R., and Ances, B. M. (2015). Effects of HIV and Combination Antiretroviral Therapy (cART) on Cortico-Striatal Functional Connectivity.

AIDS, 176(1), 139–148. https://doi.org/10.1097/QAD.0000000000000611.Effects Panikratova, Y. R. et al. (2020) 'Functional connectivity of the dorsolateral prefrontal cortex contributes to different components of executive functions', International Journal of Psychophysiology. Elsevier, 151, pp. 70–79. doi: 10.1016/j.ijpsycho.2020.02.013.

Park, B. Y., Byeon, K. and Park, H. (2019) 'FuNP (fusion of neuroimaging preprocessing) pipelines: A fully automated preprocessing software for functional magnetic resonance imaging', Frontiers in Neuroinformatics, 13, pp. 1–14. doi: 10.3389/fninf.2019.00005.

Park, J. (2016) 'Movement Disorders Following Cerebrovascular Lesion in the Basal Ganglia Circuit', Journal of Movement Disorders, 9(2), pp. 71–79. doi: 10.14802/jmd.16005.

Parker, D. B. and Razlighi, Q. R. (2019) 'The benefit of slice timing correction in common fMRI preprocessing pipelines', Frontiers in Neuroscience. doi: 10.3389/fnins.2019.00821.

Patel, A. K. et al. (2018) 'Incidence of symptomatic CSF viral escape in HIV infected patients receiving atazanavir / ritonavir (ATV / r) -containing ART: a tertiary care cohort in western India', Jounal of Neurovirology. Journal of NeuroVirology, pp. 498–505.

Pinheiro, J. C. and Bates, D. M. (2000) Mixed-Effects Models in S and S-PLUS, Springer.

Porter, J. N. et al. (2015) 'Developmental Cognitive Neuroscience Age-related changes in the intrinsic functional connectivity of the human ventral vs . dorsal striatum from childhood to middle age', Accident Analysis and Prevention. Elsevier Ltd, 11, pp. 83–95. doi: 10.1016/j.dcn.2014.08.011.

Posada, D. and Buckley, T. R. (2004) 'Model selection and model averaging in phylogenetics: Advantages of akaike information criterion and bayesian approaches over likelihood ratio tests', Systematic Biology, 53(5), pp. 793–808. doi: 10.1080/10635150490522304.

Power, J. D. et al. (2012) 'Spurious but systematic correlations in functional connectivity MRI networks arise from subject motion', NeuroImage. Elsevier Inc., 59(3), pp. 2142–2154. doi: 10.1016/j.neuroimage.2011.10.018.

Richardson, C. et al. (2018) "Development of inhibition and switching: A longitudinal study of the maturation of interference suppression and reversal processes during childhood," Developmental Cognitive Neuroscience, 34, pp. 92–100. doi:10.1016/j.dcn.2018.03.002.

Rogers, B. P. et al. (2007) 'Assessing functional connectivity in the human brain by fMRI', Magnetic Resonance Imaging, 25(10), pp. 1347–1357. doi: 10.1016/j.mri.2007.03.007.

Romero, M. C. et al. (2008) 'Activity of neurons in the caudate and putamen during a visuomotor task', NeuroReport, 19(11), pp. 1141–1145. doi: 10.1097/WNR.0b013e328307c3fc.

Ruel, T. D. et al. (2012) 'Neurocognitive and motor deficits in HIV-infected ugandan children with high CD4 cell counts', Clinical Infectious Diseases, 54(7), pp. 1001–1009. doi: 10.1093/cid/cir1037.

S.A, S. (2020) 'Statistics S.A. Mid-year population estimates 2020', (July), pp. 8–9.

Satterthwaite, T. D. et al. (2013) 'An improved framework for confound regression and filtering for control of motion artifact in the preprocessing of resting-state functional connectivity data', NeuroImage. Elsevier Inc., 64(1), pp. 240–256. doi: 10.1016/j.neuroimage.2012.08.052.

Schachar, R. et al. (2000) "Confirmation of an Inhibitory Control Deficit in Attention-Deficit/Hyperactivity Disorder," Journal of Abnormal Child Psychology, 13(3), pp. 227–235.

Scutari, R. et al. (2017) 'The Role of HIV Infection in Neurologic Injury', pp. 10–18. doi: 10.3390/brainsci7040038.

Shah, A. et al. (2016) 'Neurotoxicity in the Post-HAART Era: Caution for the Antiretroviral Therapeutics', Neurotoxicity Research. Springer US, 30(4), pp. 677–697. doi: 10.1007/s12640-016-9646-0.

Sladky, R. et al. (2011) 'Slice-timing effects and their correction in functional MRI', NeuroImage. Elsevier Inc., 58(2), pp. 588–594. doi: 10.1016/j.neuroimage.2011.06.078. Smith, R. and Chase, C. (2005) 'Effects_of_perinatal_HIV_infec.PDF'.

Smitha, K. et al. (2017) 'Resting state fMRI: A review on methods in resting state connectivity analysis and resting state networks'. doi: 10.1177/1971400917697342.

Szaflarski, J. P., Schmithorst, V. J., Altaye, M., Byars, A. W., Ret, J., Plante, E., & Holland, S. K. (2006). A longitudinal functional magnetic resonance imaging study of language development in children 5 to 11 years old.

Annals of Neurology, 59(5), 796–807. https://doi.org/10.1002/ana.20817 Szczepanski, S. M. and Knight, R. T. (2014) 'Insights into Human Behavior from Lesions to the Prefrontal Cortex', Neuron. Elsevier Inc., 83(5), pp. 1002–1018. doi: 10.1016/j.neuron.2014.08.011.

Teichmann, M., Darcy, I. and Dupoux, E. (2009) 'The role of the striatum in phonological processing . Evidence from early stages of Huntington ' s disease', CORTEX, 45, pp. 839–849. doi: 10.1016/j.cortex.2008.12.005.

Thames, A. D. et al. (2016) 'Increased Subcortical Neural Activity Among HIV+ Individuals During a Lexical Retrieval Task', Neurobiology Disease, 92, pp. 175–182. doi: 10.1016/j.nbd.2015.10.017.INCREASED.

Toich, J. T. F. et al. (2018) 'Functional connectivity alterations between networks and associations with infant immune health within networks in HIV infected children on early treatment: A study at 7 years', Frontiers in Human Neuroscience, 11(January), pp. 1–15. doi: 10.3389/fnhum.2017.00635.

Uysal, S. et al. (2020) "The effect of attention deficit and hyperactivity disorder on ART and appointment adherence among adults living with HIV," Journal of Infection in Developing Countries, 14(3), pp. 304–311. doi:10.3855/jidc.12027.

van den Heuvel, M. P. and Hulshoff Pol, H. E. (2010) 'Exploring the brain network: A review on resting-state fMRI functional connectivity', European Neuropsychopharmacology. Elsevier B.V., 20(8), pp. 519–534. doi: 10.1016/j.euroneuro.2010.03.008.

Van Rie, A. et al. (2007) 'Neurologic and neurodevelopmental manifestations of pediatric HIV/AIDS: A global perspective', European Journal of Paediatric Neurology, 11(1), pp. 1–9.

Van Rie, A. et al. (2010) 'Neurodevelopmental trajectory of HIV-infected children accessing care in Kinshasa, Democratic Republic of Congo', 52(5), pp. 636–642. doi: 10.1097/QAI.0b013e3181b32646.

VanWyhe, K. S. et al. (2021) 'Cognitive outcomes at ages seven and nine years in South African children from the children with HIV early antiretroviral (CHER) trial: a longitudinal investigation', Journal of the International AIDS Society, pp. 1–14. doi: 10.1002/jia2.25734.

Verbruggen, F. and Logan, G.D. (2008) "Response inhibition in the stop-signal paradigm," Trends in Cognitive Sciences, pp. 418–424. doi:10.1016/j.tics.2008.07.005.

Vinas-Guasch, N. and Wu, Y. J. (2017) 'The role of the putamen in language: a meta-analytic connectivity modeling study', Brain Structure and Function, pp. 3991–4004. doi: 10.1007/s00429-017-1450-y.

Violari, A. et al. (2008) 'Early antiretroviral therapy and mortality among HIV-infected infants', New England Journal of Medicine, 359(21), pp. 2233–2244. doi: 10.1056/NEJMoa0800971.

Wade, B. et al. (2019) 'Mapping abnormal subcortical neurodevelopment in a cohort of Thai children with HIV', NeuroImage: Clinical. doi: 10.1016/j.nicl.2019.101810.

Walker, S. Y., Pierre, R. B. and Chang, S. M. (2013) 'Neurocognitive function in HIV-positive children in a developing country', International Journal of Infectious Diseases, 17, pp. 862–867.

Wang, J., Zuo, X. and He, Y. (2010) 'Graph-based network analysis of resting-state functional MRI', Frontiers in Systems Neuroscience, 4(June), pp. 1–14. doi: 10.3389/fnsys.2010.00016.

Wei, W. and Wang, X.J. (2016) "Inhibitory Control in the Cortico-Basal Ganglia-Thalamocortical Loop: Complex Regulation and Interplay with Memory and Decision Processes," Neuron, 92(5), pp. 1093–1105. doi:10.1016/j.neuron.2016.10.031.

Wierenga, L. et al. (2014) 'Typical development of basal ganglia, hippocampus, amygdala and cerebellum from age 7 to 24', NeuroImage. Elsevier Inc., 96, pp. 67–72. doi: 10.1016/j.neuroimage.2014.03.072.

Yadav, S. K. et al. (2017) 'Altered structural brain changes and neurocognitive performance in pediatric HIV', NeuroImage: Clinical. The Author(s), 14, pp. 316–322. doi: 10.1016/j.nicl.2017.01.032.

Yadav, S. K. et al. (2018) 'Changes in resting-state functional brain activity are associated with waning cognitive functions in HIV-infected children', NeuroImage: Clinical. Elsevier, pp. 1204–1210. doi: 10.1016/j.nicl.2018.10.028.

Yan, C. et al. (2013) 'A comprehensive assessment of regional variation in the impact of head micromovements on functional connectomics', NeuroImage. Elsevier Inc., 76, pp. 183–201. doi: 10.1016/j.neuroimage.2013.03.004.

Yang, Z. et al. (2019) 'Robust Motion Regression of Resting-State Data Using a Convolutional Neural Network Model', Frontiers in Neuroscience, 13(February), pp. 1–14. doi: 10.3389/fnins.2019.00169.

Yin, H. H. (2019) 'The basal ganglia in action', 23(3), pp. 299–313. doi: 10.1177/1073858416654115.

Zelazo, P. D. et al. (2003) 'The Development of Executive Function in Early Childhood', Monographs of the Society for Research in Child Development, 68(3), pp. 5–24.

Zelazo, P. D. et al. (2003) 'The Development of Executive Function in Early Childhood', Monographs of the Society for Research in Child Development, 68(3), pp. 5–24.

Zhang, S. et al. (2018) 'Characterizing and Differentiating Task-based and Resting State FMRI Signals via Two-stage Sparse Representations', Physiology & behavior, 176(1), pp. 139–148. doi: 10.1016/j.physbeh.2017.03.040.

Zhuang, Y. et al. (2017) 'Combination antiretroviral therapy improves cognitive performance and functional connectivity in treatment-naïve HIV-infected individuals', Jounal of Neurovirology. Journal of NeuroVirology, pp. 704–712. doi: 10.1007/s13365-017-0553-9.

9. Bibliography

Amaro, E., and Barker, G. J. (2006). Study design in fMRI: Basic principles. Brain and Cognition, 60, 220–232. https://doi.org/10.1016/j.bandc.2005.11.009

Gore, J. C. (2003). Principles and practice of functional MRI of the human brain. The Journal of Clinical Investigation, 112(1). https://doi.org/10.1172/JCI200319010.Conventional

Grover, V. P. B., Tognarelli, J. M., Crossey, M. M. E., Cox, I. J., Taylor-robinson, S. D., and Mcphail, M. J. W. (2015). Magnetic Resonance Imaging: Principles and Techniques: Lessons for Clinicians. Journal of Clinical and Experimental Hepatology, 5(3), 246–255. https://doi.org/10.1016/j.jceh.2015.08.001

Kim, S., and Bandettini, P. A. (1890). Principles of Functional MRI. 12–13. Lindquist, M. A., and Wager, T. D. (2014). Principles of functional Magnetic Resonance Imaging. Handbook of Neuroimaging Data Analysis, 3–48.

Radue, E. W., Weigel, M., Wiest, R., and Urbach, H. (2016). Introduction to Magnetic Resonance Imaging for Neurologists. CONTINUUM Lifelong Learning in Neurology, 22(5), 1379–1398. https://doi.org/10.1212/CON.0000000000000391

Wager, T. D., and Lindquist, M. A. (n.d.). Principles of fMRI.

A. Appendix A - Preprocessing Code

```
afni_proc.py \
    -subj_id ${sub_name}                                          \
                -dsets ${resting_set}                                      \
                -copy_anat ${anat_set}                                        \
                -blocks despike tshift align tlrc volreg blur mask regress    \
                -tcat_remove_first_trs 0                                      \
          -align_opts_aea -cost lpc+ZZ -giant_move                  \
                -volreg_align_e2a                                     \
                -volreg_tlrc_warp                                     \
          -tlrc_base ~/HaskinsPeds_NL_template1.0+tlrc                  \
          -tlrc_NL_warp                           \
                -blur_size 6.0                                        \
                -mask_apply epi                                       \
                -mask_segment_anat yes                                \
                -regress_bandpass 0.01 0.1                            \
                -regress_apply_mot_types demean deriv                 \
                -regress_ROI WMe CSFe                                 \
                -regress_RSFC                                            \
                -regress_run_clustsim no                              \
                -regress_est_blur_errts
```

Figure A.1: These AFNI_proc.py commands were used to preprocess the data. The sub_name, resting_set, and anat_set define the subject's ID, subject's resting-state data, and subject's anatomical data, respectively.

B. Appendix B - R Code

READ IN DATA FOR EACH BG SEED

```
############################################################
#Read in txt and csv file

#Zscore results for left putamen and demographics
dat7 <- read.delim("7_level20thr34ROI_1.txt",
fileEncoding="UTF-8-BOM", sep = " ")
dat9A <- read.delim("9A_level20thr34ROI_1.txt",
fileEncoding="UTF-8-BOM", sep = " ")
dat9S <- read.delim("9S_level20thr34ROI_1.txt",
fileEncoding="UTF-8-BOM", sep = " ")
dat11<- read.delim("11_level20thr34ROI_1.txt",
fileEncoding="UTF-8-BOM", sep = " ")
demographics <- read.csv("HIVdemographics.csv",
fileEncoding="UTF-8-BOM", sep = ";")

#motion
mot7 <- read.csv("7_motion.csv",
fileEncoding="UTF-8-BOM", sep = ";")
mot9A <- read.csv("9A_motion.csv",
fileEncoding="UTF-8-BOM", sep = ";")
mot9S <- read.csv("9S_motion.csv",
fileEncoding="UTF-8-BOM", sep = ";")
mot11<- read.csv("11_motion.csv",
fileEncoding="UTF-8-BOM", sep = ";")


#combine Zscore7, Zscore9A
newdataframe <- merge(dat7,dat9A,
by = "id", all = TRUE)

#combine Zscore7, Zscore9A, Zscore9S
newdataframe2 <- merge(newdataframe,dat9S,
by = "id", all = TRUE)

#combine  Zscore7, Zscore9A, Zscore9S, Zscore11
newdataframe3 <- merge(newdataframe2,dat11,
by = "id", all = TRUE)

#combine demographic data with Zscores
newdataframe4 <- merge(newdataframe3, demographics,
by = "id")

#combine motion data
mot1 <- merge(mot7,mot9A, by = "id", all = TRUE)
mot2 <- merge(mot1,mot9S, by = "id", all = TRUE)
motion_all <- merge(mot2,mot11, by = "id", all = TRUE)

fulldataframe <- merge(newdataframe4,motion_all)


######
mot7_1 <- subset(mot7, select= -4)
mot9A_1 <- subset(mot9A, select= -4)
mot9S_1 <- subset(mot9S, select= -4)
```

```
mot11_1 <- subset(mot11, select= -4)

d7_1 <- merge(dat7,mot7_1,by = "id" )
d9A_1 <- merge(dat9A,mot9A_1,by = "id")
d9S_1 <- merge(dat9S,mot9S_1,by = "id")
d11_1 <- merge(dat11,mot11_1,by = "id")

d1m_1 <- merge(d7_1,d9A_1, all =TRUE)
d2m_1 <- merge(d1m_1,d9S_1, all =TRUE)
d3m_1 <- merge(d2m_1,d11_1, all =TRUE)

dfinal_1 <- merge(d3m_1, demographics, by ="id")

#################################################################
#Zscore results right putamen
dat7_2 <- read.delim("7_level20thr34ROI_2.txt",
fileEncoding="UTF-8-BOM", sep = " ")
dat9A_2 <- read.delim("9A_level20thr34ROI_2.txt",
fileEncoding="UTF-8-BOM", sep = " ")
dat9S_2 <- read.delim("9S_level20thr34ROI_2.txt",
fileEncoding="UTF-8-BOM", sep = " ")
dat11_2<- read.delim("11_level20thr34ROI_2.txt",
fileEncoding="UTF-8-BOM", sep = " ")

d7_2 <- merge(dat7_2,mot7_1,by = "id" )
d9A_2 <- merge(dat9A_2,mot9A_1,by = "id")
d9S_2 <- merge(dat9S_2,mot9S_1,by = "id")
d11_2 <- merge(dat11_2,mot11_1,by = "id")

d1m_2 <- merge(d7_2,d9A_2, all =TRUE)
d2m_2 <- merge(d1m_2,d9S_2, all =TRUE)
d3m_2 <- merge(d2m_2,d11_2, all =TRUE)

dfinal_2 <- merge(d3m_2, demographics, by ="id")
#################################################################
#Zscore results for left caudate

dat7_4 <- read.delim("7_level20thr34ROI_4.txt",
fileEncoding="UTF-8-BOM", sep = " ")
dat9A_4 <- read.delim("9A_level20thr34ROI_4.txt",
fileEncoding="UTF-8-BOM", sep = " ")
dat9S_4 <- read.delim("9S_level20thr34ROI_4.txt",
fileEncoding="UTF-8-BOM", sep = " ")
dat11_4<- read.delim("11_level20thr34ROI_4.txt",
fileEncoding="UTF-8-BOM", sep = " ")

d7_4 <- merge(dat7_4,mot7_1,by = "id" )
d9A_4 <- merge(dat9A_4,mot9A_1,by = "id")
d9S_4 <- merge(dat9S_4,mot9S_1,by = "id")
d11_4 <- merge(dat11_4,mot11_1,by = "id")

d1m_4 <- merge(d7_4,d9A_4, all =TRUE)
d2m_4 <- merge(d1m_4,d9S_4, all =TRUE)
d3m_4 <- merge(d2m_4,d11_4, all =TRUE)
```

```
dfinal_4 <- merge(d3m_4, demographics, by ="id")

#################################################################
#Zscore results for right caudate

dat7_5 <- read.delim("7_level20thr34ROI_5.txt",
fileEncoding="UTF-8-BOM", sep = " ")
dat9A_5 <- read.delim("9A_level20thr34ROI_5.txt",
fileEncoding="UTF-8-BOM", sep = " ")
dat9S_5 <- read.delim("9S_level20thr34ROI_5.txt",
fileEncoding="UTF-8-BOM", sep = " ")
dat11_5<- read.delim("11_level20thr34ROI_5.txt",
fileEncoding="UTF-8-BOM", sep = " ")

d7_5 <- merge(dat7_5,mot7_1,by = "id" )
d9A_5 <- merge(dat9A_5,mot9A_1,by = "id")
d9S_5 <- merge(dat9S_5,mot9S_1,by = "id")
d11_5 <- merge(dat11_5,mot11_1,by = "id")

d1m_5 <- merge(d7_5,d9A_5, all =TRUE)
d2m_5 <- merge(d1m_5,d9S_5, all =TRUE)
d3m_5 <- merge(d2m_5,d11_5, all =TRUE)

dfinal_5 <- merge(d3m_5, demographics, by ="id")
#################################################################
#Zscore results left GP

dat7_7 <- read.delim("7_level20thr34ROI_7.txt",
fileEncoding="UTF-8-BOM", sep = " ")
dat9A_7 <- read.delim("9A_level20thr34ROI_7.txt",
fileEncoding="UTF-8-BOM", sep = " ")
dat9S_7 <- read.delim("9S_level20thr34ROI_7.txt",
fileEncoding="UTF-8-BOM", sep = " ")
dat11_7<- read.delim("11_level20thr34ROI_7.txt",
fileEncoding="UTF-8-BOM", sep = " ")

d7_7 <- merge(dat7_7,mot7_1,by = "id" )
d9A_7 <- merge(dat9A_7,mot9A_1,by = "id")
d9S_7 <- merge(dat9S_7,mot9S_1,by = "id")
d11_7 <- merge(dat11_7,mot11_1,by = "id")

d1m_7 <- merge(d7_7,d9A_7, all =TRUE)
d2m_7 <- merge(d1m_7,d9S_7, all =TRUE)
d3m_7 <- merge(d2m_7,d11_7, all =TRUE)

dfinal_7 <- merge(d3m_7, demographics, by ="id")

#################################################################
#Zscore results right GP

dat7_8 <- read.delim("7_level20thr34ROI_8.txt",
fileEncoding="UTF-8-BOM", sep = " ")
dat9A_8 <- read.delim("9A_level20thr34ROI_8.txt",
fileEncoding="UTF-8-BOM", sep = " ")
dat9S_8 <- read.delim("9S_level20thr34ROI_8.txt",
```

```
fileEncoding="UTF-8-BOM", sep = " ")
dat11_8<- read.delim("11_level20thr34ROI_8.txt",
fileEncoding="UTF-8-BOM", sep = " ")

d7_8 <- merge(dat7_8,mot7_1,by = "id" )
d9A_8 <- merge(dat9A_8,mot9A_1,by = "id")
d9S_8 <- merge(dat9S_8,mot9S_1,by = "id")
d11_8 <- merge(dat11_8,mot11_1,by = "id")

d1m_8 <- merge(d7_8,d9A_8, all =TRUE)
d2m_8 <- merge(d1m_8,d9S_8, all =TRUE)
d3m_8 <- merge(d2m_8,d11_8, all =TRUE)

dfinal_8 <- merge(d3m_8, demographics, by ="id")

#################################################################
#Zscore results for left thalamus

dat7_10 <- read.delim("7_level20thr34ROI_10.txt",
fileEncoding="UTF-8-BOM", sep = " ")
dat9A_10 <- read.delim("9A_level20thr34ROI_10.txt",
fileEncoding="UTF-8-BOM", sep = " ")
dat9S_10 <- read.delim("9S_level20thr34ROI_10.txt",
fileEncoding="UTF-8-BOM", sep = " ")
dat11_10<- read.delim("11_level20thr34ROI_10.txt",
fileEncoding="UTF-8-BOM", sep = " ")

d7_10 <- merge(dat7_10,mot7_1,by = "id" )
d9A_10 <- merge(dat9A_10,mot9A_1,by = "id")
d9S_10 <- merge(dat9S_10,mot9S_1,by = "id")
d11_10 <- merge(dat11_10,mot11_1,by = "id")

d1m_10 <- merge(d7_10,d9A_10, all =TRUE)
d2m_10 <- merge(d1m_10,d9S_10, all =TRUE)
d3m_10 <- merge(d2m_10,d11_10, all =TRUE)

dfinal_10 <- merge(d3m_10, demographics, by ="id")

#################################################################
#Zscore results for left thalamus

dat7_11 <- read.delim("7_level20thr34ROI_11.txt",
fileEncoding="UTF-8-BOM", sep = " ")
dat9A_11 <- read.delim("9A_level20thr34ROI_11.txt",
fileEncoding="UTF-8-BOM", sep = " ")
dat9S_11 <- read.delim("9S_level20thr34ROI_11.txt",
fileEncoding="UTF-8-BOM", sep = " ")
dat11_11<- read.delim("11_level20thr34ROI_11.txt",
fileEncoding="UTF-8-BOM", sep = " ")

d7_11 <- merge(dat7_11,mot7_1,by = "id" )
d9A_11 <- merge(dat9A_11,mot9A_1,by = "id")
d9S_11 <- merge(dat9S_11,mot9S_1,by = "id")
d11_11 <- merge(dat11_11,mot11_1,by = "id")
```

```
d1m_11 <- merge(d7_11,d9A_11, all =TRUE)
d2m_11 <- merge(d1m_11,d9S_11, all =TRUE)
d3m_11 <- merge(d2m_11,d11_11, all =TRUE)

dfinal_11 <- merge(d3m_11, demographics, by ="id")

############################################################
```

FORMAT DATA INTO LONG FORMAT AND REMOVE OUTLIERS

```
############################################################
#Reshape data frame from wide format to long ROI1
datalong1 <- reshape(dfinal_1, varying = c("Age_7",
"averagemotion_7", "maxmotion_7", "Scanner7","Zscore_7",
"Age_9", "averagemotion_9A", "maxmotion_9A","Scanner9A", "Zscore_9A",
"Age_9.5", "averagemotion_9S", "maxmotion_9S","Scanner9S","Zscore_9S",
"Age_11","averagemotion_11", "maxmotion_11", "Scanner11","Zscore_11"),
timevar = "year",times = c("7", "9", "9.5", "11"),
v.names = c("Age", "averagemotion", "maxmotion", "Scanner","Zscore"),
direction = "long",
new.row.names = 1:10000, idvar = "id" )


View(datalong1)

#Model does not change when outliers are removed
datalong1 <- datalong1[-c(366), ]

#sort data by id
datalong1.sort <- datalong1[order(datalong1$id),]
#store sorted data in data frame "dat"
datalong1 <- datalong1.sort
head(datalong1)


############################################################
#Reshape data frame from wide format to long right putamen
datalong2 <- reshape(dfinal_2, varying = c("Age_7",
"averagemotion_7", "maxmotion_7", "Scanner7","Zscore_7",
"Age_9", "averagemotion_9A", "maxmotion_9A","Scanner9A", "Zscore_9A",
"Age_9.5", "averagemotion_9S", "maxmotion_9S","Scanner9S","Zscore_9S",
"Age_11","averagemotion_11", "maxmotion_11", "Scanner11","Zscore_11"),
timevar = "year",times = c("7", "9", "9.5", "11"),
v.names = c("Age", "averagemotion", "maxmotion", "Scanner","Zscore"),
direction = "long",
new.row.names = 1:10000, idvar = "id" )

View(datalong2)
#Model does not change when outliers are removed
datalong2 <- datalong2[-c(366), ]

#sort data by id
datalong2.sort <- datalong2[order(datalong2$id),]
#store sorted data in data frame "dat"
datalong2 <- datalong2.sort
```

```
head(datalong2)

#################################################################
#Reshape data frame from wide format to long left caudate
datalong4 <- reshape(dfinal_4, varying = c("Age_7",
"averagemotion_7", "maxmotion_7", "Scanner7","Zscore_7",
"Age_9", "averagemotion_9A", "maxmotion_9A","Scanner9A", "Zscore_9A",
"Age_9.5", "averagemotion_9S", "maxmotion_9S","Scanner9S","Zscore_9S",
"Age_11","averagemotion_11", "maxmotion_11", "Scanner11","Zscore_11"),
timevar = "year",times = c("7", "9", "9.5", "11"),
v.names = c("Age", "averagemotion", "maxmotion", "Scanner","Zscore"),
direction = "long",
new.row.names = 1:10000, idvar = "id" )

View(datalong4)
#Status no longer significant with outliers removed
datalong4 <- datalong4[-c(366), ]

#sort data by id
datalong4.sort <- datalong4[order(datalong4$id),]
#store sorted data in data frame "dat"
datalong4 <- datalong4.sort
head(datalong4)

#################################################################
#Reshape data frame from wide format to long right caudate
datalong5 <- reshape(dfinal_5, varying = c("Age_7",
"averagemotion_7", "maxmotion_7", "Scanner7","Zscore_7",
"Age_9", "averagemotion_9A", "maxmotion_9A","Scanner9A", "Zscore_9A",
"Age_9.5", "averagemotion_9S", "maxmotion_9S","Scanner9S","Zscore_9S",
"Age_11","averagemotion_11", "maxmotion_11", "Scanner11","Zscore_11"),
timevar = "year",times = c("7", "9", "9.5", "11"),
v.names = c("Age", "averagemotion", "maxmotion", "Scanner","Zscore"),
direction = "long",
new.row.names = 1:10000, idvar = "id" )

View(datalong5)
#Model does not change when outliers are removed
datalong5 <- datalong5[-c(366), ]

#sort data by id
datalong5.sort <- datalong5[order(datalong5$id),]
#store sorted data in data frame "dat"
datalong5 <- datalong5.sort
head(datalong5)

#################################################################
#Reshape data frame from wide format to long left GP
datalong7 <- reshape(dfinal_7, varying = c("Age_7",
"averagemotion_7", "maxmotion_7", "Scanner7","Zscore_7",
"Age_9", "averagemotion_9A", "maxmotion_9A","Scanner9A", "Zscore_9A",
"Age_9.5", "averagemotion_9S", "maxmotion_9S","Scanner9S","Zscore_9S",
"Age_11","averagemotion_11", "maxmotion_11", "Scanner11","Zscore_11"),
timevar = "year",times = c("7", "9", "9.5", "11"),
v.names = c("Age", "averagemotion", "maxmotion", "Scanner","Zscore"),
```

```
direction = "long",
new.row.names = 1:10000, idvar = "id" )

View(datalong7)

datalong7 <- datalong7[-c(366), ]

#sort data by id
datalong7.sort <- datalong7[order(datalong7$id),]
#store sorted data in data frame "dat"
datalong7 <- datalong7.sort
head(datalong7)

#################################################################
#Reshape data frame from wide format to long right GP
datalong8 <- reshape(dfinal_8, varying = c("Age_7",
"averagemotion_7", "maxmotion_7", "Scanner7","Zscore_7",
"Age_9", "averagemotion_9A", "maxmotion_9A","Scanner9A", "Zscore_9A",
"Age_9.5", "averagemotion_9S", "maxmotion_9S","Scanner9S","Zscore_9S",
"Age_11","averagemotion_11", "maxmotion_11", "Scanner11","Zscore_11"),
timevar = "year",times = c("7", "9", "9.5", "11"),
v.names = c("Age", "averagemotion", "maxmotion", "Scanner","Zscore"),
direction = "long",
new.row.names = 1:10000, idvar = "id" )

View(datalong8)

datalong8 <- datalong8[-c(366), ]

#sort data by id
datalong8.sort <- datalong8[order(datalong8$id),]
#store sorted data in data frame "dat"
datalong8 <- datalong8.sort
head(datalong8)

#################################################################
#Reshape data frame from wide format to long left thalamus
datalong10 <- reshape(dfinal_10, varying = c("Age_7",
"averagemotion_7", "maxmotion_7", "Scanner7","Zscore_7",
"Age_9", "averagemotion_9A", "maxmotion_9A","Scanner9A", "Zscore_9A",
"Age_9.5", "averagemotion_9S", "maxmotion_9S","Scanner9S","Zscore_9S",
"Age_11","averagemotion_11", "maxmotion_11", "Scanner11","Zscore_11"),
timevar = "year",times = c("7", "9", "9.5", "11"),
v.names = c("Age", "averagemotion", "maxmotion", "Scanner","Zscore"),
direction = "long",
new.row.names = 1:10000, idvar = "id" )

View(datalong10)
#status significant when outliers are removed from data set
datalong10<- datalong10[-c(366), ]


#sort data by id
datalong10.sort <- datalong10[order(datalong10$id),]
#store sorted data in data frame "dat"
```

```
datalong10 <- datalong10.sort
head(datalong10)

#################################################################
#Reshape data frame from wide format to long right thalamus
datalong11 <- reshape(dfinal_11, varying = c("Age_7",
"averagemotion_7", "maxmotion_7", "Scanner7","Zscore_7",
"Age_9", "averagemotion_9A", "maxmotion_9A","Scanner9A", "Zscore_9A",
"Age_9.5", "averagemotion_9S", "maxmotion_9S","Scanner9S","Zscore_9S",
"Age_11","averagemotion_11", "maxmotion_11", "Scanner11","Zscore_11"),
timevar = "year",times = c("7", "9", "9.5", "11"),
v.names = c("Age", "averagemotion", "maxmotion", "Scanner","Zscore"),
direction = "long",
new.row.names = 1:10000, idvar = "id" )

View(datalong11)

#status significant when outliers are removed from data set
datalong11<- datalong11[-c(366), ]


#sort data by id
datalong11.sort <- datalong11[order(datalong11$id),]
#store sorted data in data frame "dat"
datalong11 <- datalong11.sort
head(datalong11)

#################################################################
```

PLOT ZSCORE FC OVER TIME FOR EACH BG SEED

```
#################################################################
#create theme function for plotting
mytheme <- function(){
list(theme_minimal(),theme(legend.position = "none"),
theme(plot.title = element_text(size = 22, hjust = 0.5)),
theme(axis.text = element_text(size = 20),
axis.title = element_text(size = 20, face = "bold")),
labs(title = "",
x = "", y = ""),
theme(panel.grid.minor = element_blank(),
panel.border = element_blank(), axis.line = element_line()))
}
#################################################################
#Scatter plot of Zscore ROI1
pp<-ggplot(data = datalong1,aes(x=Age,y=Zscore,colour=status),
inherit.aes = FALSE) +
geom_point(size=3, data = datalong1, aes(shape = Scanner)) +
xlab("Age ") + ylab("Zscore") +
theme(axis.title = element_text(size=28,family="Verdana")) +
theme(text = element_text(size=20,family="Verdana")) +
stat_smooth(method = "gam", formula = y ~ x, size = 1,
fullrange = TRUE, se=FALSE)
```

```
plot1 <- pp + mytheme() + labs(x = "Age",
y = "Left Putamen Z-score") +
scale_shape_manual( name = "Scanner", values = c(1,2)) +
scale_colour_manual(name = "Status",
values=c("firebrick3", "dodgerblue3"))

plot1

#############################################################
#Scatter plot of Zscore ROI2
pp2<-ggplot(data = datalong2,aes(x=Age,y=Zscore,colour=status),
inherit.aes = FALSE) +
geom_point(size=3, data = datalong2, aes(shape = Scanner)) +
xlab("Age ") + ylab("Zscore") +
theme(axis.title = element_text(size=28,family="Verdana")) +
theme(text = element_text(size=20,family="Verdana")) +
stat_smooth(method = "gam", formula = y ~ x, size = 1,
fullrange = TRUE, se=FALSE)

plot2 <- pp2 + mytheme() + labs(x = "Age",
y = "Right Putamen Z-score") +
scale_shape_manual( name = "Scanner", values = c(1,2)) +
scale_colour_manual(name = "Status",
values=c("firebrick3", "dodgerblue3"))

plot2
#############################################################
#Scatter plot of Zscore ROI4
pp4<-ggplot(data = datalong4,aes(x=Age,y=Zscore,colour=status),
inherit.aes = FALSE) +
geom_point(size=3, data = datalong4, aes(shape = Scanner)) +
xlab("Age ") + ylab("Zscore") +
theme(axis.title = element_text(size=28,family="Verdana")) +
theme(text = element_text(size=20,family="Verdana")) +
stat_smooth(method = "gam", formula = y ~ x,
size = 1, fullrange = TRUE, se=FALSE)

plot4 <- pp4 + mytheme() + labs(x = "Age",
y = "Left Caudate Z-score") +
scale_shape_manual( name = "Scanner", values = c(1,2)) +
scale_colour_manual(name = "Status",
values=c("firebrick3", "dodgerblue3"))


plot4
#############################################################
#Scatter plot of Zscore ROI5
pp5<-ggplot(data = datalong5,aes(x=Age,y=Zscore,colour=status),
inherit.aes = FALSE) +
geom_point(size=3, data = datalong5, aes(shape = Scanner)) +
xlab("Age ") + ylab("Zscore") +
theme(axis.title = element_text(size=28,family="Verdana")) +
theme(text = element_text(size=20,family="Verdana")) +
stat_smooth(method = "gam", formula = y ~ x, size = 1,
fullrange = TRUE, se=FALSE)
```

```
plot5 <- pp5 + mytheme() + labs(x = "Age",
y = "Right Caudate Z-score") +
scale_shape_manual( name = "Scanner", values = c(1,2)) +
scale_colour_manual(name = "Status",
values=c("firebrick3", "dodgerblue3"))

plot5
#################################################################
#Scatter plot of Zscore ROI7
pp7<-ggplot(data = datalong7,aes(x=Age,y=Zscore,colour=status),
inherit.aes = FALSE) +
geom_point(size=3, data = datalong7, aes(shape = Scanner)) +
xlab("Age ") + ylab("Zscore") +
theme(axis.title = element_text(size=28,family="Verdana")) +
theme(text = element_text(size=20,family="Verdana")) +
stat_smooth(method = "gam", formula = y ~ x, size = 1,
fullrange = TRUE, se=FALSE)


plot7 <- pp7 + mytheme() + labs(x = "Age", y = "Left GP Z-score") +
scale_shape_manual( name = "Scanner", values = c(1,2)) +
scale_colour_manual(name = "Status",
values=c("firebrick3", "dodgerblue3"))

plot7
#################################################################
#Scatter plot of Zscore ROI8
pp8<-ggplot(data = datalong8,aes(x=Age,y=Zscore,colour=status),
inherit.aes = FALSE) +
geom_point(size=3, data = datalong8, aes(shape = Scanner)) +
xlab("Age ") + ylab("Zscore") +
theme(axis.title = element_text(size=28,family="Verdana")) +
theme(text = element_text(size=20,family="Verdana")) +
stat_smooth(method = "gam", formula = y ~ x, size = 1,
fullrange = TRUE, se=FALSE)


plot8 <- pp8 + mytheme() + labs(x = "Age",
y = "Right GP Z-score") +
scale_shape_manual( name = "Scanner", values = c(1,2)) +
scale_colour_manual(name = "Status",
values=c("firebrick3", "dodgerblue3"))

plot8

#################################################################
#Scatter plot of Zscore ROI10
pp10<-ggplot(data = datalong10,aes(x=Age,y=Zscore,colour=status),
inherit.aes = FALSE) +
geom_point(size=3, data = datalong10, aes(shape = Scanner)) +
xlab("Age ") + ylab("Zscore") +
theme(axis.title = element_text(size=28,family="Verdana")) +
theme(text = element_text(size=20,family="Verdana")) +
stat_smooth(method = "gam", formula = y ~ x, size = 1,
fullrange = TRUE, se=FALSE)
```

```
plot10 <- pp10 + mytheme() + labs(x = "Age",
y = "Left Thalamus Z-score") +
scale_shape_manual( name = "Scanner", values = c(1,2)) +
scale_colour_manual(name = "Status",
values=c("firebrick3", "dodgerblue3"))

plot10

#############################################################
#Scatter plot of Zscore ROI11
pp11<-ggplot(data = datalong11,aes(x=Age,y=Zscore,colour=status),
inherit.aes = FALSE) +
geom_point(size=3, data = datalong11, aes(shape = Scanner)) +
xlab("Age ") + ylab("Zscore") +
theme(axis.title = element_text(size=28,family="Verdana")) +
theme(text = element_text(size=20,family="Verdana")) +
stat_smooth(method = "gam", formula = y ~ x, size = 1,
fullrange = TRUE, se=FALSE)


plot11 <- pp11 + mytheme() + labs(x = "Age",
y = "Right Thalamus Z-score") +
scale_shape_manual( name = "Scanner", values = c(1,2)) +
scale_colour_manual(name = "Status",
values=c("firebrick3", "dodgerblue3"))

plot11

#############################################################
#Combine all plots into a grid
library(gridExtra)
grid1<- grid.arrange(plot1, plot2, plot4, plot5,ncol = 2)
grid2 <- grid.arrange(plot7, plot8, plot10, plot11, ncol =2)

#############################################################
```

LME MODEL FORMULATION

```
#############################################################
#Model building
#grouped data object
z_dat <- groupedData(Zscore ~ Age|id, data = datalong1)

#############################################################

#Age effect
mod1 <- lme(Zscore ~ Age, data = z_dat, random = ~1|id,
na.action = na.exclude, method = "ML")
summary(mod1)

#Age and status
mod2 <- lme(Zscore ~ Age + status, data = z_dat,
random = ~1|id,na.action = na.exclude, method = "ML")
```

```
summary(mod2)
anova(mod1,mod2) #used for model comparison

#Age and status interaction
mod2b <- lme(Zscore ~ Age*status, data = z_dat,
random = ~1|id, na.action = na.exclude, method = "ML")
summary(mod2b)
anova(mod2,mod2b)

#Age and scanner
mod3 <- lme(Zscore ~ Age + Scanner, data = z_dat,
random = ~1|id, na.action = na.exclude, method = "ML")
summary(mod3)

#Age and gender
mod4 <- lme(Zscore ~ Age + Gender, data = z_dat,
random = ~1|id, na.action = na.exclude, method = "ML")
summary(mod4)

#Inclusion of motion
mod5 <- lme(Zscore ~ Age*status + Scanner,
data = z_dat, random = ~1|id, na.action = na.exclude,
method = "ML")
summary(mod5)
#maxmotion
mod5b <- lme(Zscore ~ Age*status + Scanner + maxmotion,
data = z_dat, random = ~1|id, na.action = na.exclude,
method = "ML")
summary(mod5b)
anova(mod5,mod5b)
#averagemotion (mean displacement)
mod6<-  lme(Zscore ~ Age*status + Scanner + averagemotion,
data = z_dat, random = ~1|id, na.action = na.exclude,
method = "ML")
summary(mod6)
anova(mod5,mod6)

#################################################################
```

MODEL VERIFICATION

```
#################################################################
#create function for plotting histograms
hist_func <- function(x){
test <- hist(x, plot = FALSE)
dat <- data.frame(d=x)
hist <- ggplot(dat, aes(x=d)) +
geom_histogram(breaks=test$breaks,
fill = "lightgreen",
color = "darkgreen", bins = length(test$breaks),alpha=.2) +
mytheme() + ggtitle("Between-subject Residuals")
+ labs(x = "Residuals", y = "Freqeuncy")
}

hist_func2 <- function(x){
```

```
test <- hist(x, plot = FALSE)
dat <- data.frame(d=x)
hist <- ggplot(dat, aes(x=d)) +
geom_histogram(breaks=test$breaks,
fill = "yellow",
color = "orange", bins = length(test$breaks),alpha=.2) +
mytheme() + ggtitle("Within-subject Residuals")
+ labs(x = "Residuals", y = "Freqeuncy")
}

df <- augment(mod6)

############################################################
#Plot residuals for each BG seed
r1 <- ggplot(df, aes(x = .fitted, y = .resid))+
geom_point(size=2)+
theme(axis.title = element_text(size=20,family="Verdana")) +
theme(text = element_text(size=20,family="Verdana"))

res1 <- r1+
mytheme()+
labs(x = "Fitted Values", y = "Residuals")+
ggtitle("Between-subject Fitted Values vs Residuals ")

hist1_1 <- hist_func(mod6$residuals[,1])
hist2_1 <- hist_func2(mod6$residuals[,2])

grid.arrange(
arrangeGrob(hist1_1,hist2_1, ncol = 2),res1,
nrow = 2)
############################################################
r2 <- ggplot(df, aes(x = .fitted, y = .resid))+
geom_point(size=2)+
theme(axis.title = element_text(size=20,family="Verdana")) +
theme(text = element_text(size=20,family="Verdana"))

res2 <- r2+
mytheme()+
labs(x = "Fitted Values", y = "Residuals")+
ggtitle("Between-subject Fitted Values vs Residuals")


hist1_2 <- hist_func(mod6$residuals[,1])
hist2_2 <- hist_func2(mod6$residuals[,2])

grid.arrange(
arrangeGrob(hist1_2,hist2_2, ncol = 2),res2,
nrow = 2)
############################################################

r4 <- ggplot(df, aes(x = .fitted, y = .resid))+
geom_point(size=2)+
theme(axis.title = element_text(size=20,family="Verdana")) +
theme(text = element_text(size=20,family="Verdana"))
```

```
res4 <- r4+
mytheme()+
labs(x = "Fitted Values", y = "Residuals")+
ggtitle("Between-subject Fitted Values vs Residuals")


hist1_4 <- hist_func(mod6$residuals[,1])
hist2_4 <- hist_func2(mod6$residuals[,2])

grid.arrange(
arrangeGrob(hist1_4,hist2_4, ncol = 2),res4,
nrow = 2)
#################################################################

r5 <- ggplot(df, aes(x = .fitted, y = .resid))+
geom_point(size=2)+
theme(axis.title = element_text(size=20,family="Verdana")) +
theme(text = element_text(size=20,family="Verdana"))

res5 <- r5+
mytheme()+
labs(x = "Fitted Values", y = "Residuals")+
ggtitle("Between-subject Fitted Values vs Residuals")

hist1_5 <- hist_func(mod6$residuals[,1])
hist2_5 <- hist_func2(mod6$residuals[,2])

grid.arrange(
arrangeGrob(hist1_5,hist2_5, ncol = 2),res5,
nrow = 2)

#################################################################
r7 <- ggplot(df, aes(x = .fitted, y = .resid))+
geom_point(size=2)+
theme(axis.title = element_text(size=20,family="Verdana")) +
theme(text = element_text(size=20,family="Verdana"))

res7 <- r7+
mytheme()+
labs(x = "Fitted Values", y = "Residuals")+
ggtitle("Between-subject Fitted Values vs Residuals")

hist1_7 <- hist_func(mod6$residuals[,1])
hist2_7 <- hist_func2(mod6$residuals[,2])

grid.arrange(
arrangeGrob(hist1_7,hist2_7, ncol = 2),res7,
nrow = 2)
#################################################################

r8 <- ggplot(df, aes(x = .fitted, y = .resid))+
geom_point(size=2)+
theme(axis.title = element_text(size=20,family="Verdana")) +
theme(text = element_text(size=20,family="Verdana"))
```

```
res8 <- r8+
mytheme()+
labs(x = "Fitted Values", y = "Residuals")+
ggtitle("Between-subject Fitted Values vs Residuals")

hist1_8 <- hist_func(mod6$residuals[,1])
hist2_8 <- hist_func2(mod6$residuals[,2])

grid.arrange(
arrangeGrob(hist1_8,hist2_8, ncol = 2),res8,
nrow = 2)

#############################################################

r10 <- ggplot(df, aes(x = .fitted, y = .resid))+
geom_point(size=2)+
theme(axis.title = element_text(size=20,family="Verdana")) +
theme(text = element_text(size=20,family="Verdana"))

res10 <- r10+
mytheme()+
labs(x = "Fitted Values", y = "Residuals")+
ggtitle("Between-subject Fitted Values vs Residuals")

hist1_10 <- hist_func(mod6$residuals[,1])
hist2_10 <- hist_func2(mod6$residuals[,2])

grid.arrange(
arrangeGrob(hist1_10,hist2_10, ncol = 2),res10,
nrow = 2)


#############################################################

r11 <- ggplot(df, aes(x = .fitted, y = .resid))+
geom_point(size=2)+
theme(axis.title = element_text(size=20,family="Verdana")) +
theme(text = element_text(size=20,family="Verdana"))

res11 <- r11+
mytheme()+
labs(x = "Fitted Values", y = "Residuals")+
ggtitle("Between-subject Fitted Values vs Residuals")


hist1_11 <- hist_func(mod6$residuals[,1])
hist2_11 <- hist_func2(mod6$residuals[,2])

grid.arrange(
arrangeGrob(hist1_11,hist2_11, ncol = 2),res11,
nrow = 2)

#############################################################
```

C. Appendix C - Model Selection

Table C.1: LME model estimates in which a forward step-wise approach was used to determine significant covariates for the model. If a variable did not improve the model fit, it was removed.

Model	Fixed Effect	Estimate	P-value
1	Intercept	-0.09	0.133
	Age	0.01	0.087
2	Intercept	-0.12	0.075
	Age	0.01	0.08
	Status (HIV)	0.03	0.199
3	Intercept	-0.21	0.08
	Age	0.02	0.061
	Status (HIV)	-0.07	0.598
	Age*Status (HIV)	-0.01	0.278
4	Intercept	-0.28	<0.001
	Age	0.04	<0.001
	Scanner (Skyra)	-0.17	<0.001
5	Intercept	-0.1	0.12
	Age	0.01	0.095
	Gender (Male)	0.01	0.552
6	Intercept	-0.12	0.254
	Age	0.01	0.085
	Volume	<0.001	0.77
7	Intercept	-0.38	0.001
	Age	0.05	<0.001
	Status (HIV)	0.14	0.251
	Scanner (Skyra)	-0.17	<0.001
	Age*Status (HIV)	-0.01	0.331
8	Intercept	-0.44	<0.001
	Age	0.06	<0.001
	Status (HIV)	0.15	0.216
	Scanner (Skyra)	-0.18	<0.001
	Average motion	0.23	0.02
	Age*Status (HIV)	-0.01	0.275
9	Intercept	-0.43	<0.001
	Age	0.05	<0.001
	Status (HIV)	0.14	0.258
	Scanner (Skyra)	-0.16	<0.001
	Max motion	0.02	0.01
	Age*Status (HIV)	-0.01	0.331

D. Appendix D - Model Validation

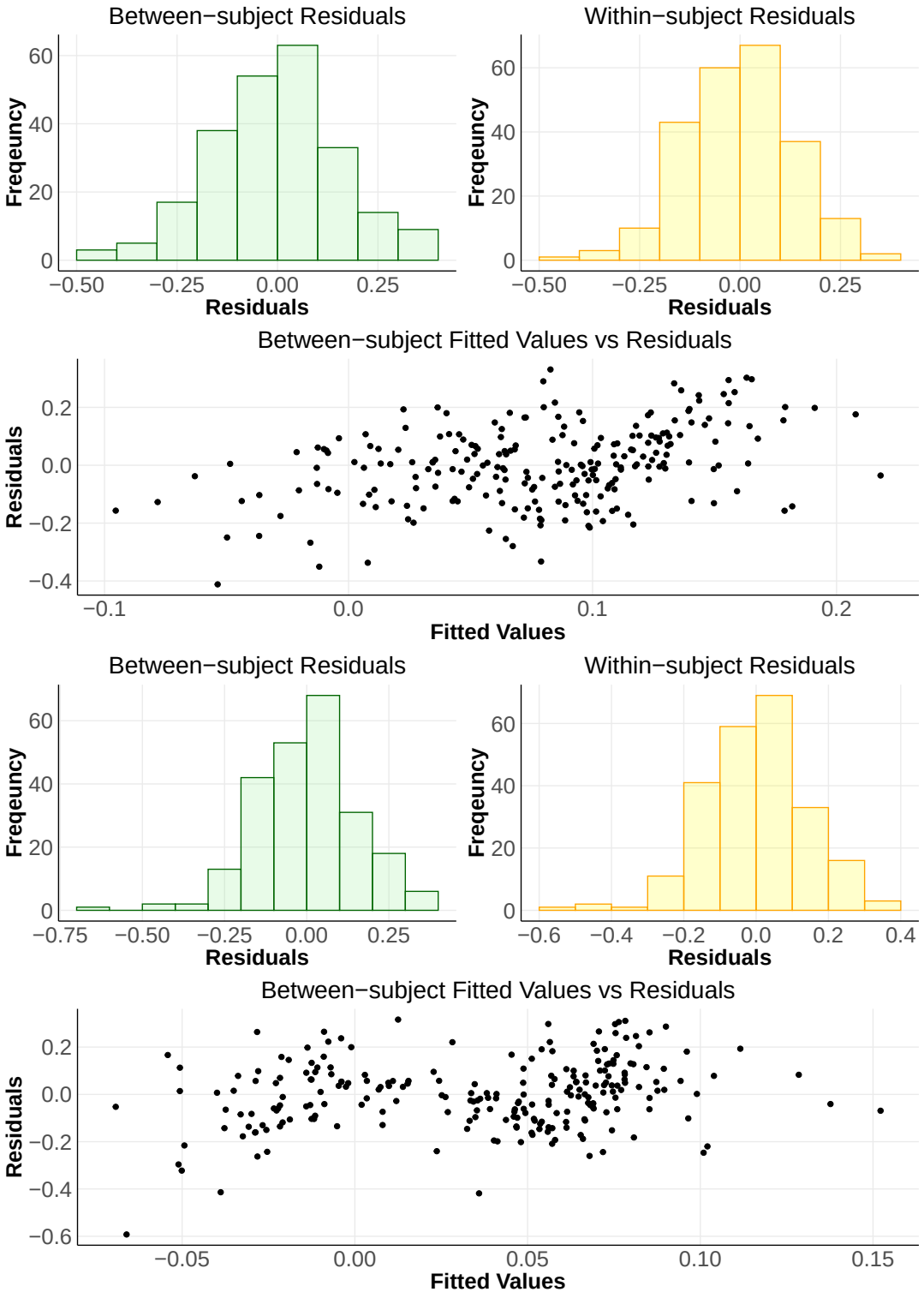

Figure D.1: Between-subject and within-subject residuals are represented by histograms and a scatter plot for Z-score FC measures between left DLPFC region and the left and right putamen.

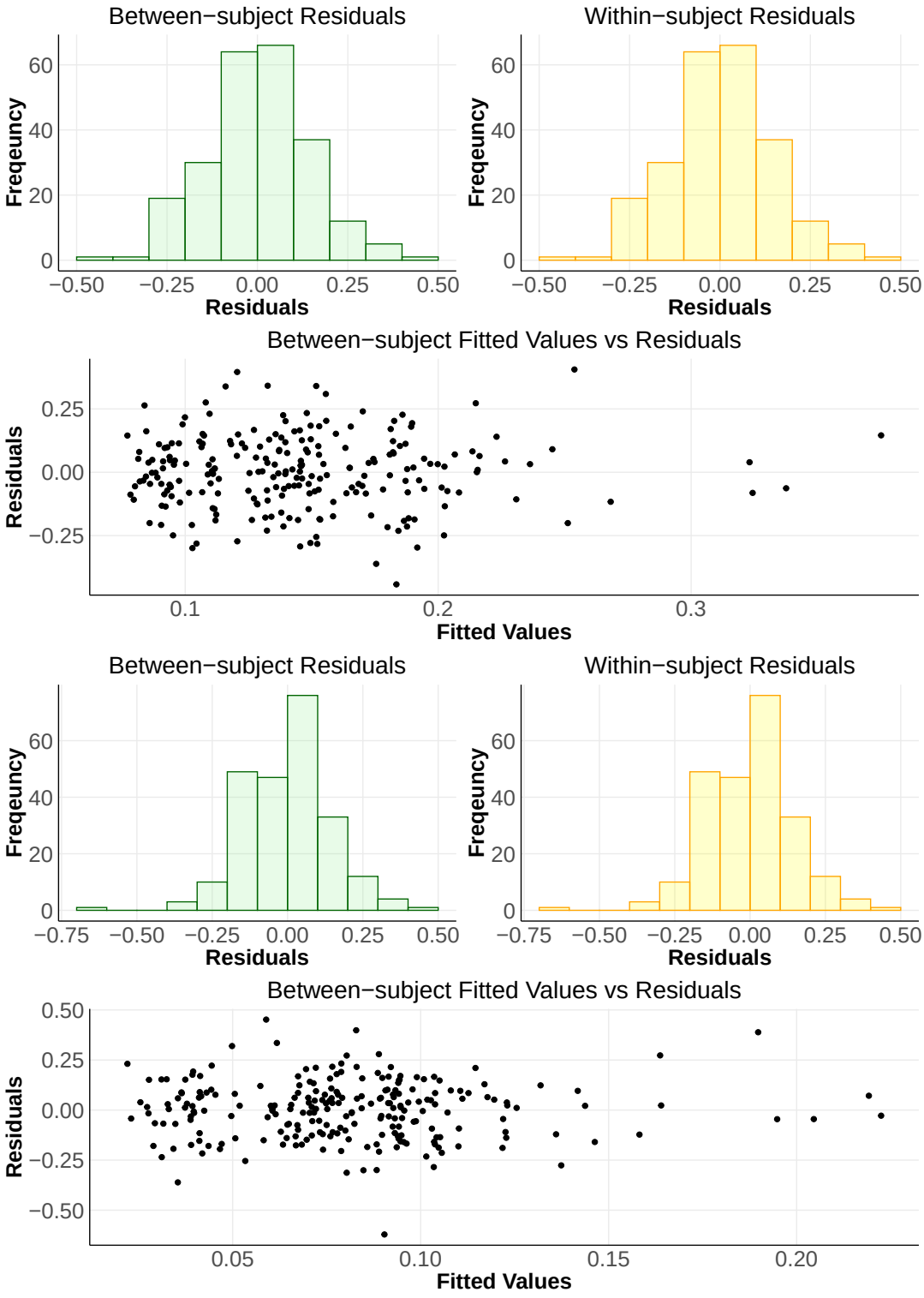

Figure D.2: Between-subject and within-subject residuals are represented by histograms and a scatter plot for Z-score FC measures between left DLPFC region and the left and right caudate.

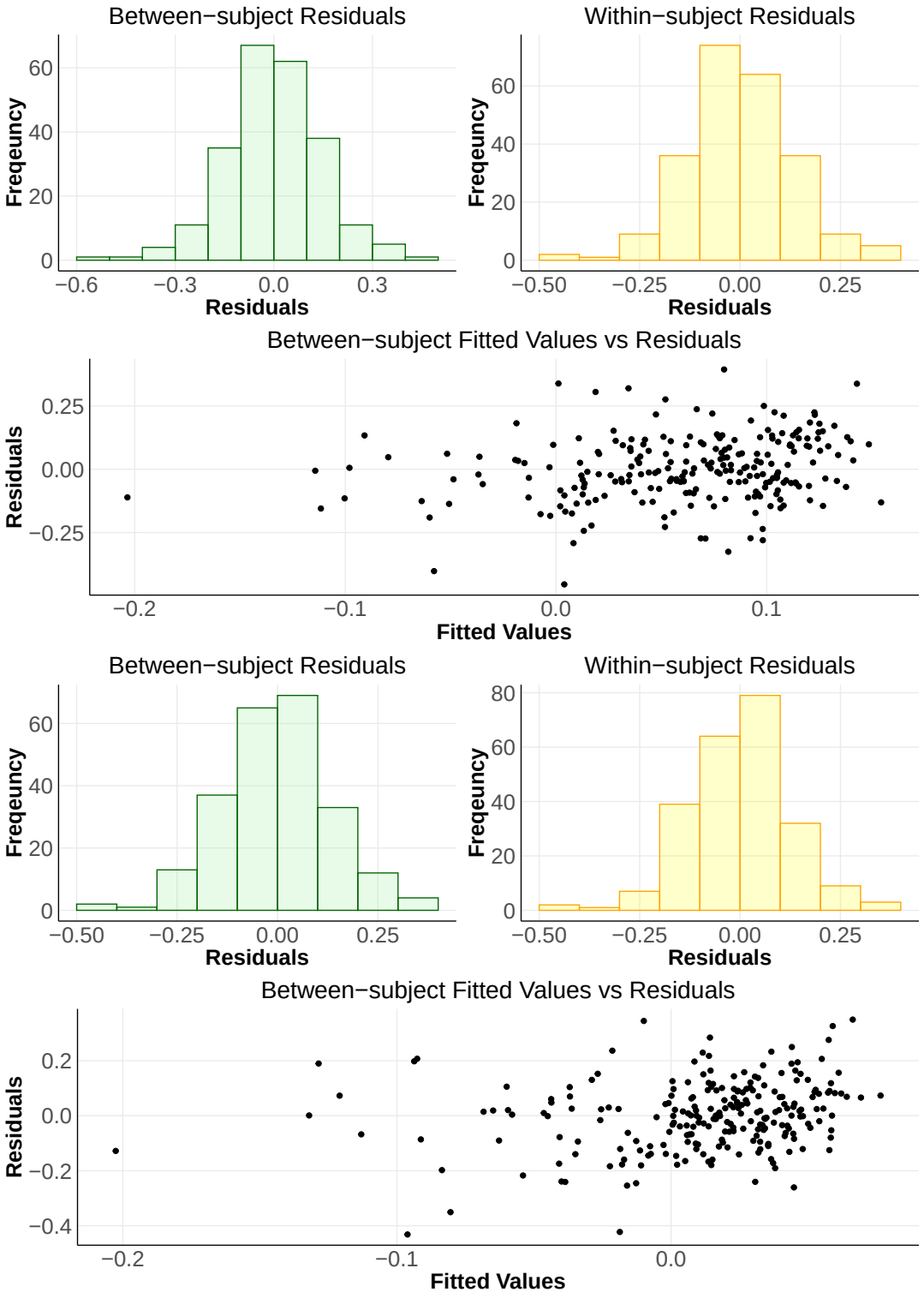

Figure D.3: Between-subject and within-subject residuals are represented by histograms and a scatter plot for Z-score FC measures between left DLPFC region and the left and right GP.

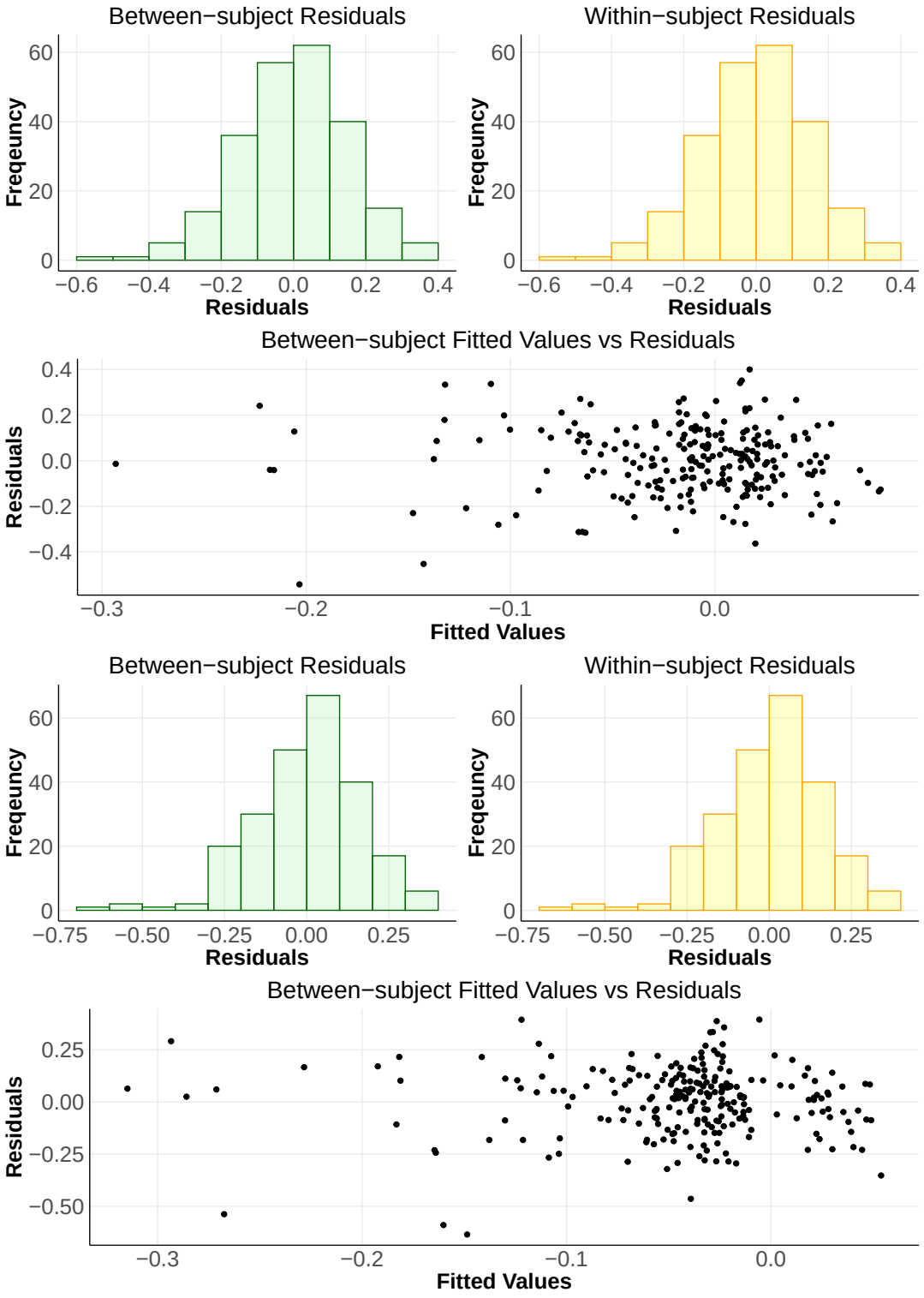

Figure D.4: Between-subject and within-subject residuals are represented by histograms and a scatter plot for Z-score FC measures between left DLPFC region and the left and right thalamus.

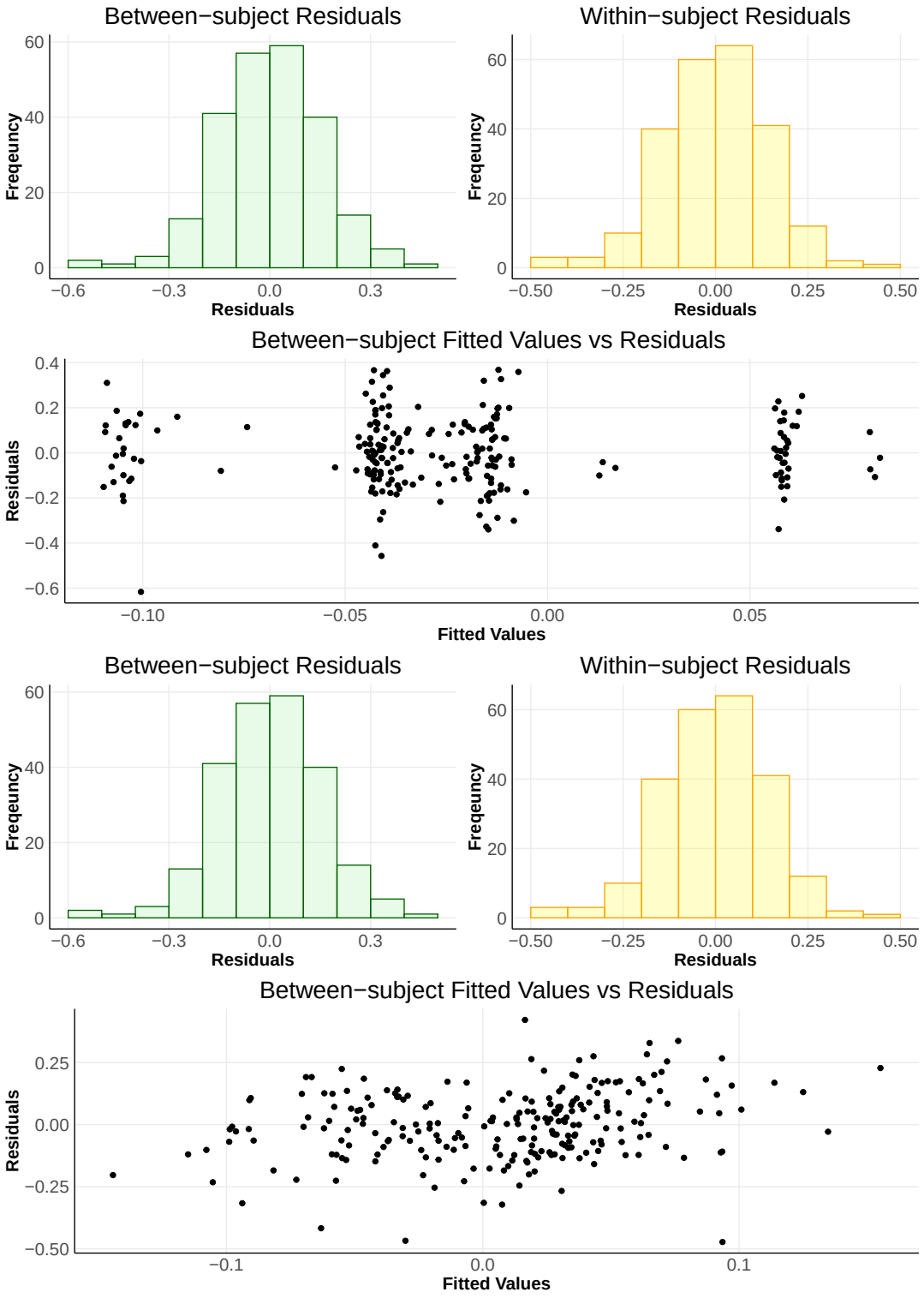

Figure D.5: Between-subject and within-subject residuals are represented by histograms and a scatter plot for Z-score FC measures between right DLPFC region and the left and right putamen.

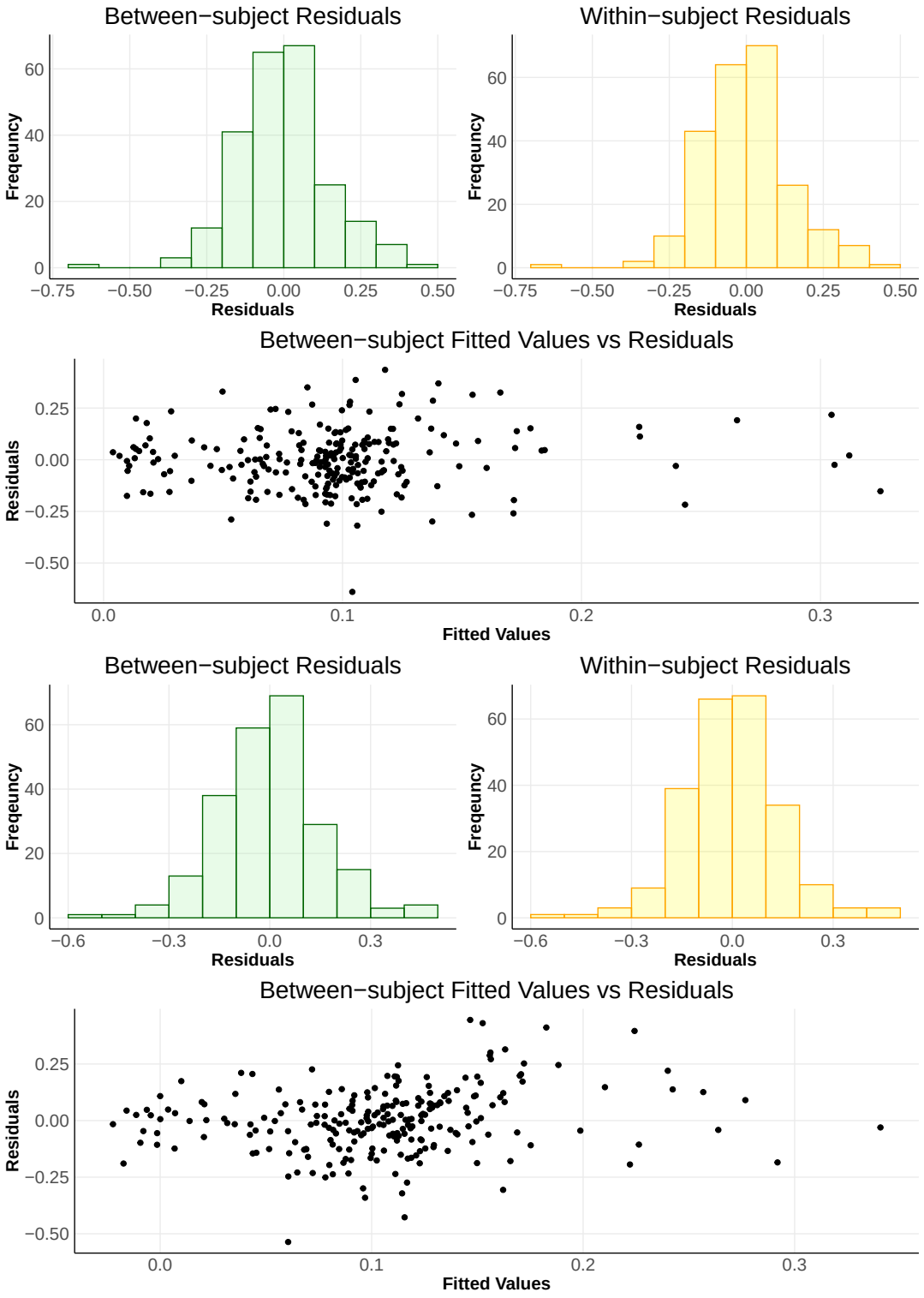

Figure D.6: Between-subject and within-subject residuals are represented by histograms and a scatter plot for Z-score FC measures between right DLPFC region and the left and right caudate.

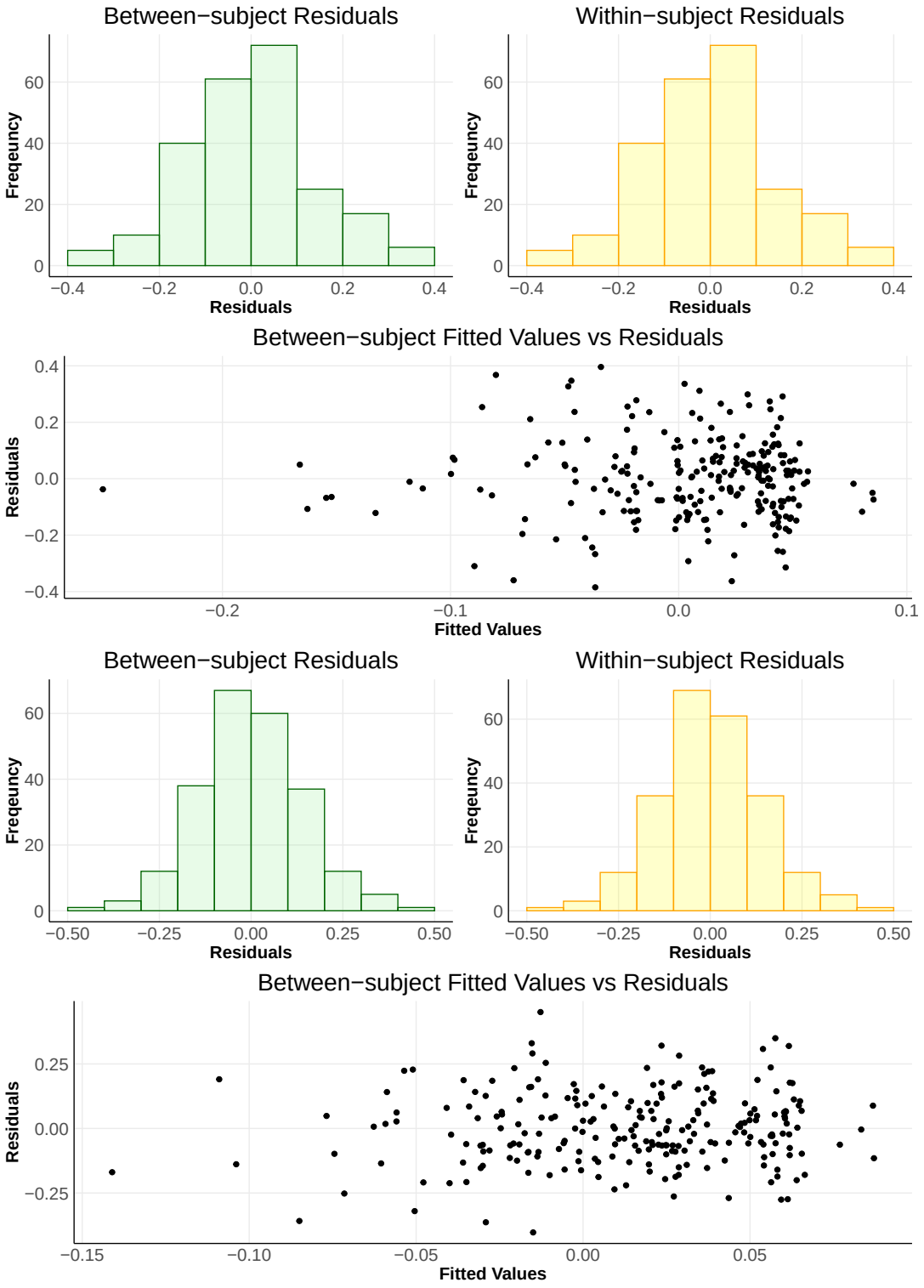

Figure D.7: Between-subject and within-subject residuals are represented by histograms and a scatter plot for Z-score FC measures between right DLPFC region and the left and right GP.

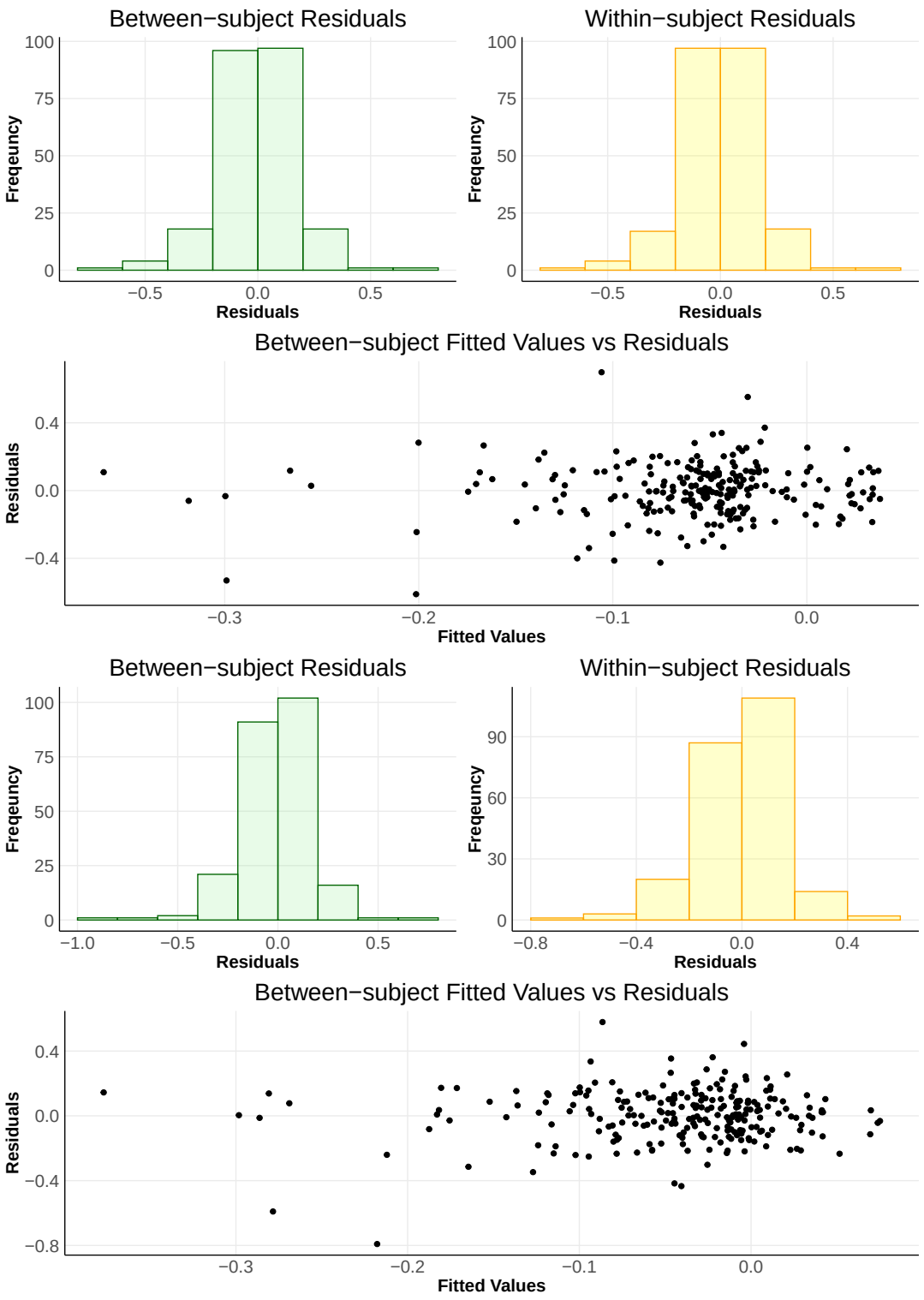

Figure D.8: Between-subject and within-subject residuals are represented by histograms and a scatter plot for Z-score FC measures between right DLPFC region and the left and right thalamus.

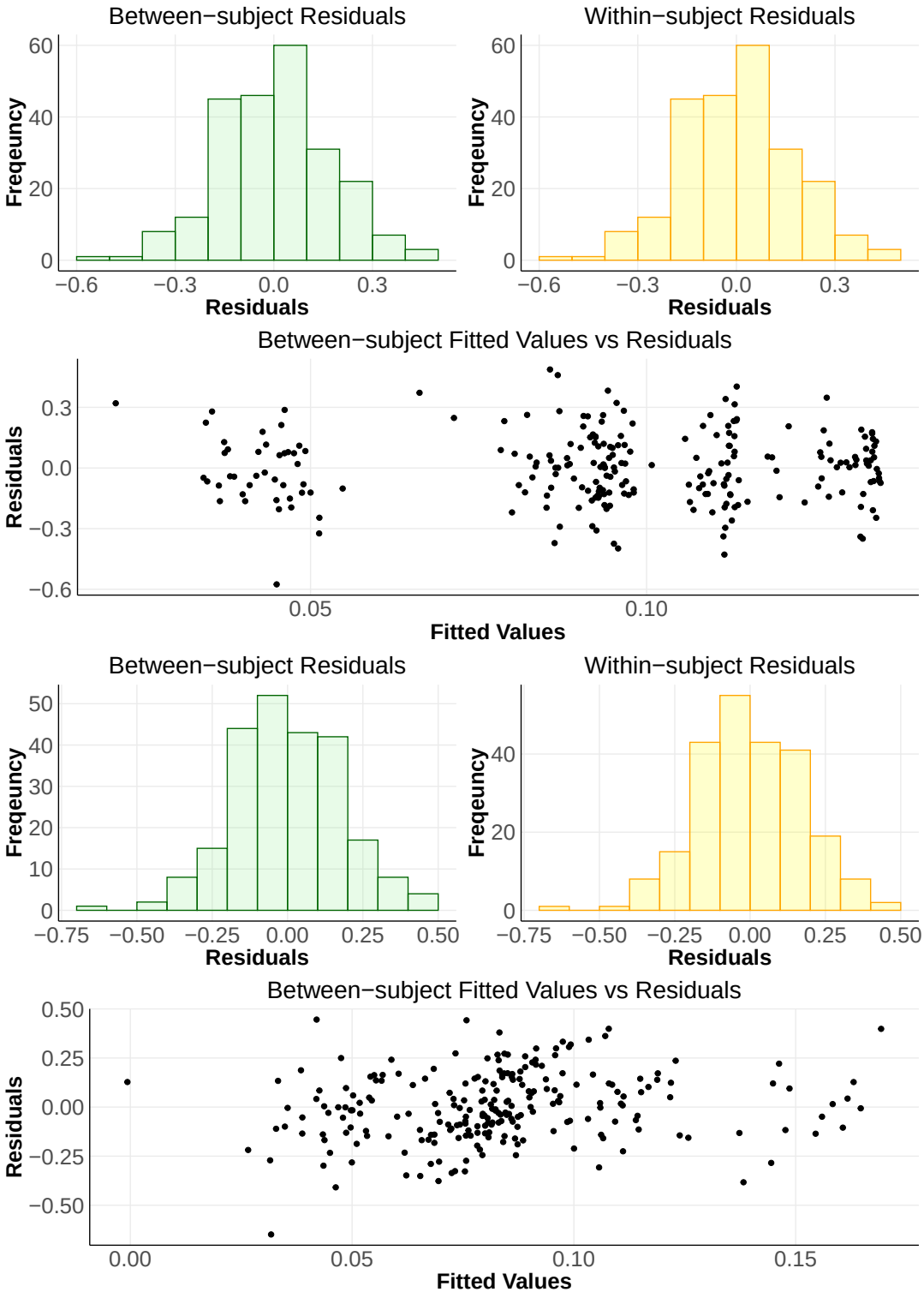

Figure D.9: Between-subject and within-subject residuals are represented by histograms and a scatter plot for Z-score FC measures between the motor region and the left and right putamen.

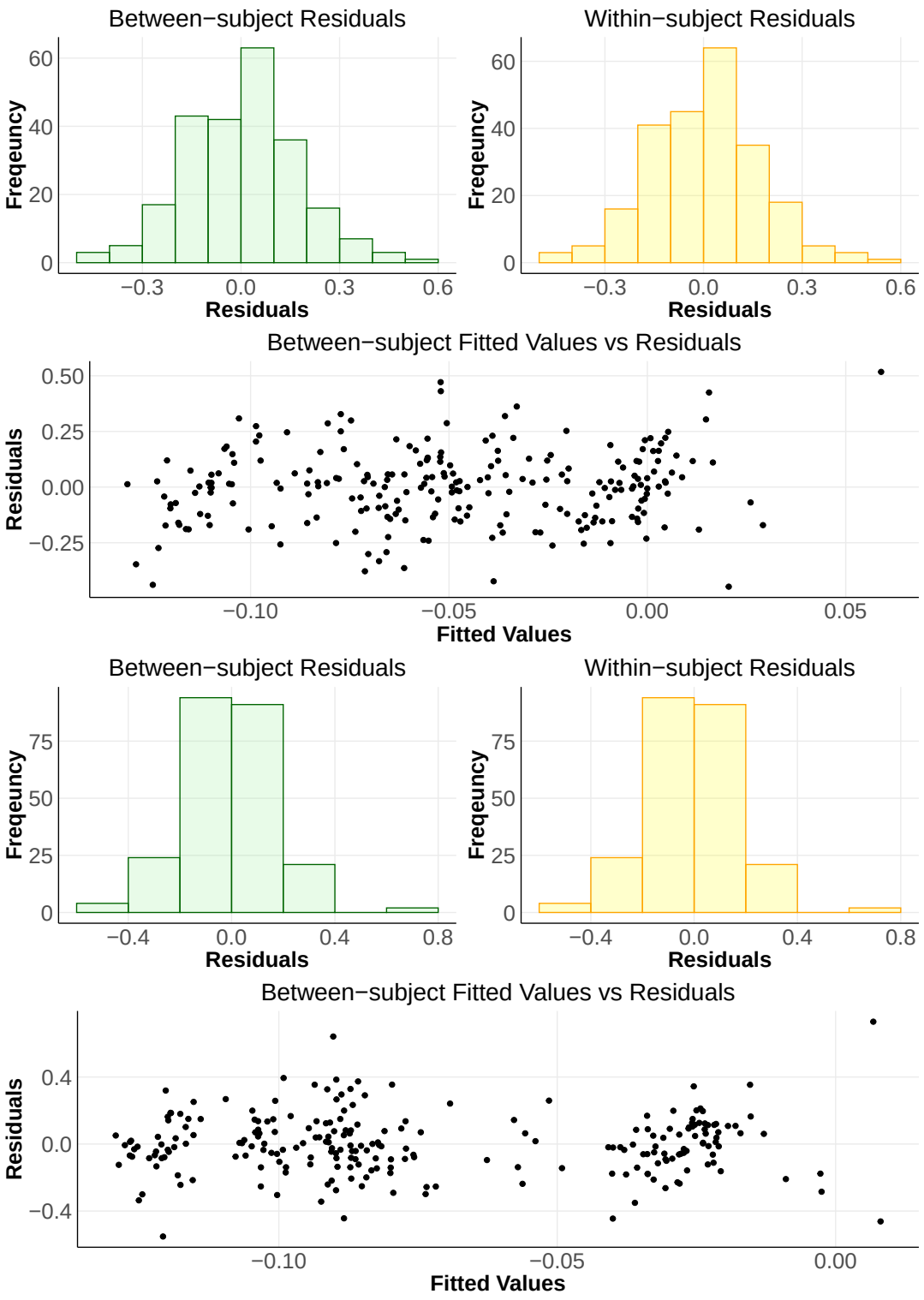

Figure D.10: Between-subject and within-subject residuals are represented by histograms and a scatter plot for Z-score FC measures between the motor region and the left and right caudate.

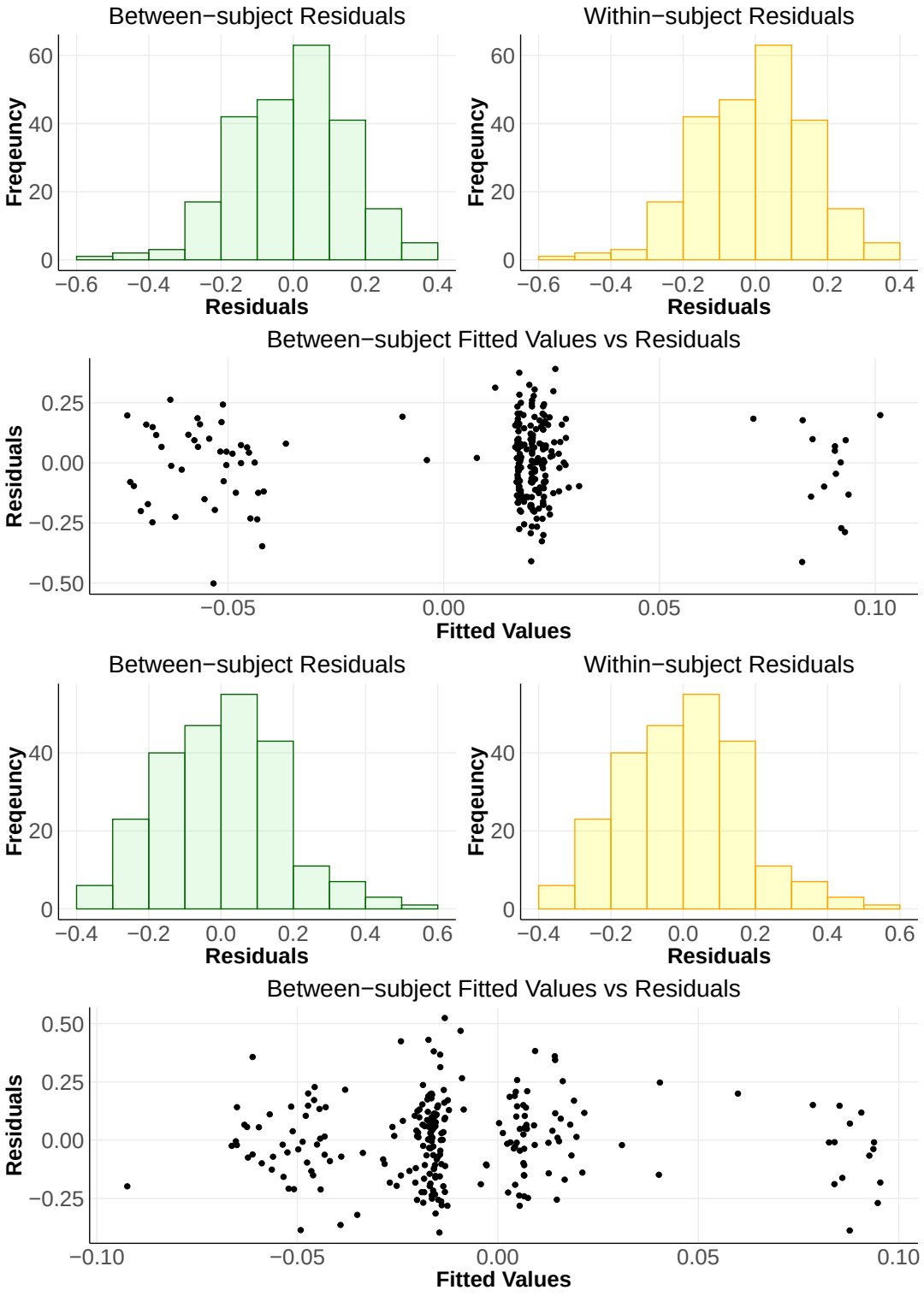

Figure D.11: Between-subject and within-subject residuals are represented by histograms and a scatter plot for Z-score FC measures between the motor region and the left and right GP.

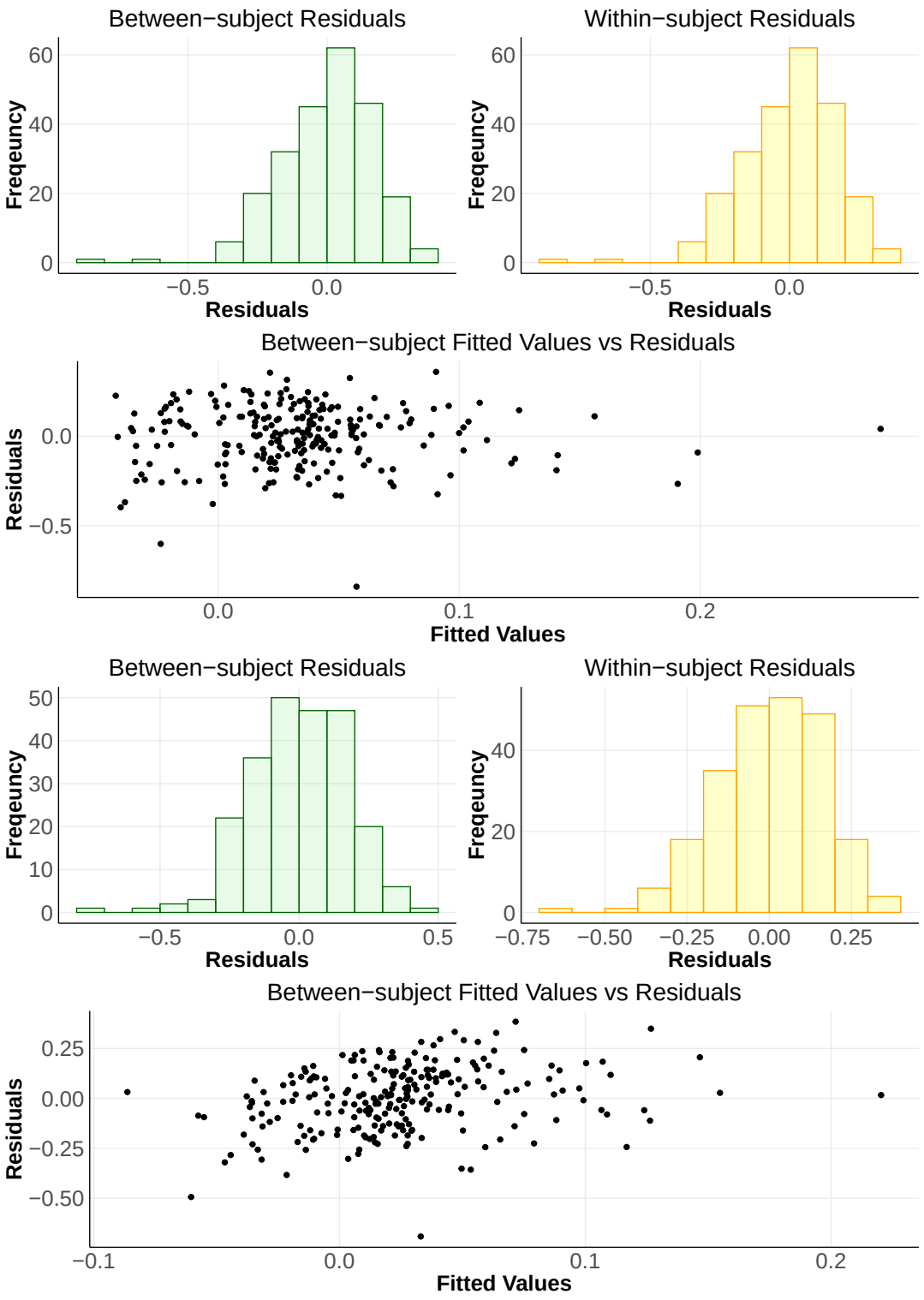

Figure D.12: Between-subject and within-subject residuals are represented by his-tograms and a scatter plot for Z-score FC measures between motor region and the left and right thalamus.

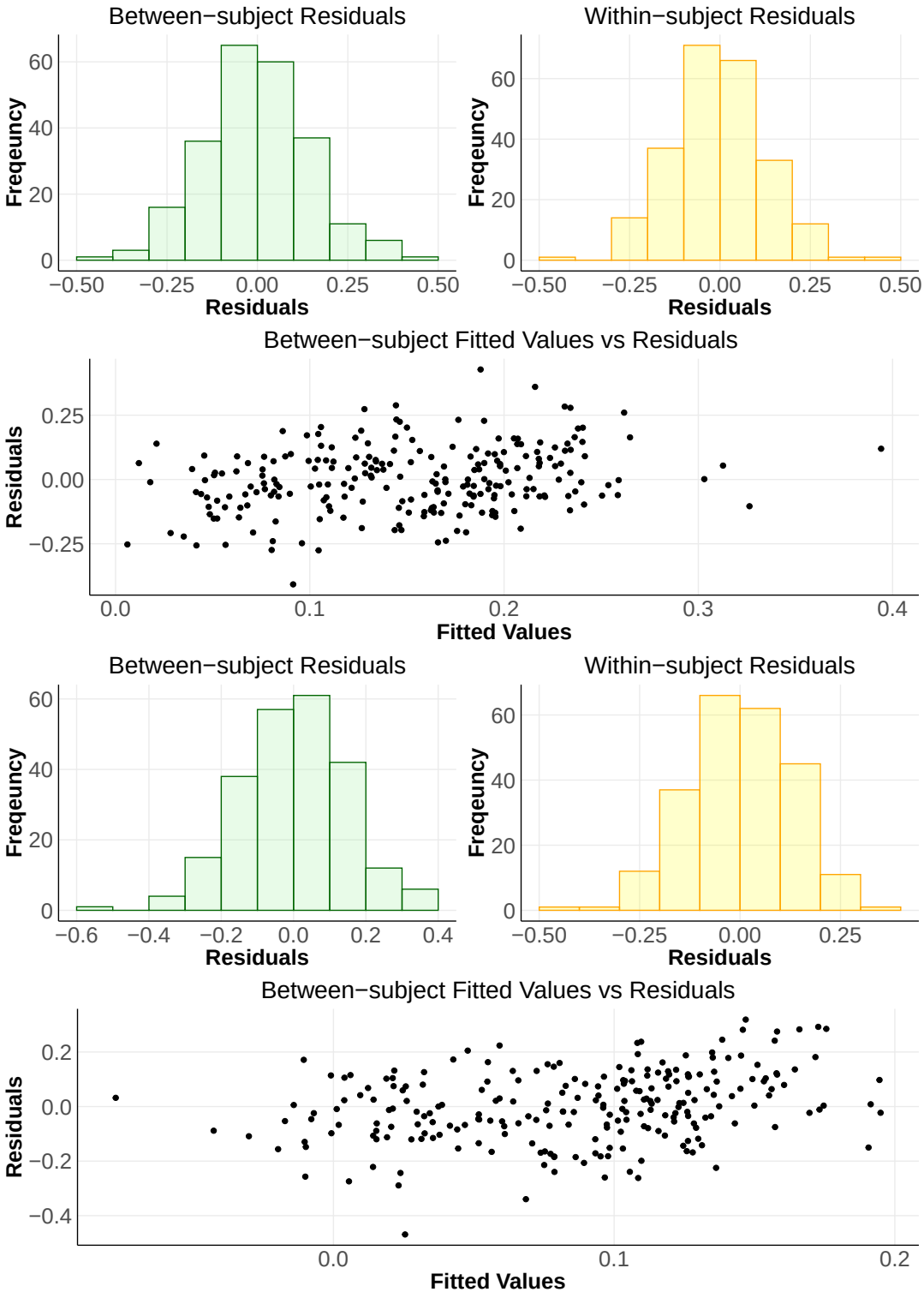

Figure D.13: Between-subject and within-subject residuals are represented by histograms and a scatter plot for Z-score FC measures between the language region and the left and right putamen.

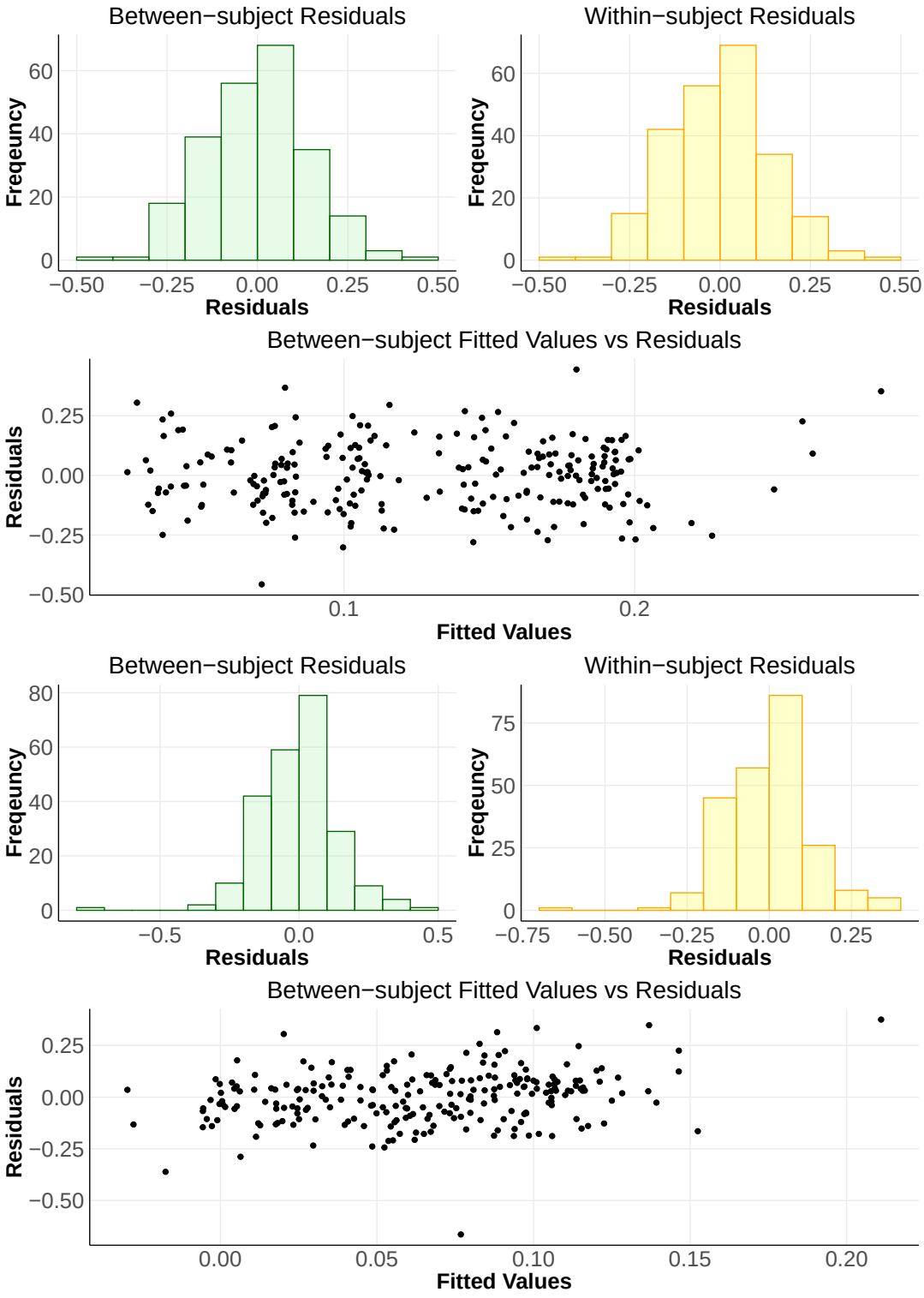

Figure D.14: Between-subject and within-subject residuals are represented by histograms and a scatter plot for Z-score FC measures between the language region and the left and right caudate.

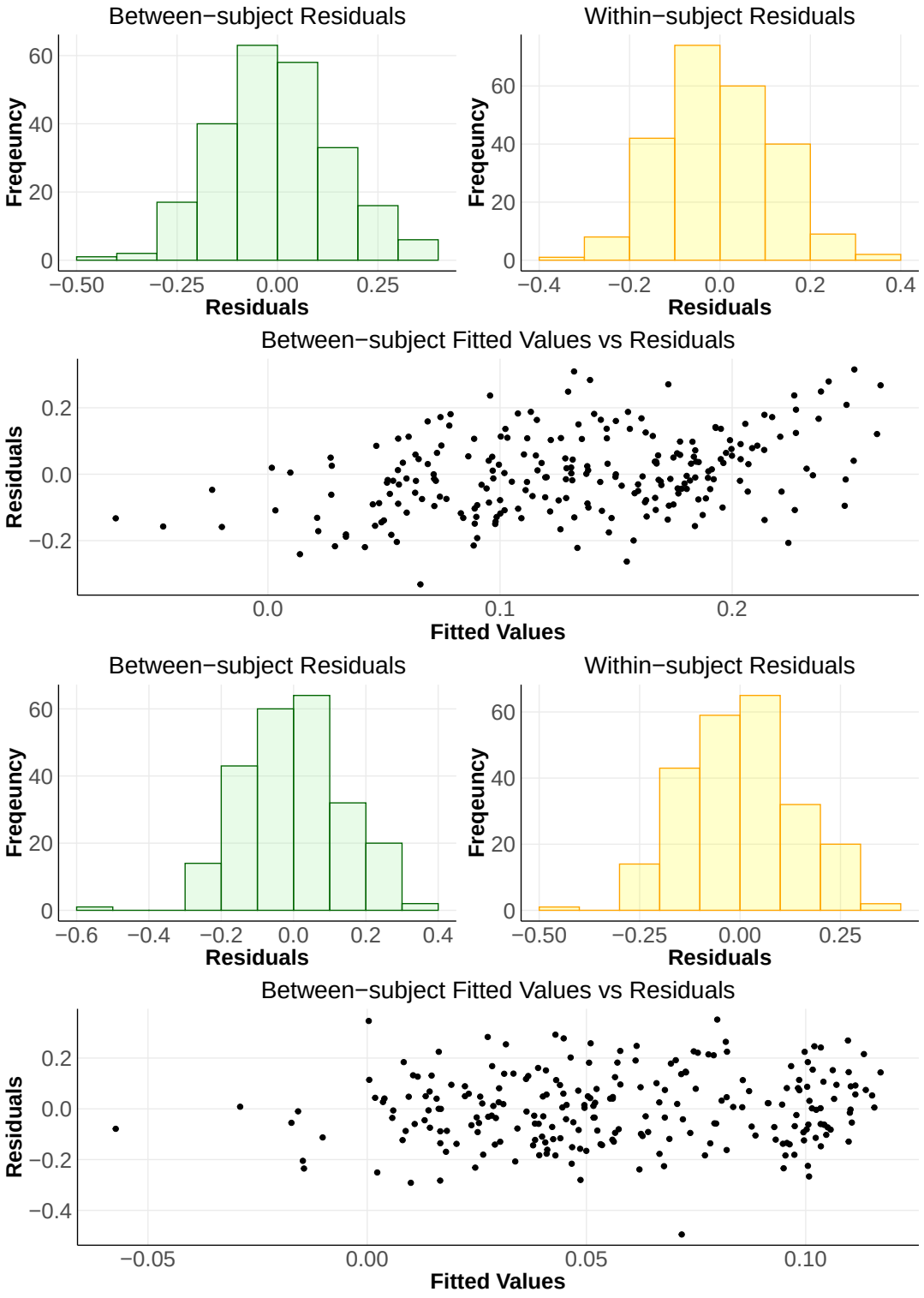

Figure D.15: Between-subject and within-subject residuals are represented by histograms and a scatter plot for Z-score FC measures between the language region and the left and right GP.

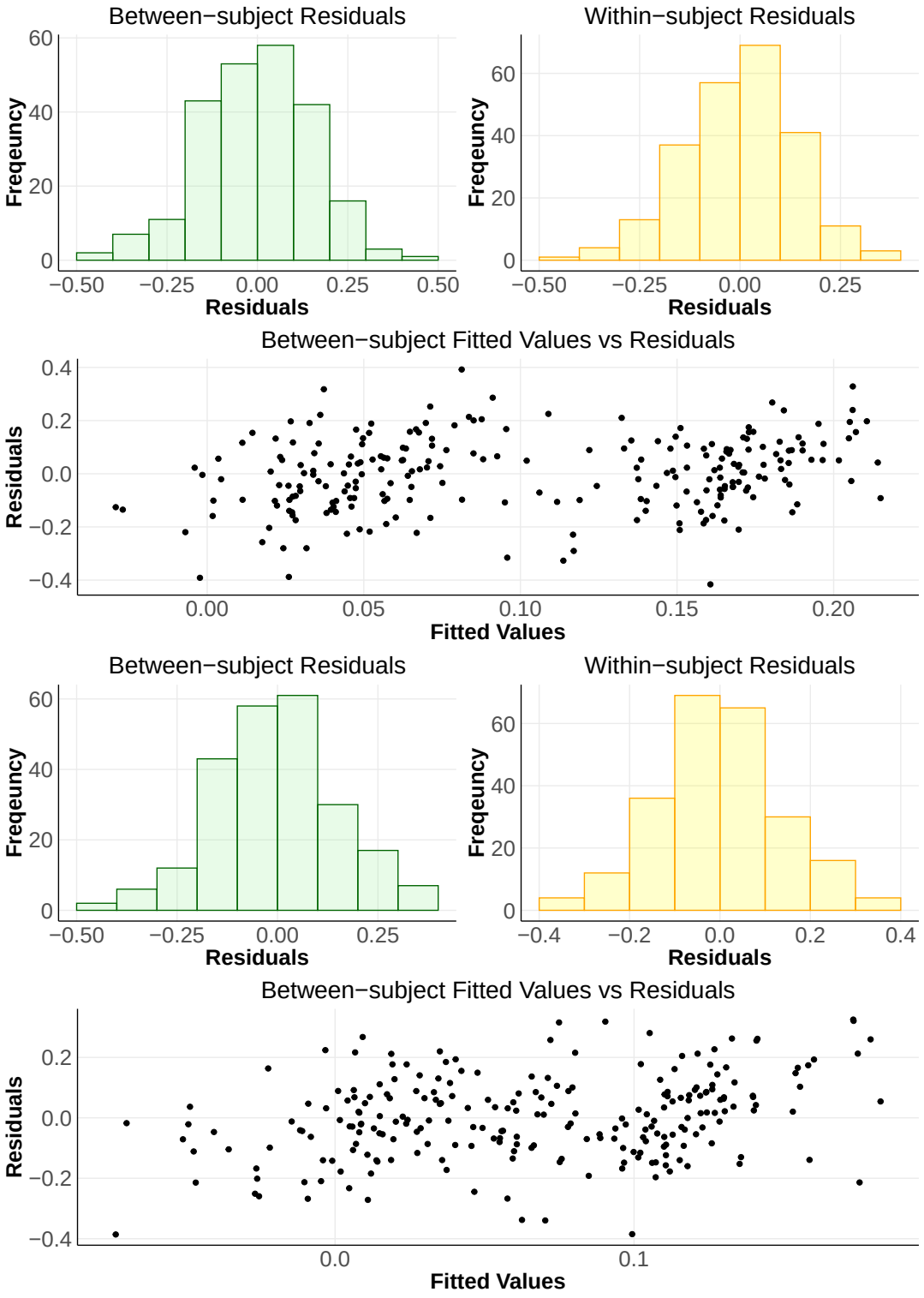

Figure D.16: Between-subject and within-subject residuals are represented by histograms and a scatter plot for Z-score FC measures between the language region and the left and right thalamus.

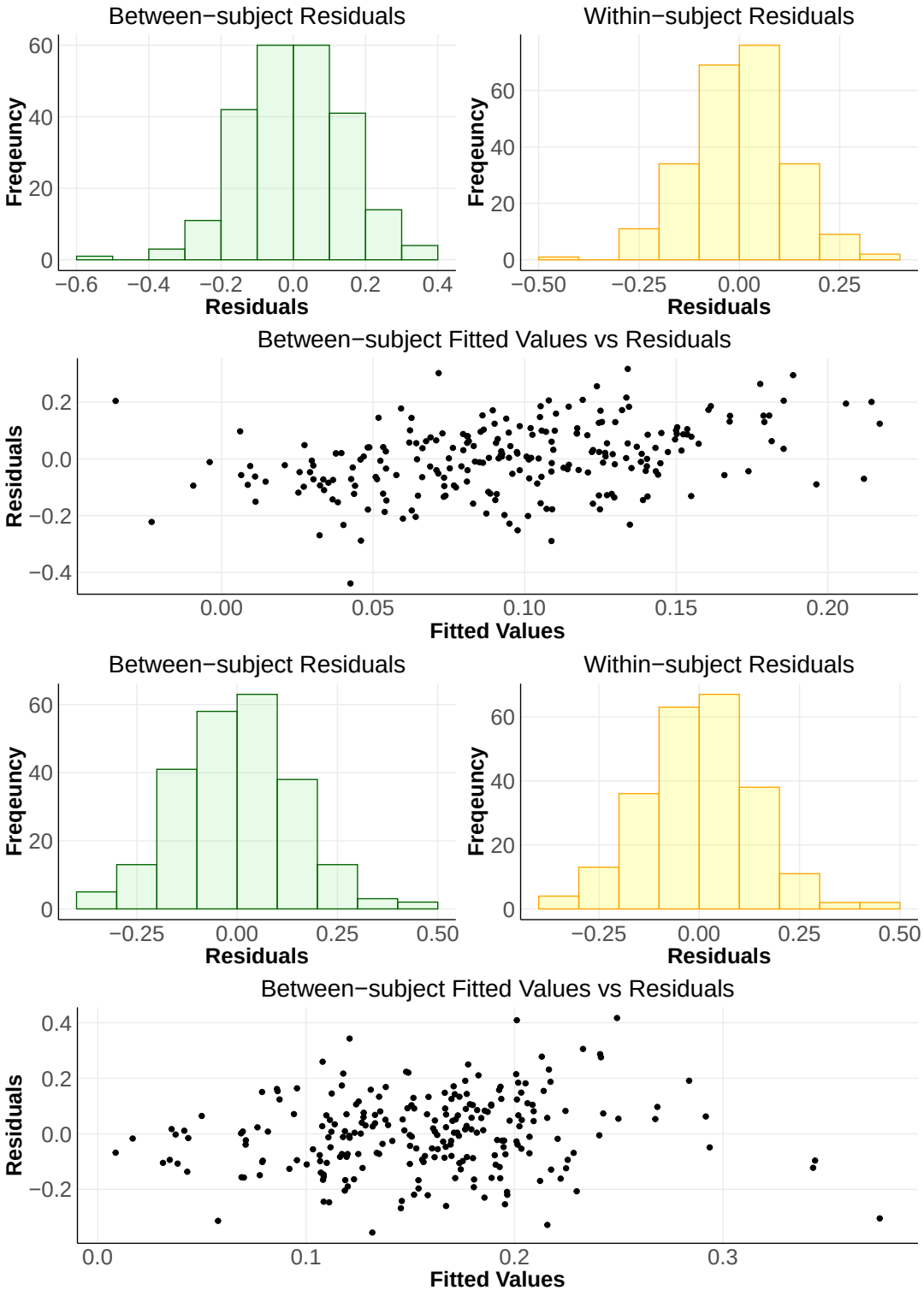

Figure D.17: Between-subject and within-subject residuals are represented by histograms and a scatter plot for Z-score FC measures between right IFG region and the left and right putamen.

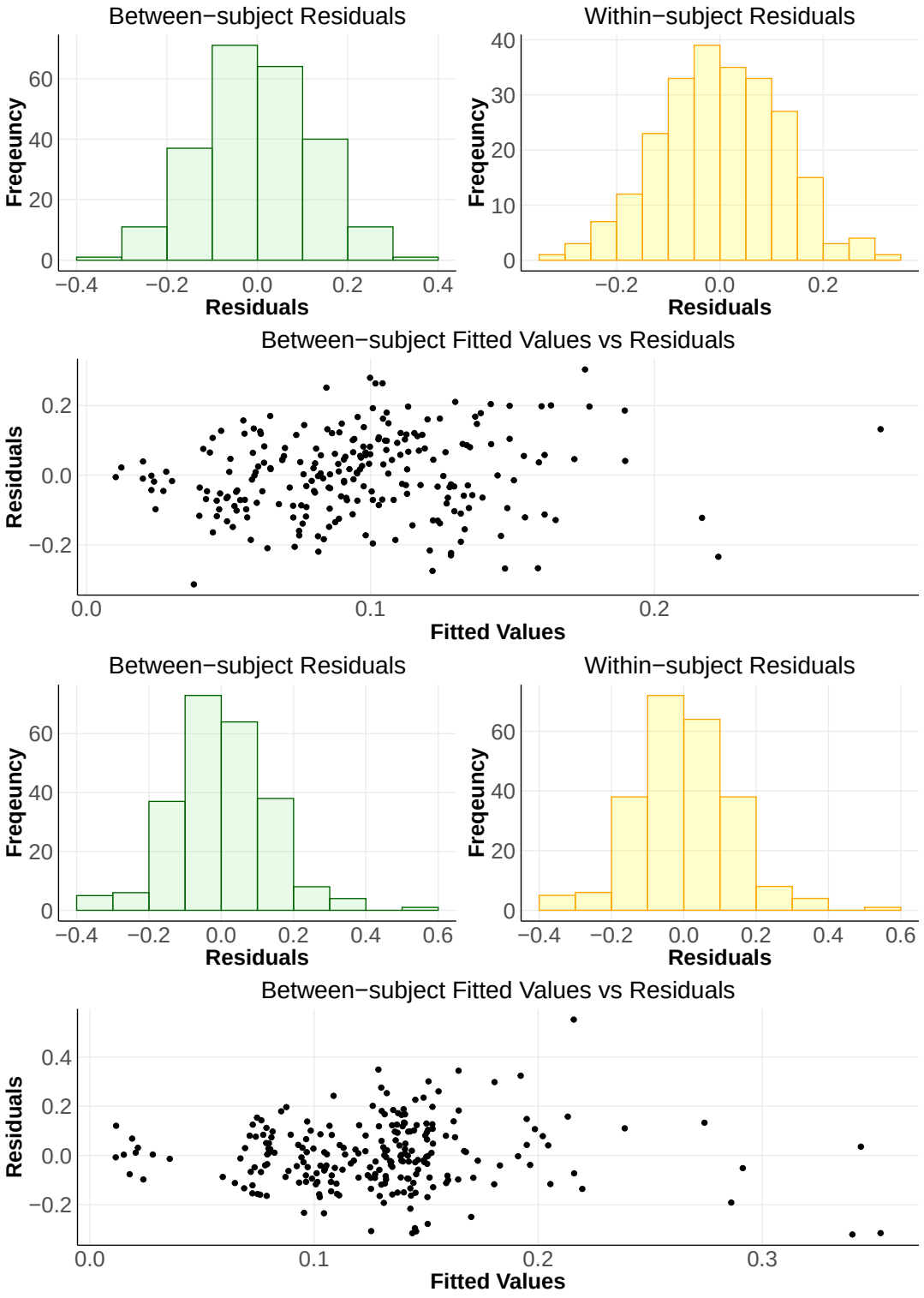

Figure D.18: Between-subject and within-subject residuals are represented by histograms and a scatter plot for Z-score FC measures between right IFG region and the left and right caudate.

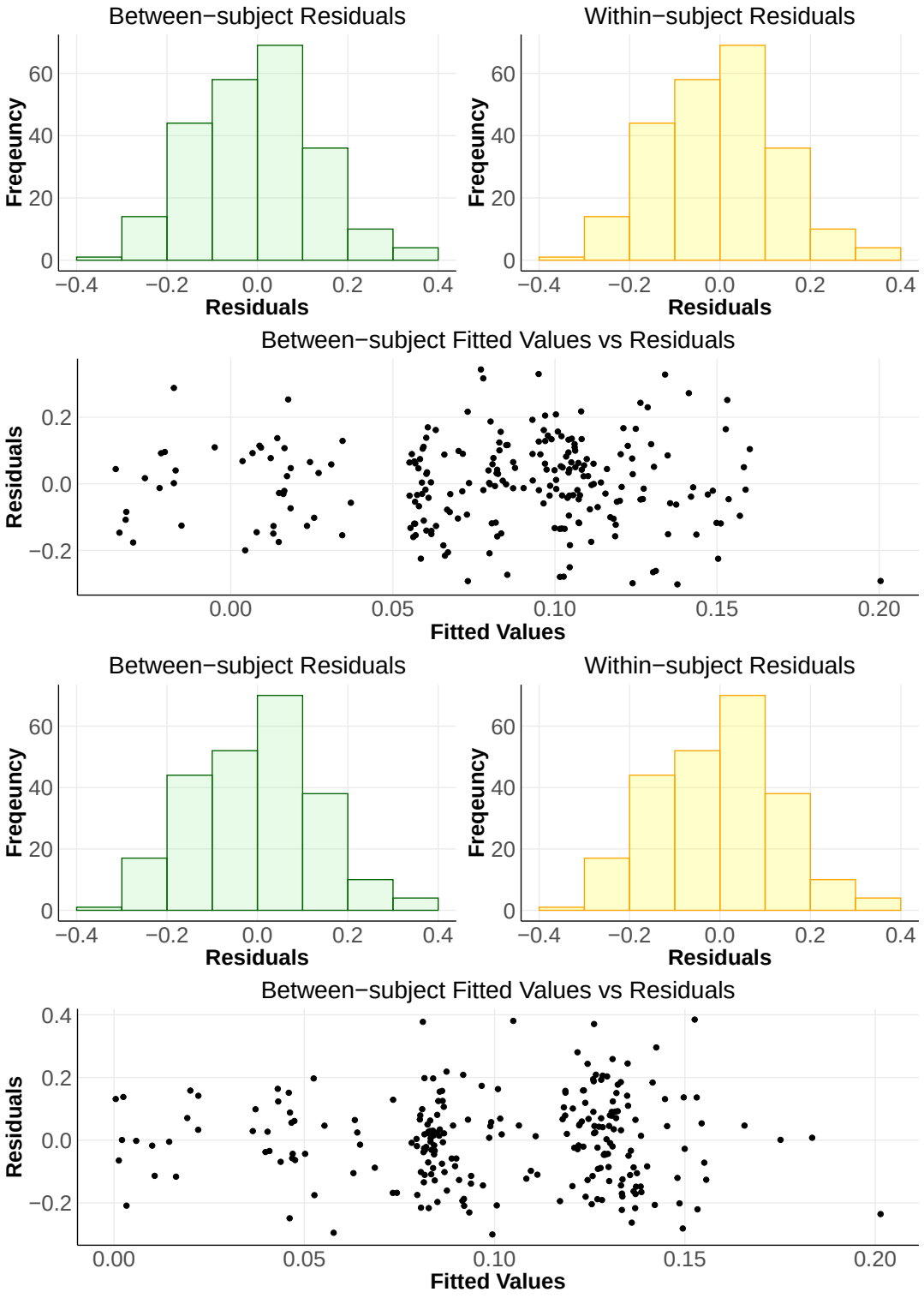

Figure D.19: Between-subject and within-subject residuals are represented by histograms and a scatter plot for Z-score FC measures between right IFG region and the left and right GP.

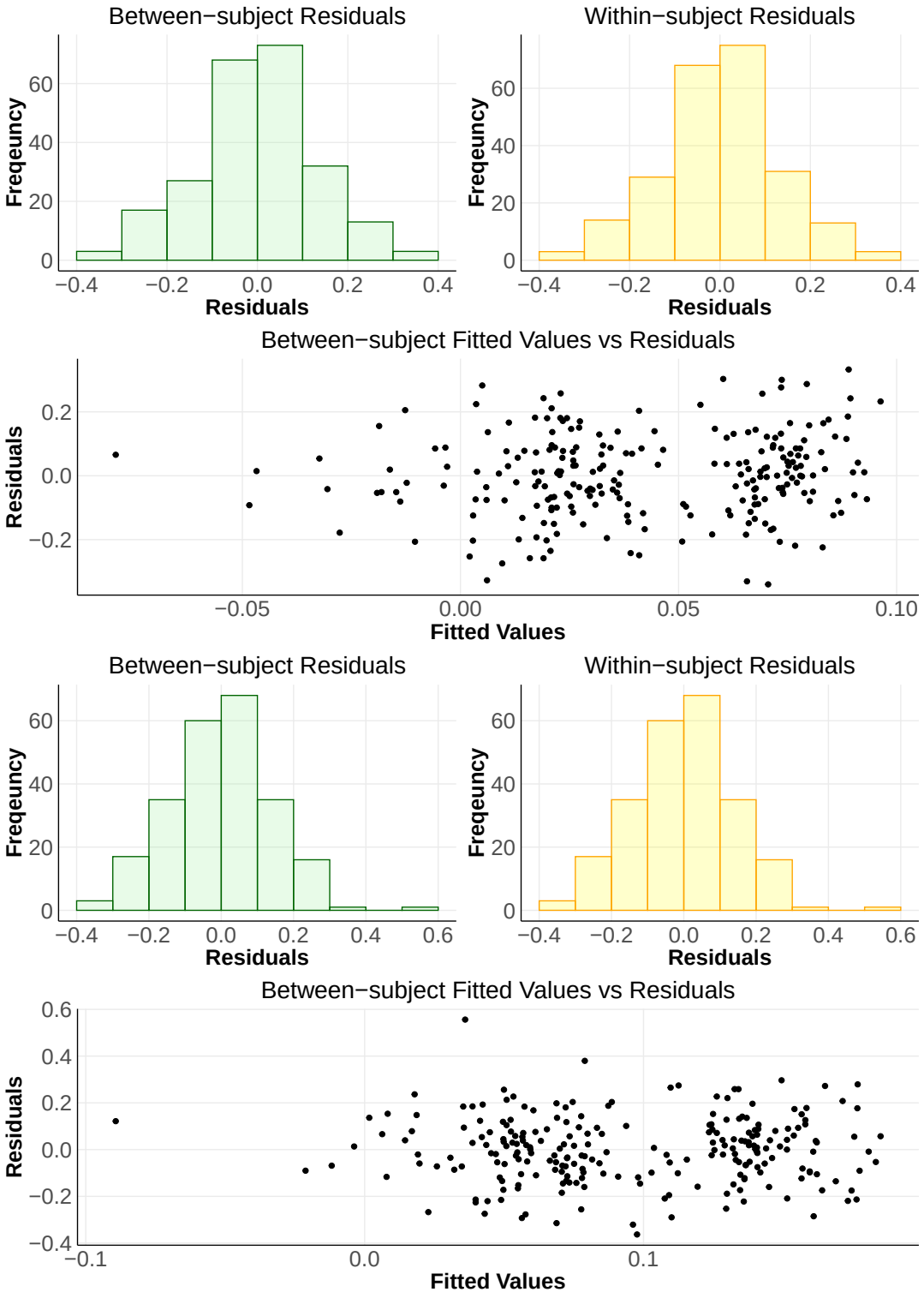

Figure D.20: Between-subject and within-subject residuals are represented by histograms and a scatter plot for Z-score FC measures between right IFG region and the left and right thalamus.

E. Appendix E - Model Validation - K-S Test

Table E.1: K-S Test for Left DLPFC

BG ROI	K-S Test Statistic	P-value
Left Putamen	0.377	<2.2e-16
Right Putamen	0.376	<2.2e-16
Left Caudate	0.374	<2.2e-16
Right Caudate	0.374	<2.2e-16
Left GP	0.377	<2.2e-16
Right GP	0.384	<2.2e-16
Left Thalamus	0.371	<2.2e-16
Right Thalamus	0.336	<2.2e-16

Table E.2: K-S Test for Right DLPFC Region

BG ROI	K-S Test Statistic	P-value
Left Putamen	0.377	<2.2e-16
Right Putamen	0.376	<2.2e-16
Left Caudate	0.374	<2.2e-16
Right Caudate	0.374	<2.2e-16
Left GP	0.377	<2.2e-16
Right GP	0.384	<2.2e-16
Left Thalamus	0.371	<2.2e-16
Right Thalamus	0.3361	<2.2e-16

Table E.3: K-S Test for Motor Region

BG ROI	K-S Test Statistic	P-value
Left Putamen	0.345	<2.2e-16
Right Putamen	0.346	<2.2e-16
Left Caudate	0.355	<2.2e-16
Right Caudate	0.351	<2.2e-16
Left GP	0.364	<2.2e-16
Right GP	0.364	<2.2e-16
Left Thalamus	0.375	<2.2e-16
Right Thalamus	0.366	<2.2e-16

Table E.4: K-S Test for Left IFG Region

BG ROI	K-S Test Statistic	P-value
Left Putamen	0.387	<2.2e-16
Right Putamen	0.381	<2.2e-16
Left Caudate	0.381	<2.2e-16
Right Caudate	0.391	<2.2e-16
Left GP	0.399	<2.2e-16
Right GP	0.381	<2.2e-16
Left Thalamus	0.380	<2.2e-16
Right Thalamus	0.376	<2.2e-16

Table E.5: K-S Test for Right IFG Region

BG ROI	**K-S Test Statistic**	**P-value**
Left Putamen	0.393	<2.2e-16
Right Putamen	0.377	<2.2e-16
Left Caudate	0.395	<2.2e-16
Right Caudate	0.377	<2.2e-16
Left GP	0.381	<2.2e-16
Right GP	0.386	<2.2e-16
Left Thalamus	0.381	<2.2e-16
Right Thalamus	0.377	<2.2e-16